CORENTIN HERBERT

AN INTRODUCTION TO FLUID TURBULENCE

Contents

These lecture notes cover the material for the course *Advanced Fluid Mechanics and Turbulence*, which is part of the Masters program *Physics: concepts and applications* offered at *ENS de Lyon*. This class is mostly an introduction to classical fluid turbulence, aimed at physicists. Typically, the class covers the Navier-Stokes equations, Kolmogorov Theory, and touches briefly upon intermittency and 2D and geophysical turbulence. This corresponds to Chapters 1– 7 in the lecture notes. Some additional paragraphs about other topics are included in this document as a bonus, I might add more in the future. The class on 2D and geophysical turbulence will be presented as a seminar and is not covered in this version of the lecture notes.

Many topics which could be treated in an Advanced Fluid Mechanics class, such as hydrodynamic instabilities, waves in fluids, buoyancy driven flows, compressible and reactive flows, complex fluids, etc, will be left aside here, for lack of time. Geophysical Fluid Dynamics will be very briefly touched upon as a seminar at the end of the term.

These notes are based mostly on classical textbooks and the lecture notes from my colleagues who taught the class previously: Laurent Chevillard and Freddy Bouchet. The class is taught jointly by Mickael Bourgoin and myself: this document covers only the material that I teach (essentially Kolmogorov theory) and leaves aside topics like Lagrangian approaches and experimental aspects. For the sake of precision, I sometimes give references in the text which go beyond the scope of the present course. You should feel free to have a look at these, but if I were to single out only one reference, it would be the book by Uriel Frisch (1995), which is closest in spirit to a course like this one. A second useful reference for this course is the book by Pope (2000).

These lecture notes are still pretty much in a draft stage; please let me know if you find any mistakes, inaccurracies or typos.

Part I

Homogeneous Isotropic Turbulence

1
Introduction: What is turbulence?

TURBULENCE is the name given to the seemingly random fluctuations appearing in fluid flows under certain conditions, basically when the flow speed is large or when the scale of the flow is large.

Turbulence is essentially a very efficient way to dissipate energy or mix stuff. There are exceptions to this rule in geophysical flows, where turbulence plays a part on the large scale organization of the flow.

1.1 Some examples of turbulent flows

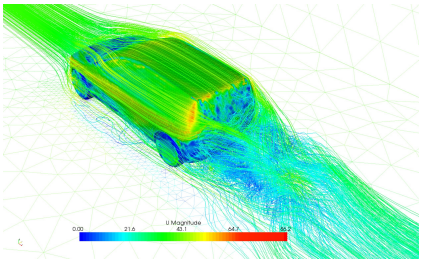

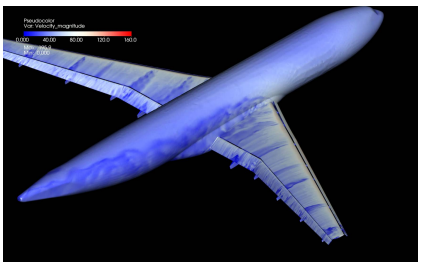

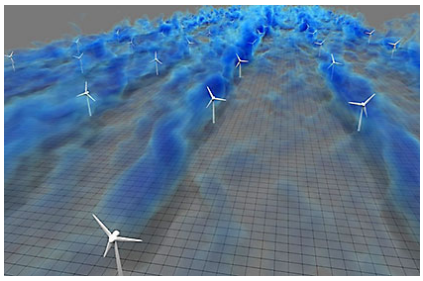

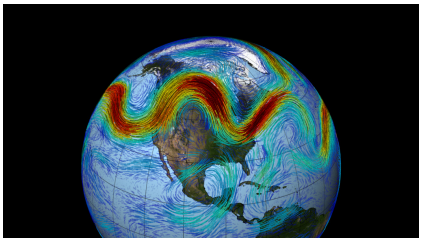

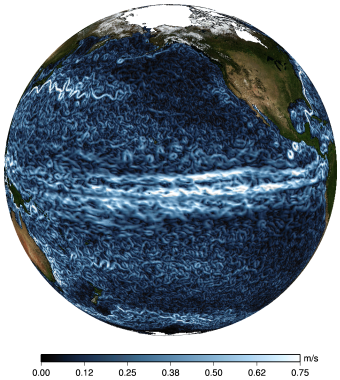

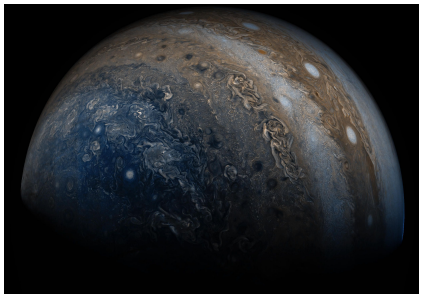

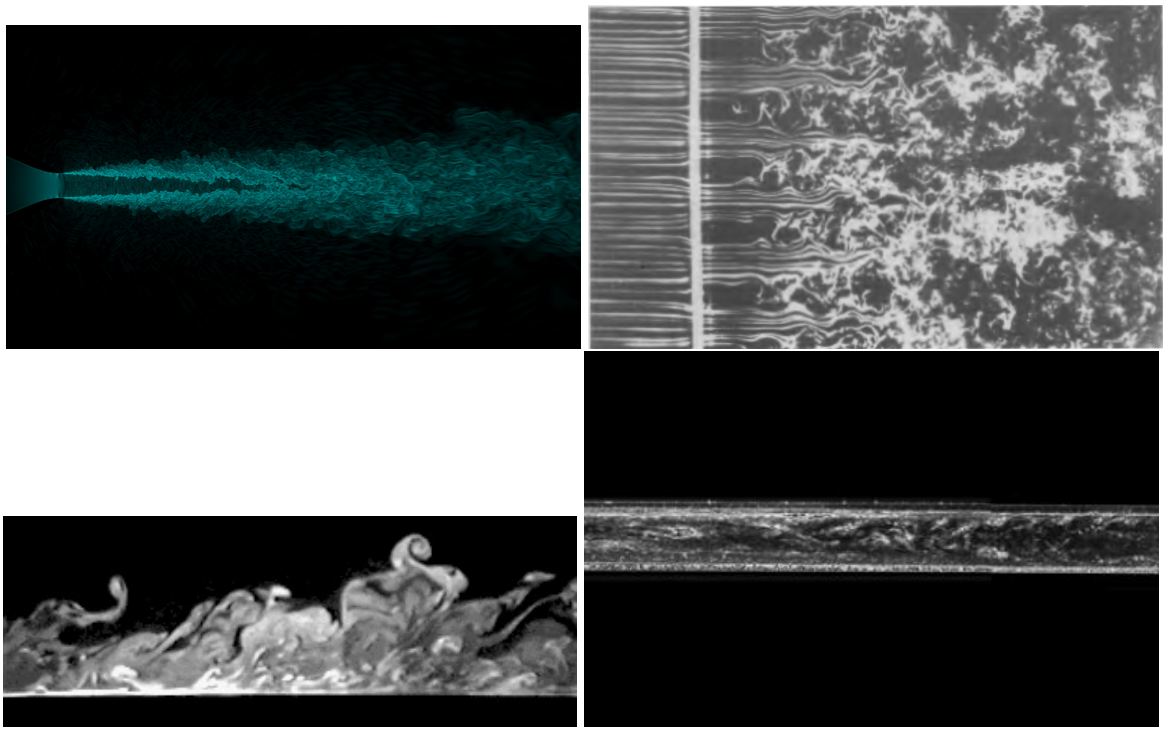

Figure 1.1: Examples of classical laboratory experiments for turbulent flows: turbulent jet (top left), grid turbulence (top right), boundary layer (bottom left) and pipe flows (bottom right).

1.2 *The impact of turbulence*

1.2.1 *Mixing: the coffee cup*

Let us consider the diffusion of a particle in a medium with diffusivity D, described by a Wiener process. As is well known, the mean-square displacement grows linearly with time, i.e. $\langle \Delta \mathbf{x}^2 \rangle = 6Dt$ in 3D space. The mass diffusion coefficient D depends on the two species involved, but typically for an aqueous solution at room temperature, it is on the order of 10^{-5} cm².s⁻¹. This means that the typical time for diffusion of sugar in a cup of coffee (a few centimeters wide) is on the order of $10/(6D)$, i.e. $\approx$ 2 days. Because thermal diffusion is faster by about two orders of magnitude (not even taking into account convection above the cup), one would be doomed to choose between drinking hot and sweet coffee. The answer to this conundrum is twofold: first, don't put sugar in your coffee. Second, turbulence. As we know from experience, stirring the cup dramatically speeds up the mixing process. The trajectory $\mathbf{R}(t)$ of a particle is now governed by:

$$d\mathbf{R}(t) = \mathbf{u}(\mathbf{R}, t)dt + \sqrt{2D}d\mathbf{W}(t), \tag{1.1}$$

where $\mathbf{u}$ is the Eulerian velocity field and $d\mathbf{W}(t)$ is the standard Wiener process (i.e. Brownian motion). The mean-square displacement $\langle \Delta \mathbf{x}^2 \rangle = 2D_{\text{eff}}t^{\alpha}$ now depends on the statistical properties of

$D \sim 10^{-5}$ cm².s⁻¹
$\kappa \sim 10^{-3}$ cm².s⁻¹

the velocity field $\mathbf{u}$: both subdiffusion ($\alpha < 1$) and superdiffusion ($\alpha > 1$) can be observed. Computing the effective diffusivity D_{eff} based on the statistical properties of $\mathbf{u}$ and molecular diffusivity D is an outstanding challenge. In a turbulent flow, we expect $D_{\text{eff}} \gg D$; turbulent diffusion is much more efficient than molecular diffusion. An intuitive understanding of this fact is that stirring the fluid deforms the isodensity contours of the substance we are mixing. First of all, there is the simple effect that advection alleviates the burden of travelling throughout the volume by diffusion only, but in addition to it, the isodensity contours develop finer and finer scales, which make it easier for molecular diffusion to do its job.

In the particular case of the coffee cup, the turbulent character of the flow can be questioned. Although the Reynolds number is quite modest (it can be reasonably estimated to be of order 100, using the viscosity of water ν on the order of 10^{-6} m^2.s^{-1}), mixing milk in a cup of coffee exhibits features characteristic of turbulent flows.

1.2.2 *Dissipation: the Rhône river*

Let us estimate the velocity of the Rhône river if the flow was laminar. We note $\alpha \sim h/d$ the angle of the canal with the horizontal, H the depth, g the gravity acceleration and ν the kinematic viscosity.

Estimating the total energy (per unit mass) dissipated over the course of the flow from Lyon to the Mediterranean sea as $\nu U^2/H^2 \times d/U$, and balancing it with the potential energy (per unit mass) in Lyon gh, we get the back-of-the-enveloppe estimate $U \sim gH^2\alpha/\nu$.

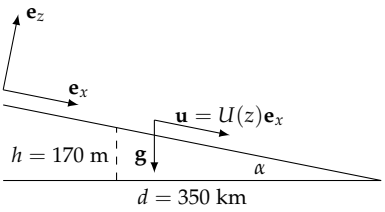

To be slightly more precise, we remember from kindergarten that the flow should be of Poiseuille type: we should have $\nu U''(z) = -g \sin\alpha$. It follows that the flow profile is parabolic, and the velocity at the surface is given by $U = gH^2 \sin\alpha/(2\nu)$.

BC: $\begin{cases} U(z=0) = 0, \\ U'(z=H) = 0 \end{cases}$

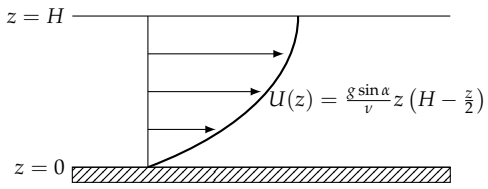

In the case of the Rhône, the elevation of Lyon is about 170m, the distance to the sea is roughly 350 km, so that $\alpha \approx 5.10^{-4}$. We obtain the following order of magnitude for the flow velocity: $U \approx 0.5 \times 10 \times 5.10^{-4} \times 10^2/10^{-6} \approx 2.5 \times 10^5$ m.s^{-1}.

Two conclusions can be drawn:

- The Rhône is an example of a relativistic flow.
- Alternatively, there exists a dissipation mechanism which transfers energy towards smaller scales, where viscosity acts much more efficiently to dissipate energy. In that case, there is not a direct balance between forcing and dissipation, that balance is mediated by the nonlinear term, which is the mechanism transferring energy towards smaller scales. One of the main goals of this course is to give a precise meaning to this statement.

At large Reynolds number, there is no steady solution: the Poiseuille flow becomes unstable, and the flow fluctuates around a different mean profile.

1.2.3 *Dissipation: the drag force*

Of course, the efficiency of turbulence as a dissipation mechanism has many practical consequences.

Let us consider the drag force F acting on a body (e.g. a car) with cross-section L^2 moving through a fluid with viscosity ν and density ρ at constant velocity U. The drag coefficient C_D is defined as (twice) the fraction of the momentum $\rho L^2 U^2 \tau$ transferred to the object in a time τ, which yields the drag equation:

$$F = \frac{C_D}{2} \rho L^2 U^2. \tag{1.2}$$

The drag coefficient should depend on the shape of the body, and the Reynolds number.

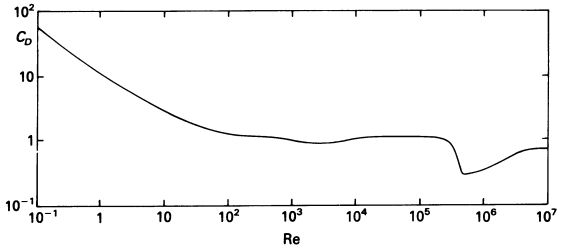

Figure 1.2: Drag coefficient as a function of the Reynolds number for a circular cylinder, based on experimental data (Tritton 2012, p. 33).

At low Reynolds number, the drag force is proportional to the velocity (i.e. the drag coefficient varies as Re^{-1}), but it becomes quadratic at higher Reynolds number (i.e. the drag coefficient becomes constant). The associated energy dissipation (per unit mass) is $\epsilon = \frac{C_D}{2} \frac{U^3}{L}$; constant drag is equivalent to a finite limit for energy dissipation as $\nu \to 0$. This is called *anomalous dissipation* (see § 5.1) and is due to turbulence.

$\epsilon = \frac{W}{\rho L^3} = \frac{FU}{\rho L^3}$. We implicitly assume that the injected energy is dissipated (into heat) in a region of the fluid of volume L^3, in the wake of the flow past the object.

1.2.4 *Summary*

Turbulence has good and bad sides. On the good side, it allows rivers to flow without encountering unnerving relativistic effects. On the bad side, it makes it much more difficult to move around for animals, people and the things they make, beyond a certain speed. Turbulence also allows you to drink coffee at the same time hot and sweet. Whether this is on the good or on the bad side remains disputed.

Exercise: estimate the contribution of turbulence to global warming.

2
The Euler and Navier-Stokes equations

A NATURAL MODEL TO CONSIDER for turbulence is the *Navier-Stokes equations* for incompressible flows:

$$\partial_t \mathbf{u} + \mathbf{u} \cdot \nabla \mathbf{u} = -\nabla p + \nu \Delta \mathbf{u}, \tag{2.1}$$

$$\nabla \cdot \mathbf{u} = 0, \tag{2.2}$$

or in coordinates

$$\partial_t u_i + u_j \partial^j u_i = -\partial_i p + \nu \partial_j \partial^j u_i, \tag{2.3}$$

$$\partial^i u_i = 0, \tag{2.4}$$

where $\mathbf{u}$ is the velocity field, p the pressure and ν the kinematic viscosity. Here and in the rest of these notes, we have adopted the Einstein summation convention for repeated indices. When $\nu = 0$, these equations are referred to as the *Euler equations*[1].

[1] Of course, historically the Euler equations came first (1757).

These equations are well-defined on a domain of arbitrary dimension, i.e. for $\mathbf{u}$ a vector field in $\mathbb{R}^d$ or more generally on a d-dimensional manifold. However, the most common case for applications is $d = 3$, and we should stick to this case for the purpose of this course. The two-dimensional case also reveals many interesting aspects, with applications for instance to geophysical flows, but we should barely touch upon those (see § **??**).

In this course, we shall take these equations for granted; we refer to classical fluid mechanics textbooks for further discussion of their validity (e.g. Landau and Lifchitz 1971). In particular, we should work in the simplest possible framework and ignore phenomena such as compressibility, density variations, rotation, magnetic fields,etc.

2.1 *Domain walls, turbulence generation and the random character of turbulence*

The Euler and Navier-Stokes equations should be supplemented by boundary conditions. For the Euler equations, the impermeability

condition $\mathbf{u} \cdot \mathbf{n} = 0$ suffices, where the vector $\mathbf{n}$ is locally normal to the domain boundary. Because they involve a second-order differential operator, the Navier-Stokes equations require all the components of the velocity to be specified on the domain boundary. For simplicity, we shall work with the *no-slip* condition here, i.e. $\mathbf{u} = 0$ on the domain boundary, or sometimes with periodic boundary conditions.

In experiments, energy is virtually always injected through the interaction of a wall with the fluid, be it the domain boundary or an object moving in the fluid. The flow may be forced steadily (e.g. von Karman flow, wind tunnel) or freely decaying after an initial perturbation (e.g. moving a grid through a tank). In both cases, the general idea is that if we shake the fluid sufficiently vigorously, we will try to impose a flow which will be unstable, thereby generating turbulence.

In numerical simulations, on the other hand, the effect of walls is more cumbersome to represent. An easier way to generate turbulence is either to pick a sufficiently energetic initial condition (*decaying turbulence*) or to inject energy in the system continuously by adding a forcing term on the right hand side of Eq. (2.1). We are free to choose the space and time structure of this forcing term.

In principle we expect the experimental process as well as the laws of motion to be deterministic. Yet, carrying out the same experiment multiple times yields different outcomes; as turbulence develops, the flow takes on a random character and only statistical properties of the flow should be robustly reproducible. As a consequence, it is quite common in numerical simulations and in theoretical studies to add explicitly a random forcing term $\mathbf{f}$ in the right hand side of the Navier-Stokes equations (2.1), which become stochastic partial differential equations. Such equations make sense only for random velocity fields. Alternatively, we may stick to deterministic initial value problems but with random initial conditions. In both cases, we are interested in the statistical properties of the solutions of the Euler and Navier-Stokes equations. It is expected that these statistical properties, at scales small enough to be unaltered by the shape of the container or details of the energy injection mechanism, should not depend on the experimental setup or the space-time structure of the imposed forcing. This is referred to as *universality*.

In this chapter, we start with a few reminders about some important aspects of the Euler and Navier-Stokes equations seen as deterministic systems before actually diving into the stochastic nature of turbulent flows.

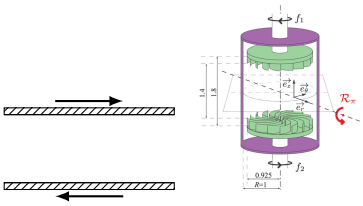

Figure 2.1: In Couette flow or van Karman flow, turbulence is generated by the motion of the domain boundaries.

2.2 *Pressure and incompressibility*

2.2.1 *Solving the Poisson equation*

Using incompressibility, the pressure can be deduced by taking the divergence of the Navier-Stokes equations:

$$\nabla \cdot (\mathbf{u} \cdot \nabla \mathbf{u}) = -\Delta p. \tag{2.5}$$

This is a Poisson problem. The Laplacian can be inverted by considering the Green function $G(x)$: $\Delta G(x) = \delta(x)$, where δ is the Dirac distribution.

Hence, the pressure reads:

$$p(\mathbf{x}) = -\int d\mathbf{y} G(\mathbf{x}-\mathbf{y}) \nabla \cdot (\mathbf{u} \cdot \nabla \mathbf{u})(\mathbf{y}). \tag{2.7}$$

In particular, in dimension $d = 3$, $G(x) = -1/(4\pi\|x\|)$, so that

$$p(\mathbf{x}) = \frac{1}{4\pi} \int_{\mathbb{R}^3} d\mathbf{y} \frac{1}{\|\mathbf{x}-\mathbf{y}\|} \partial_i u_j(\mathbf{y}) \partial^j u^i(\mathbf{y}). \tag{2.8}$$

It is clear based on this formula that pressure is a non-local quantity. It is also clear (and reassuring) that the Navier-Stokes equations are closed equations. They can be written in the form:

$$\frac{\partial u_i(\mathbf{x})}{\partial t} + u_j(\mathbf{x}) \frac{\partial u_i(\mathbf{x})}{\partial x_j} = \frac{1}{4\pi} \int_{\mathbb{R}^3} d\mathbf{y} \frac{x_i - y_i}{\|\mathbf{x}-\mathbf{y}\|^3} \frac{\partial u_j(\mathbf{y})}{\partial y_k} \frac{\partial u_k(\mathbf{y})}{\partial y_j} + \nu \frac{\partial}{\partial x_j} \frac{\partial}{\partial x^j} u_i(\mathbf{x}), \tag{2.9}$$

or in more compact form,

$$\partial_t \mathbf{u} + \mathbf{u} \cdot \nabla \mathbf{u} = \frac{1}{4\pi} \int_{\mathbb{R}^3} d\mathbf{y} \frac{\mathbf{x}-\mathbf{y}}{\|\mathbf{x}-\mathbf{y}\|^3} \operatorname{Tr}(\nabla \mathbf{u})^2(\mathbf{y}) + \nu \Delta \mathbf{u}. \tag{2.10}$$

It is important to keep in mind that pressure acts to maintain incompressibility.

2.2.2 *Vorticity*

Another way to eliminate the pressure is to work with vorticity.

Let us define the vector field $\boldsymbol{\omega} = \nabla \times \mathbf{u}$. In coordinates, we have $\omega_i = \epsilon_{ijk} \partial^j u^k$, where ϵ_{ijk} is the standard, rank 3, totally antisymmetric *Levi-Civita tensor*. Taking the curl of the Navier-Stokes equations (2.3) (hint: with the tensor contraction identity $\epsilon_{ijk}\epsilon^{ilm} = \delta^l_j \delta^m_k - \delta^m_j \delta^l_k$, prove and use the vector identity $\mathbf{u} \times \nabla \times \mathbf{u} = \nabla u^2/2 - \mathbf{u} \cdot \nabla \mathbf{u}$), we obtain the equation governing vorticity dynamics:

$$\partial_t \boldsymbol{\omega} = \nabla \times (\mathbf{u} \times \boldsymbol{\omega}) + \nu \Delta \boldsymbol{\omega}, \tag{2.11}$$

$$\partial_t \boldsymbol{\omega} = \boldsymbol{\omega} \cdot \nabla \mathbf{u} - \mathbf{u} \cdot \nabla \boldsymbol{\omega} + \nu \Delta \boldsymbol{\omega}. \tag{2.12}$$

In arbitrary dimension d (let us not be cheap), the Green function of the Laplacian reads:

$$G(x) = \begin{cases} \frac{1}{2\pi} \ln\|x\| & \text{if } d = 2, \\ \frac{1}{(2-d)\Omega_d} \|x\|^{2-d} & \text{if } d \geq 3, \end{cases} \tag{2.6}$$

where $\Omega_d = 2\pi^{d/2}/\Gamma(d/2)$ is the surface of the unit sphere in dimension d, and $\Gamma(x) = \int_0^{+\infty} t^{x-1} e^{-t} dt$ is the Gamma function.

The second term on the right-hand side is just advection of vorticity by the flow, while the first term describes *vorticity stretching*.

Of course, no miracle occurs: the vorticity equation depends on the velocity field $\mathbf{u}$. To close it, we need to invert vorticity first, which again introduces a non-local operator. Nevertheless, it can sometimes be useful to work with vorticity rather than velocity, This is particularly true in two-dimensional turbulence, where the vorticity stretching term vanishes, implying that vorticity is a material invariant in 2D inviscid flows.

2.3 *The Reynolds number*

2.3.1 *Naive definition*

Two physical effects compete in the Navier-Stokes equations: inertia (represented by the advection term $\mathbf{u} \cdot \nabla \mathbf{u}$) and viscous dissipation (represented by the diffusion term $\nu \Delta \mathbf{u}$). Roughly speaking, turbulence occurs when inertia prevails over viscosity.

A very naive way to measure this competition is to estimate the order of magnitude of the advection and dissipation terms as U^2/L and $\nu U/L^2$, respectively, where U and L are characteristic velocity and length scales, respectively. The ratio of these two quantities defines a non-dimensional number, the *Reynolds number*:

$$Re = \frac{UL}{\nu}. \tag{2.13}$$

Based on the above reasoning, we expect turbulence to occur when the Reynolds number is large. We can already guess that a large Reynolds number also means that nonlinearity will play a crucial part. In fact, we shall see later that the Reynolds number provides an estimate of the range of scales coupled by the nonlinear term (see § 6.1.4).

Note that there is some arbitrariness in the choice of the characteristic velocity U and length scale L; we shall come back to this problem later (see § 3.1.4 and § 3.1.5).[2]

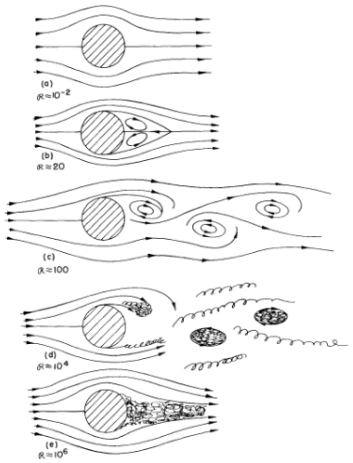

Figure 2.2: Flow past a cylinder as a function of the Reynolds number (Feynman, Leighton, and Sands 1965).

[2] While viscosity ν is a property of the fluid, Re is a property of the flow.

2.3.2 *Hydrodynamic similarity principle*

Let us make the above arguments a little more precise by non-dimensionalizing the Navier-Stokes equations. We introduce arbitrary length and time scales L and T, and denote $U = L/T$. Now, we define non-dimensional coordinates:

$$\mathbf{x}' = \mathbf{x}/L, \qquad t' = t/T. \tag{2.14}$$

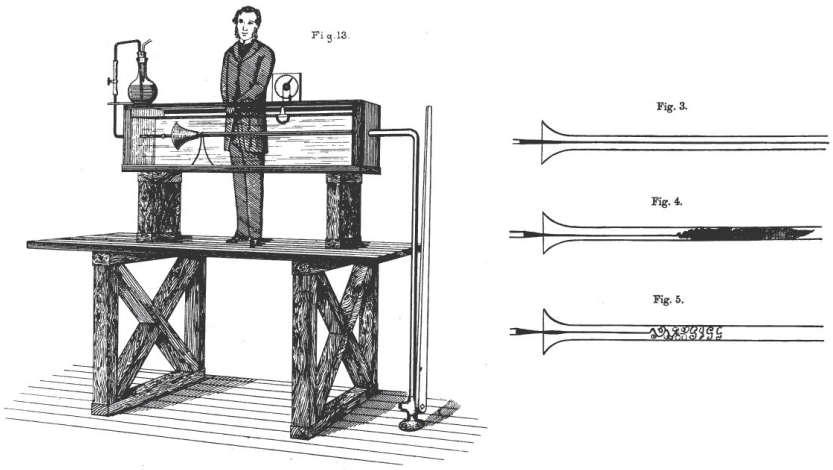

Figure 2.3: The classical experiment of flow in a pipe by Osborne Reynolds (1883).

Non-dimensional velocity and pressure read:

$$\mathbf{u}'(\mathbf{x}', t') = \mathbf{u}(\mathbf{x}'L, t'T)/U, \qquad p'(\mathbf{x}', t') = p(\mathbf{x}'L, t'T)/U^2, \qquad (2.15)$$

which satisfy the non-dimensional Navier-Stokes equations:

$$\partial_{t'}\mathbf{u}' + \mathbf{u}' \cdot \nabla'\mathbf{u}' = -\nabla' p' + Re^{-1}\Delta'\mathbf{u}',$$
$$\nabla' \cdot \mathbf{u}' = 0,$$

where the Reynolds number is given by Eq. (2.13).

This means that the behavior of solutions of the Navier-Stokes equations is governed by only one non-dimensional number, the Reynolds number.

From a more pragmatic point of view, two flows are "the same" if they have the same Reynolds number. This is referred to as the *hydrodynamic similarity principle*. It is the basis on which engineers rely to design aircrafts or other vehicles by studying models in wind tunnels, for instance (prior to the advent of numerical simulations, it was essentially the only option).

A caveat is the role of boundary conditions, on which we shall modestly refrain from commenting.

In the limit of large Reynolds number, we would expect to recover the Euler equations. However, it is far from clear whether solutions of the Navier-Stokes equations (or their statistical properties) converge to solutions of the Euler equations in some sense when $Re \to +\infty$.

2.4 *Symmetries*

As is customary in theoretical physics, we shall say that dynamical equations have a symmetry group G if the space of solutions is invariant under the action of G. We refer to a course on group theory for more formal definitions.

Let us start by listing the symmetries of the Euler equations in an infinite domain.

Continuous symmetries:

- Space and time translation invariance: $(t, \mathbf{x}, \mathbf{u}) \longmapsto (t, \mathbf{x} + \mathbf{x}_0, \mathbf{u})$ for $\mathbf{x}_0 \in \mathbb{R}^d$ and $(t, \mathbf{x}, \mathbf{u}) \longmapsto (t + t_0, \mathbf{x}, \mathbf{u})$ for $t_0 \in \mathbb{R}$.

- Galilean transforms: $(t, \mathbf{x}, \mathbf{u}) \longmapsto (t, \mathbf{x} + t\mathbf{U}, \mathbf{u} + \mathbf{U})$ for $\mathbf{U} \in \mathbb{R}^d$.

- Rotations: $(t, \mathbf{x}, \mathbf{u}) \longmapsto (t, \mathbf{R}\mathbf{x}, \mathbf{R}\mathbf{u})$ for $\mathbf{R} \in SO(d)$.

- Scaling transforms: $(t, \mathbf{x}, \mathbf{u}) \longmapsto (\lambda^{1-h} t, \lambda \mathbf{x}, \lambda^h \mathbf{u})$ for $\lambda \in \mathbb{R}_+, h \in \mathbb{R}$.

Discrete symmetries:

- Parity: $(t, \mathbf{x}, \mathbf{u}) \longmapsto (t, -\mathbf{x}, -\mathbf{u})$.

- Time reversal: $(t, \mathbf{x}, \mathbf{u}) \longmapsto (-t, \mathbf{x}, -\mathbf{u})$.

With finite viscosity, i.e. for the Navier-Stokes equations, all these symmetries hold except for time reversal (broken by molecular diffusion) and some scaling transforms (only the $h = -1$ scaling transformation group remains).

It should be noted that, except for scale invariance, all the above symmetries of the hydrodynamic equations correspond to symmetries of the underlying microscopic equations.

Note that some of these symmetries may be broken explicitly, for instance by the domain boundaries, the forcing mechanism, or by imposing a transverse field (e.g. gravity or magnetic field) on the flow (see § **??**).

In any case, those symmetries are expected to be restored at a statistical level (i.e. for the invariant measure of the system or correlation functions), away from the mechanisms which break them (e.g. at small scales). In particular, we shall focus in the following on stationary, homogeneous and isotropic turbulence, which essentially means that ensemble averages should be invariant under time and space translations as well as rotations.

A symmetry which is not restored at a statistical level is referred to as an *anomaly*. Perhaps the most famous examples of anomalies in turbulence are the *dissipation anomaly* (time reversal invariance is not restored in the limit $\nu \to 0$, see § 5.1) or *anomalous scaling*, i.e. *intermittency* (see § 7).

2.5 *Energy budget*

E.g. Landau and Lifchitz (1971, § 16).

From the Navier-Stokes equations (2.1), it is easy to obtain the evolution equations for the kinetic energy density $u^2 = \mathbf{u}^2$:

$$\frac{1}{2}\frac{\partial u^2}{\partial t} = -u_i u_j \frac{\partial u^i}{\partial x_j} - u_i \frac{\partial p}{\partial x_i} + \nu u_i \frac{\partial}{\partial x_j}\frac{\partial}{\partial x^j} u^i + u_i f^i, \tag{2.16}$$

$$= -\partial_j[(u^2/2 + p)u^j] + \nu u_i \partial_j \partial^j u^i + u_i f^i, \tag{2.17}$$

exploiting incompressibility. The first term in Eq. (2.17) vanishes upon integration over the whole domain $\mathcal{D}$, using the Gauss theorem and the no-penetration condition. Integrating by parts, we obtain the evolution of the global energy $E = 1/2 \int_\mathcal{D} u^2$:

$$\frac{\partial E}{\partial t} = \mathcal{P}_{inj} + \nu \oint_{\partial\mathcal{D}} u_i \partial^j u^i dS_j - \nu \int_\mathcal{D} \partial_j u_i \partial^j u^i, \tag{2.18}$$

where $\mathcal{P}_{inj} = \int_\mathcal{D} \mathbf{u} \cdot \mathbf{f}$ is the energy injection rate. The surface integral again vanishes, and we have

$$\frac{\partial E}{\partial t} = \mathcal{P}_{inj} - \epsilon, \tag{2.19}$$

where $\epsilon = \nu \int_\mathcal{D} (\nabla \mathbf{u})^2 > 0$ is the energy dissipation rate.

Using the classical relation $\epsilon_{ijk}\epsilon^{ilm} = \delta^l_j \delta^m_k - \delta^m_j \delta^l_k$ and incompressibility, we can write $\partial_j u_i \partial^j u^i = \omega_i \omega^i + \partial^i (u_j \partial^j u_i)$. The surface term vanishes once more, and we obtain $\epsilon = 2\nu\Omega$, where $\Omega = \int_\mathcal{D} \omega^2/2$ is the enstrophy.

Alternatively, the energy budget can be written by replacing the velocity gradient tensor $\partial_i u_j$ with the *strain rate* $s_{ij} = (\partial_i u_j + \partial_j u_i)/2$, i.e. the symmetric part of the velocity gradient tensor. Indeed, $\partial_i u_j$ can be decomposed as usual into symmetric and antisymmetric parts, s_{ij} and $\Omega_{ij} = (\partial_i u_j - \partial_j u_i)/2$ (often called *rotation rate tensor*). A general result is that antisymmetric matrices in 3D are entirely determined by a vector: in the case of the rotation rate, this vector is just vorticity: $\Omega_{ij} = \frac{1}{2}\epsilon_{ijk}\omega^k$. It follows that

$$\epsilon = \nu \int_\mathcal{D} s_{ij} s^{ij} + \nu \int_\mathcal{D} \Omega_{ij}\Omega^{ij} = \nu \int_\mathcal{D} s_{ij} s^{ij} + \nu \int_\mathcal{D} \frac{\omega_i \omega^i}{2}. \tag{2.20}$$

Because we have seen in the previous paragraph that $\epsilon = 2\nu\Omega$, it follows that we also have $\epsilon = 2\nu \int_\mathcal{D} s_{ij} s^{ij}$.

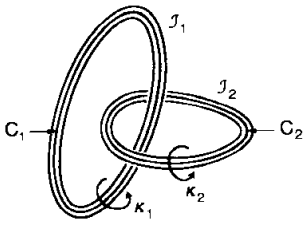

Figure 2.4: Helicity measures the knottedness of vortex lines (Moffatt and Tsinober 1992).

Conservation laws

In the absence of forcing, inviscid flows (i.e. flows with $\nu = 0$) conserve energy. This is related to the fact that the Euler equations are reversible, while the Navier-Stokes equations are dissipative. Inviscid

flows in 3D conserve another global quantity, *helicity* $H = \int_{\mathcal{D}} \mathbf{u} \cdot \boldsymbol{\omega}$, related to topological properties (see Frisch (1995, § 2.3), or Moffatt and Tsinober (1992) for more details). Roughly speaking, helicity measures parity breaking: $H \mapsto -H$ under P, so that parity invariant flows must have $H = 0$.

Inviscid 2D flows have an infinity of additional conservation laws: all the moments of the vorticity field are conserved: $\frac{d}{dt} \int_{\mathcal{D}} \omega^n = 0$ (more generally, $\frac{d}{dt} \int_{\mathcal{D}} s(\omega) = 0$). This fundamental property has far-reaching consequences (see § **??**).

Note that to derive the conservation laws, we have assumed that the velocity field was sufficiently smooth. This is a reasonable assumption for finite viscosity (the velocity field needs to be at least twice differentiable for the Navier-Stokes equations to make sense) but not necessarily for the Euler equations. In principle, singularities could break energy conservation, as observed early on by Onsager (1949).

3
Statistical Description of Homogeneous Isotropic Turbulence

Statistics and probabilities are the proper tools to characterize turbulent flows, since they are fluctuating by nature. In this section, we introduce basic objects to describe the statistical properties of turbulent flows (essentially the velocity covariance and the kinetic energy spectrum), and exploit symmetries to simplify as much as possible these objects. This approach is quite old[1]. At the end of the chapter, we show that the statistics cannot be determined directly from first principles; in future chapters we will see how they can be determined empirically and explained phenomenologically.

[1] Most of the results shown here can already be found in the book of Batchelor (1953)

3.1 Real space statistics

3.1.1 Statistical Symmetries

It is natural to assume that the symmetries of the Navier-Stokes equations, which may be broken by the forcing, are restored in a statistical sense, i.e. should be recovered at the level of moments, correlation functions, PDFs or joint PDFs. For instance, translation invariance implies that averages of the form $\langle \phi_1(\mathbf{x}_1) \cdots \phi_n(\mathbf{x}_n) \rangle = \langle \phi_1(\mathbf{x}_1 + \mathbf{x}) \cdots \phi_n(\mathbf{x}_n + \mathbf{x}) \rangle$ are homogeneous. In particular, this means that quantities observed at a given point have a space-independent average: e.g. $\langle u_i(\mathbf{x}) \rangle$ does not depend on the position $\mathbf{x}$, the only possible mean-flow in homogeneous turbulence is trivial. In the sequel, we shall assume $\langle u_i(\mathbf{x}) \rangle = 0$.

When there is no mean-flow, the typical velocity estimate, used for instance to compute the Reynolds number, is based on the *root mean square velocity*: $U_{rms} = \sqrt{\langle u_i(\mathbf{x})^2 \rangle}$. It is also the standard deviation of the turbulent velocity. By homogeneity and isotropy this does not depend on the choice of $\mathbf{x}$ or the index i (no summation here).

3.1.2 *Local energy budget in homogeneous isotropic turbulence*

The global energy budget derived in Sec. 2.5 holds locally in an homogeneous turbulent flow.

Indeed, let us now consider a random velocity field $\mathbf{u}$ solution of the Navier-Stokes equations. We introduce the ensemble average $\langle\cdot\rangle$. Assuming that the statistics are homogeneous, we have $\langle\cdot\rangle = \lim_{V\to\infty} \frac{1}{V}\int d\mathbf{r}$. Assuming in addition isotropy, we have $\langle u^2\rangle = 3U_{\rm rms}^2$, where $U_{\rm rms}^2 = \langle u_x^2\rangle = \langle u_y^2\rangle = \langle u_z^2\rangle$. To make it clear that we are using isotropy, we shall denote as $u_\parallel$ the projection of the velocity field on an arbitrary direction, and write $U_{\rm rms}^2 = \langle u_\parallel^2\rangle$.

Now, using incompressibility again, we have

$$\frac{3}{2}\frac{\partial U_{\rm rms}^2}{\partial t} = \langle u_i f^i\rangle - \nu\langle \partial_j u_i \partial^j u^i\rangle. \tag{3.1}$$

We shall denote

$$\epsilon = \nu\langle \partial_j u_i \partial^j u^i\rangle \tag{3.2}$$

the energy dissipation rate. Most often, we shall consider stationary statistics, so that ϵ also coincides with the energy injection rate.

As in section 2.5 it can be expressed using vorticity or strain rate: $\epsilon = \nu\langle\omega^2\rangle = 2\nu\langle s_{ij}s^{ij}\rangle$.

3.1.3 *Two-point statistics: velocity covariance tensor*

Batchelor (1953, § 3.4)

Let us introduce the velocity covariance:

$$U_{ij}(\mathbf{x},\mathbf{y}) = \langle u_i(\mathbf{x})u_j(\mathbf{y})\rangle. \tag{3.3}$$

Assuming homogeneity, U_{ij} is only a function of $\mathbf{r} = \mathbf{x}-\mathbf{y}$, and assuming isotropy, it can be written as (see § B.1)

$$U_{ij}(\mathbf{r}) = F(r)r_i r_j + G(r)\delta_{ij}. \tag{3.4}$$

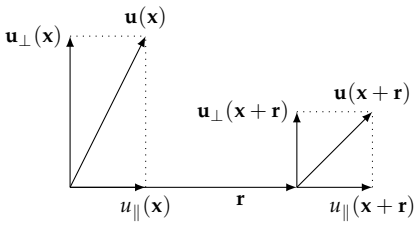

The functions F and G are directly related to the longitudinal and transverse autocorrelation functions: introducing, as above, the notations $u_\parallel = \mathbf{u}\cdot\mathbf{r}/r$ and $\mathbf{u}_\perp = \mathbf{u} - u_\parallel\mathbf{r}/r$, we have

$$f(r) = \langle u_\parallel(\mathbf{x})u_\parallel(\mathbf{x}+\mathbf{r})\rangle, \tag{3.5}$$
$$= \frac{r_i r_j}{r^2}U^{ij}(\mathbf{r}), \tag{3.6}$$
$$= F(r)r^2 + G(r), \tag{3.7}$$

f and g are even functions: $f(-r) = f(r)$, $g(-r) = g(r)$.

and

$$g(r) = \langle \mathbf{u}_\perp(\mathbf{x})\cdot\mathbf{u}_\perp(\mathbf{x}+\mathbf{r})\rangle/2, \tag{3.8}$$
$$= (U_i^i(\mathbf{r}) - f(r))/2, \tag{3.9}$$
$$= G(r). \tag{3.10}$$

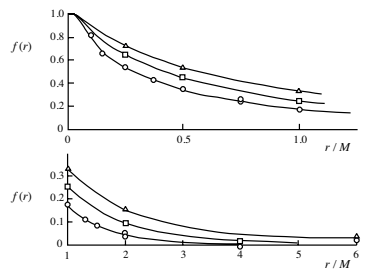

Autocorrelation function in grid turbulence, after Comte-Bellot and Corrsin (1971).

Incompressibility implies $\frac{\partial U_{ij}(\mathbf{r})}{\partial r_j} = 0$, which yields after some algebra $g(r) = f(r) + rf'(r)/2$. This shows that the longitudinal autocorrelation function determines the whole velocity covariance.

Helical flows The form of the velocity covariance tensor given by Eq. (3.4) holds if we include reflection symmetry in the definition of isotropy, rather than only rotations. If we do not enforce reflection symmetry, an additional term arises (see § B.1):

$$U_{ij}(\mathbf{r}) = F(r)r_i r_j + G(r)\delta_{ij} + H(r)\epsilon_{ijk}\mathbf{r}^k. \tag{3.11}$$

Lesieur (2008, § 5.9.6); be careful, our definition of helicity differs by a factor 2.

The coefficient $H(r)$ contains information about the helical character of the flow. For instance, it can be easily shown that $H(0) = -H/6$, where $H = \langle \mathbf{u} \cdot \boldsymbol{\omega} \rangle$ is the mean helicity:

$$\begin{aligned} H &= \langle \epsilon_{ijk} u^i \partial^j u^k \rangle, && (3.12)\\ &= \lim_{r\to 0} \epsilon_{ijk} \frac{\partial}{\partial r_j} U^{ik}(\mathbf{r}), && (3.13)\\ &= \lim_{r\to 0} \epsilon_{ijk}\epsilon^{ikl} \frac{\partial}{\partial r_j} H(r) r_l, && (3.14)\\ &= \lim_{r\to 0} -2\delta^l_j [\delta^j_l H(r) + \frac{r^j r_l}{r} H'(r)], && (3.15)\\ &= -6H(0). && (3.16) \end{aligned}$$

3.1.4 *Integral scale*

The *integral scale* is the length scale associated with the largest eddies in the flow, or in other words, the energy containing scale. It could be approximated very roughly as the size of the domain (in a finite domain).

A more precise definition is the autocorrelation scale of velocity:

$$L_0 = \int_0^{+\infty} \frac{\langle u_\parallel(\mathbf{x}) u_\parallel(\mathbf{x}+\mathbf{r}) \rangle}{U_{rms}^2} dr, \tag{3.17}$$

Technically, this is the *longitudinal* integral scale; using the notations from § 3.1.3, we have $L_0 = \int_0^\infty f(r)dr/f(0)$. Note that some references (e.g. Pope 2000, p. 197) factor out the RMS energy $U_{rms}^2 = f(0) = g(0)$ out of f and g in the velocity autocorrelation tensor; in this case the integral scale is simply the integral of the longitudinal velocity autocorrelation function f. One could define similarly a *transverse integral scale* $L_0^\perp = \int_0^\infty g(r)dr/g(0)$. In isotropic turbulence, the two are directly related: the relation between f and g established in § 3.1.3 yields $L_0^\perp = L_0/2$.

where we have used the shorthand $u_\parallel(\mathbf{x}) = \mathbf{u}(\mathbf{x}) \cdot \mathbf{r}/r$. By isotropy, this does not depend on the direction of the $\mathbf{r}$ vector.

In decaying turbulence, the integral scale is typically used to estimate the Reynolds number and the energy injection rate: $Re = U_{rms}L_0/\nu$, $\epsilon = U_{rms}^3/L_0$. In the presence of a forcing acting at a definite scale (e.g. in many Direct Numerical Simulation (DNS) studies), the forcing scale is often preferred.

3.1.5 *Taylor scale*

Taylor (1935)

We are interested in the universal properties of velocity fluctuations, which should be independent of the forcing mechanism or

the boundaries. It would be useful to construct a Reynolds number independent of the large scales properties (like, for instance, the integral scale, which is difficult to estimate precisely in practice). Another way to define a characteristic length scale is to combine the rms velocity and the velocity gradients: let us define the *Taylor microscale* λ such that

$$\frac{U_{rms}^2}{\lambda^2} = \left\langle \left(\frac{\partial u_i}{\partial x_i}(\mathbf{x}) \right)^2 \right\rangle, \tag{3.18}$$

again independently of the index i by isotropy (no summation is implied).

The Taylor scale is related to the longitudinal autocorrelation function: it can be easily shown that $\langle (\partial_\parallel u_\parallel)^2 \rangle = -f''(0)$, from which it follows that $\lambda^2 = -f(0)/f''(0)$.

Based on that definition, we can introduce the Reynolds number at the Taylor microscale:

$$R_\lambda = \frac{U_{rms}\lambda}{\nu}. \tag{3.19}$$

Taylor initially thought that λ was the scale of the smallest eddies dissipating energy. This incorrectly assumes that the velocity at the Taylor scale is U_{rms}, i.e. that $R_\lambda = Re(\lambda) = 1$. In fact, the scale which plays that role is the Kolmogorov scale.

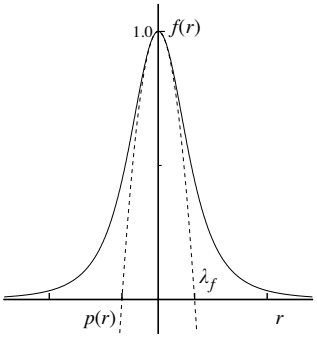

The parabola osculating the autocorrelation function f intersects the axis at $r = \lambda_f = \sqrt{2}\lambda$.

3.1.6 *Energy dissipation rate as a function of the longitudinal velocity gradient*

Computing the energy dissipation rate using Eq. (3.2) requires the knowledge of all the components of the velocity gradient tensor. Even with the progress of velocimetry techniques (see lecture by Mickael Bourgoin), this is difficult to achieve in laboratory experiments. A classical technique is hot-wire measurements, which gives access only to longitudinal velocity gradients (under the Taylor hypothesis, see § A). But exploiting statistical homogeneity and isotropy, it should be possible to express the mean energy dissipation rate as a function of the longitudinal velocity gradient only. Let us do so by relying on the results of Sec. 3.1.3.

The energy dissipation rate is given by

$$\begin{aligned}
\epsilon &= \nu \langle \partial_j u_i \partial^j u^i \rangle, && (3.20)\\
&= -\nu \Delta_{\mathbf{r}} U_i^i(\mathbf{r})|_{\mathbf{r}=0}, && (3.21)\\
&= -\nu [8f'(r)/r + 7f''(r) + rf'''(r)]_{r=0}, && (3.22)\\
&= -15\nu f''(0), && (3.23)\\
&= 15\nu \langle (\partial_\parallel u_\parallel)^2 \rangle. && (3.24)
\end{aligned}$$

where we have used the expression of the Laplacian in spherical coordinates $\Delta = r^{-2}\partial_r r^2 \partial_r$ and the fact that f is an even function.

The energy dissipation rate can be expressed conveniently in terms of the Taylor microscale: $\epsilon = 15\nu U_{rms}^2/\lambda^2$ (Taylor 1935).

3.1.7 *Second-order structure functions*

Above we have considered the velocity covariance tensor; another statistical quantity of interest is the second-order structure function: $D_{ij}(\mathbf{r}) = \langle [u_i(\mathbf{x}+\mathbf{r}) - u_i(\mathbf{x})][u_j(\mathbf{x}+\mathbf{r}) - u_j(\mathbf{x})]\rangle$. Like in Sec. 3.1.3, this tensor can be decomposed as follows:

$$D_{ij}(\mathbf{r}) = D_\perp(r)\delta_{ij} + [D_\parallel(r) - D_\perp(r)]\frac{r_i r_j}{r^2}. \tag{3.25}$$

Choosing the coordinate system such that $\mathbf{r}$ is one of the base vectors (e.g. $\mathbf{r} = \mathbf{e}_1$), we see that $D_\parallel(r) = S_2(r) = \langle(\delta_\parallel u)^2\rangle$ is the usual longitudinal structure function (from $i = j = 1$) and $D_\perp(r) = \langle(\delta\mathbf{u}_\perp)^2\rangle/2$ the transverse structure function (form $i = j = 2$ or 3).

Again, the second-order structure function is entirely determined by the longitudinal velocity autocorrelation function: we first express the structure function in terms of the velocity covariance tensor:

$$D_{ij}(\mathbf{r}) = \langle [u_i(\mathbf{x}+\mathbf{r}) - u_i(\mathbf{x})][u_j(\mathbf{x}+\mathbf{r}) - u_j(\mathbf{x})]\rangle, \tag{3.26}$$
$$= 2U_{ij}(0) - U_{ij}(\mathbf{r}) - U_{ji}(\mathbf{r}), \tag{3.27}$$

which, using $U_{ij}(0) = g(0)\delta_{ij} = f(0)\delta_{ij}$ and assuming reflection symmetry, yields

$$= 2g(0)\delta_{ij} - 2U_{ij}(\mathbf{r}), \tag{3.28}$$
$$= 2[g(0) - g(r)]\delta_{ij} - 2[f(r) - g(r)]\frac{r_i r_j}{r^2}. \tag{3.29}$$

By identification, we find:

$$D_\parallel(r) = S_2(r) = 2[f(0) - f(r)], \quad D_\perp(r) = 2[g(0) - g(r)]. \tag{3.30}$$

From the relation between f and g (due to incompressibility), we deduce a relation between $D_\parallel$ and $D_\perp$:

$$D_\perp(r) = D_\parallel(r) + \frac{rD'_\parallel(r)}{2}. \tag{3.31}$$

3.2 *Spectral description of homogeneous turbulence*

3.2.1 *Navier-Stokes equations in Fourier space*

See for instance Lesieur (2008, chap. 5).

Let us first introduce the Fourier transform operator $\mathcal{F}$:

$$\mathcal{F} : \phi \longmapsto \hat{\phi} \text{ such that } \hat{\phi}(\mathbf{k}) = \frac{1}{(2\pi)^3}\int d\mathbf{x}\phi(\mathbf{x})e^{-i\mathbf{k}\cdot\mathbf{x}}, \tag{3.32}$$

and the inverse Fourier transform:

$$\mathcal{F}^{-1} : \hat{\phi} \longmapsto \phi \text{ such that } \phi(\mathbf{x}) = \int d\mathbf{k} \hat{\phi}(\mathbf{k}) e^{i\mathbf{k}\cdot\mathbf{x}}. \tag{3.33}$$

In particular, the Fourier transform of the velocity fields writes $\hat{u}_i(\mathbf{k}) = \mathcal{F}[u_i](\mathbf{k})$. Note that for the velocity field to be real-valued, the hermitian condition $\hat{u}_i(-\mathbf{k}) = \hat{u}_i(\mathbf{k})^*$ should hold. From a computational point of view, it means that we only need to solve the equations on half the Fourier space.

As usual with Fourier transforms, alternative normalizations may be chosen.

Taking the Fourier transform of the Navier-Stokes equations (2.3), we obtain

$$\begin{aligned} \partial_t \hat{u}_i(\mathbf{k}) + \widehat{u_j \partial^j u_i}(\mathbf{k}) &= -ik_i \hat{p}(\mathbf{k}) - \nu k^2 \hat{u}_i(\mathbf{k}), \\ k^i \hat{u}_i(\mathbf{k}) &= 0. \end{aligned}$$

It should be noted that incompressibility in Fourier space corresponds to the fact that each Fourier coefficient is orthogonal to the wave vector. Before treating the non-linear term, let us note that the Fourier transform of pressure can be obtained readily using equation (2.5): $k^2 \hat{p}(\mathbf{k}) = ik^j \widehat{u_l \partial^l u_j}(\mathbf{k})$, so that the Navier-Stokes equations in Fourier space now read:

$$(\partial_t + \nu k^2)\hat{u}_i(\mathbf{k}) = -P_{ij}(\mathbf{k}) \widehat{u_l \partial^l u^j}(\mathbf{k}), \tag{3.34}$$

with $P_{ij}(\mathbf{k}) = \delta_{ij} - k_i k_j / k^2$. Now, using incompressibility, $\widehat{u_l \partial^l u_j}(\mathbf{k}) = ik^l \widehat{u_l u_j}(\mathbf{k})$, and because the tensor $\widehat{u_l u_j}$ is symmetric, we can also symmetrize $k^l P_{ij}(\mathbf{k})$: let $\mathcal{P}_{ijl}(\mathbf{k}) = k_j P_{il}(\mathbf{k}) + k_l P_{ij}(\mathbf{k})$, and because the Fourier transform of a product is a convolution, we can finally write the closed Navier-Stokes equations in Fourier space:

$$(\partial_t + \nu k^2)\hat{u}_i(\mathbf{k}) = -\frac{i}{2} \mathcal{P}_i^{\ jl}(\mathbf{k}) \int d\mathbf{p} d\mathbf{q} \delta(\mathbf{p} + \mathbf{q} - \mathbf{k}) \hat{u}_j(\mathbf{p}) \hat{u}_l(\mathbf{q}). \tag{3.35}$$

This equation involves the interaction of three modes with wavevectors satisfying $\mathbf{k} = \mathbf{p} + \mathbf{q}$, referred to as a *triad*.

$P_{ij}(\mathbf{k})$ is actually the Fourier transform of the operator $\mathcal{P} : \mathbf{u} \longmapsto \mathbf{u} - \nabla\Delta^{-1}\nabla \cdot \mathbf{u}$: $\widehat{(\mathcal{P}\mathbf{u})}_i(\mathbf{k}) = P_{ij}(\mathbf{k})\hat{u}^j(\mathbf{k})$. As can be checked explicitly, $\mathcal{P}$ is a projector ($\mathcal{P}^2 = \mathcal{P}$, or $P_{ij}(\mathbf{k})P_l^j(\mathbf{k}) = P_{il}(\mathbf{k})$) on the space of divergence-free velocity fields ($\nabla \cdot \mathcal{P}\mathbf{u} = 0$, or $k^i P_{ij}(\mathbf{k}) = 0$).

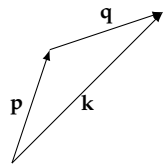

Figure 3.1: An example of a triadic interaction.

3.2.2 *Scale-by-scale energy budget*

As an aside, let us note that writing the Navier-Stokes equations in Fourier space allows us to derive easily a scale-by-scale energy budget: from the Parseval-Plancherel theorem, energy, enstrophy and helicity now read

$$E = \frac{1}{2} \int d\mathbf{k} \hat{u}^j(\mathbf{k}) \hat{u}_j(\mathbf{k})^*, \tag{3.36}$$

$$\Omega = \frac{1}{2} \int d\mathbf{k} \hat{\omega}^j(\mathbf{k}) \hat{\omega}_j(\mathbf{k})^* = \frac{1}{2} \int d\mathbf{k} k^2 \hat{u}^j(\mathbf{k}) \hat{u}_j(\mathbf{k})^*, \tag{3.37}$$

$$H = \frac{1}{2} \int d\mathbf{k} \hat{\omega}^j(\mathbf{k}) \hat{u}_j(\mathbf{k})^* = \frac{i}{2} \epsilon_{jlm} \int d\mathbf{k} k^j \hat{u}^l(\mathbf{k}) \hat{u}^m(\mathbf{k})^*, \tag{3.38}$$

where ϵ is the standard, rank 3, totally antisymmetric, Levi-Civita tensor. Let us now define the *cumulative energy spectrum* $E_<(k)$ (resp. enstrophy spectrum $\Omega_<(k)$) by restricting the integration above to the ball of radius k: $\|\mathbf{k}\| \leq k$, and the *energy spectrum* $E(k) = dE_<(k)/dk$. $E_<(k)$ measures the kinetic energy at wave numbers smaller than k, i.e. scales larger than $1/k$. One could define similarly the enstrophy spectrum $\Omega(k) = d\Omega_<(k)/dk$; as is easily checked, $\Omega(k) = k^2 E(k)$. From equation (3.35), ading a forcing term f, it is straightforward to obtain the scale-by-scale energy budget:

$$\partial_t E_<(k) = -\Pi(k) - 2\nu\Omega_<(k) + F_<(k), \tag{3.39}$$

and

$$(\partial_t + 2\nu k^2)E(k) = -\partial_k \Pi(k) + F(k), \tag{3.40}$$

with

$$\Pi(k) = \frac{i}{2}\int_{\|\mathbf{k}\|\leq k} d\mathbf{k}\mathcal{P}^{ijl}(\mathbf{k})\hat{u}_i(\mathbf{k})^* \int d\mathbf{p}d\mathbf{q}\delta(\mathbf{p}+\mathbf{q}-\mathbf{k})\hat{u}_j(\mathbf{p})\hat{u}_l(\mathbf{q}). \tag{3.41}$$

There are three contributions to the scale-by-scale energy budget: energy injection by the forcing, viscous dissipation, and inertial transfer. When $\Pi(k) > 0$, the energy is transferred, by the nonlinear term, on average from wave numbers smaller than k (i.e. scales larger than $1/k$) to wave numbers larger than k (i.e. scales smaller than $1/k$). This is called a *direct energy transfer*. When $\Pi(k) < 0$, the converse is true. This is called an *inverse energy transfer*.

Note that by definition, $\Pi(0) = 0$, but we also have $\lim_{k\to+\infty}\Pi(k) = 0$ i.e. $\int_0^{+\infty}\partial_k\Pi(k)dk = 0$: the nonlinear term only acts to redistribute energy across scales, but does not have any net effect on the global budget, as seen above (§ 2.5).

3.2.3 *Autocovariance in Fourier space: energy and helicity spectra*

We introduce the Fourier transform of the velocity field:

$$\hat{u}_i(\mathbf{k}) = \frac{1}{(2\pi)^3}\int d\mathbf{x}u_i(\mathbf{x})e^{-i\mathbf{k}\cdot\mathbf{x}}., \tag{3.42}$$

and we consider the covariance tensor for the Fourier coefficients:

$$\langle\hat{u}_i(\mathbf{k})\hat{u}_j(\mathbf{p})\rangle = \frac{1}{(2\pi)^6}\int\langle u_i(\mathbf{x})u_j(\mathbf{y})\rangle e^{-i\mathbf{k}\cdot\mathbf{x}-i\mathbf{p}\cdot\mathbf{y}}d\mathbf{x}d\mathbf{y}, \tag{3.43}$$

$$= \frac{1}{(2\pi)^6}\int d\mathbf{r}U_{ij}(\mathbf{r})e^{-i\mathbf{p}\cdot\mathbf{r}}\int d\mathbf{x}e^{-i(\mathbf{k}+\mathbf{p})\cdot\mathbf{x}}, \tag{3.44}$$

which, using $\int d\mathbf{x}e^{-i\mathbf{k}\cdot\mathbf{x}} = (2\pi)^3\delta(\mathbf{k})$, yields

$$= \delta(\mathbf{k}+\mathbf{p})\hat{U}_{ij}(\mathbf{p}). \tag{3.45}$$

The Dirac delta is the signature of homogeneity: translations in real space corresponds to multiplication by a phase factor in Fourier space. The average of products of Fourier coefficients should be invariant under such transforms, i.e. the phase factors should cancel out. In general, this means that a product of the form $\langle \hat{u}_{i_1}(\mathbf{k}_1) \cdots \hat{u}_{i_n}(\mathbf{k}_n) \rangle$ will vanish unless $\mathbf{k}_1 + \cdots + \mathbf{k}_n = 0$.

Like in the above, the tensor $\hat{U}_{ij}(\mathbf{k})$ can be decomposed in the following manner (we treat directly the general case of a flow with nonzero mean helicity, i.e. without enforcing reflection symmetry):

$$\hat{U}_{ij}(\mathbf{k}) = A(k)\delta_{ij} + B(k)k_i k_j + C(k)\epsilon_{ijl}k^l. \tag{3.46}$$

The incompressibility condition in Fourier space reads $k^i \hat{u}_i(\mathbf{k}) = 0$; taking the scalar product with the velocity covariance in Fourier space yields $k^i \hat{U}_{ij}(\mathbf{k}) = 0 = A(k)k_j + B(k)k^2 k_j$, from which we obtain

$$\hat{U}_{ij}(\mathbf{k}) = A(k)P_{ij}(\mathbf{k}) + C(k)\epsilon_{ijl}k^l, \tag{3.47}$$

with $P_{ij}(\mathbf{k}) = \delta_{ij} - \frac{k_i k_j}{k^2}$. The mean kinetic energy per unit mass is $E = U_i^i(0)/2 = \int A(k)d\mathbf{k} = \int_0^{+\infty} 4\pi k^2 A(k)dk$. In other words, the trace part of the tensor, $A(k)$, is related to $E(k)$ the kinetic energy density in Fourier space integrated over a sphere of radius k, often simply called "the energy spectrum" and defined such that $E = \int_0^{+\infty} E(k)dk$, by the relation $E(k) = 4\pi k^2 A(k)$.

The traceless part, on the other hand, is related to the mean helicity (per unit mass):

$$H = \langle \mathbf{u} \cdot \boldsymbol{\omega} \rangle = \lim_{r \to 0} \epsilon_{ijl} \frac{\partial}{\partial r_j} U^{il}(\mathbf{r}), \tag{3.48}$$

$$= i\epsilon_{ijl} \int k^j \hat{U}^{il}(\mathbf{k})d\mathbf{k}, \tag{3.49}$$

$$= -2i\delta_j^m \int k^j k_m C(k)d\mathbf{k}, \tag{3.50}$$

$$= -2i \int_0^{+\infty} 4\pi k^4 C(k)dk, \tag{3.51}$$

so that $H(k) = -8\pi i k^4 C(k)$. Finally, the velocity covariance tensor in Fourier space reads:

$$\hat{U}_{ij}(\mathbf{k}) = \frac{E(k)}{4\pi k^2} P_{ij}(\mathbf{k}) + i\frac{H(k)}{8\pi k^4} \epsilon_{ijl} k^l. \tag{3.52}$$

We note that in general, $\hat{U}_{ij}(\mathbf{k})$ is a Hermitian tensor: $\hat{U}_{ji}(\mathbf{k}) = \hat{U}_{ij}(\mathbf{k})^*$; it is symmetric only if there is no mean helicity (in that, case, it takes real values).

3.3 *Turbulence, an out-of-equilibrium phenomenon: failure of equilibrium statistical mechanics*

Because inviscid flows form a Hamiltonian system, a very natural question to ask is how well does equilibrium statistical mechanics describe the statistics of turbulent velocity fields? The idea is simply to introduce a measure on phase space which is proportional to the Lebesgue measure, and whose density depends only on conserved quantities (e.g. the microcanonical measure which is uniform on surfaces of constant energy) or their associated Lagrange multiplier (e.g. the canonical measure).

Let us first note that unlike the systems considered in undergraduate statistical physics courses, we are dealing here with classical fields, i.e. an infinite dimensional phase space. This implies considerable technical difficulties. Let us therefore consider a finite-dimensional approximation of the system: a typical approach is Galerkin truncation, which retains only a finite number of Fourier modes (hoping that we can take the limit of an infinite number of modes later). It has been shown in this context (Lee 1952) that the Lebesgue measure is invariant under the Hamiltonian flow, i.e. the Liouville theorem holds, and the classical equilibrium measure are indeed invariant measures. As noted early on by Lee (1952), the canonical measure corresponds to energy equipartition, which leads to an energy spectrum of the form $E(k) \propto k^2$: the energy concentrates in the small scales. If we let the cutoff wave-number tend to infinity, we obtain an infinite energy. This ultraviolet catastrophe, typical of classical fields, is known as the Rayleigh-Jeans paradox (Pomeau 1995).

$$
\begin{aligned}
u_j(\mathbf{x}) &= \sum_{\mathbf{k}} \hat{u}_j(\mathbf{k}) e^{i\mathbf{k}\cdot\mathbf{x}}, \\
E &= \frac{1}{2}\int u^2 = \frac{1}{2}\sum_{\mathbf{k}} \hat{u}_j(\mathbf{k})\hat{u}^j(\mathbf{k})*, \\
p(\{\hat{u}_j(\mathbf{k})\}_{\mathbf{k}}) &= \frac{1}{\mathcal{Z}} e^{-\beta E}, \\
\mathcal{Z} &= \prod_{\mathbf{k}} \frac{2\pi}{\beta}, \\
\langle E \rangle &= -\frac{\partial \ln \mathcal{Z}}{\partial \beta}, \\
&= \sum_{\mathbf{k}} \frac{1}{\beta}, \\
E &= \int E(k) dk, \\
\langle E(k) \rangle &= \frac{4\pi k^2}{\beta}.
\end{aligned}
$$

Taking helicity into account does not change fundamentally the conclusions (Kraichnan 1973), unless specific constraints are enforced (Herbert 2014).

2D flows, on the other hand, because of their different conservation laws (§ 2.5), can be described to some extent using equilibrium statistical mechanics methods (see § **??** or Eyink and Sreenivasan (2006), Bouchet and Venaille (2012), and Herbert (2015) for reviews).

3.4 *Turbulence, a non-linear phenomenon: The closure problem*

We have just seen that turbulence is an out-of-equilibrium statistical physics problem. As a consequence, the dynamics cannot be dismissed[2]. Let us go back to the Navier-Stokes equations and try to deduce the statistical properties of the velocity field from there.

[2] An interesting read in this respect is Ruelle (2004).

Let us assume that the statistics are homogeneous and introduce the Fourier transform of the velocity covariance $\hat{U}_{ij}(\mathbf{k})$. Using the

Navier-Stokes equations in Fourier space (3.35), we easily obtain the equation governing the dynamics of $\hat{U}_{ij}$:

$$(\partial_t + 2\nu k^2)\hat{U}_{ij}(\mathbf{k}) = -\frac{i}{2}\mathcal{P}_i^{\ lm}(\mathbf{k})\int d\mathbf{p} T_{jlm}(-\mathbf{k},\mathbf{p}) - \frac{i}{2}\mathcal{P}_j^{\ lm}(-\mathbf{k})\int d\mathbf{p} T_{ilm}(\mathbf{k},\mathbf{p}) \tag{3.53}$$

with $T_{ijk}(\mathbf{k},\mathbf{p}) = (2\pi)^{-6}\int d\mathbf{r}d\mathbf{r}'\langle u_i(\mathbf{x})u_j(\mathbf{x}+\mathbf{r})u_k(\mathbf{x}+\mathbf{r}')\rangle e^{-i\mathbf{k}\cdot\mathbf{r}-i\mathbf{p}\cdot\mathbf{r}'}$. In other words, the equations governing the evolution of the second order statistics depend on the third order statistics. If we were to write the equations for the third-order tensor T_{ijk}, it would involve the fourth-order statistics, and so on. This is the problem of closure of the hierarchy of momentum for the Navier-Stokes equations. Many strategies have been developed to close this hierarchy, but they all contain some degree of arbitrariness (see § 9 or Orszag (1970) for more details).

The idea may be conveyed simply by denoting in a symbolic manner the Navier-Stokes equations as $Lu = uu$, where L is a linear operator, so that:

$$L_1\langle u\rangle = \langle uu\rangle$$
$$L_2\langle uu\rangle = \langle uuu\rangle$$
$$L_3\langle uuu\rangle = \langle uuuu\rangle$$
$$\dots$$

In general the linear operators on the left hand side are not all the same; they do in the inviscid case where they boil down to the time derivative.

4
Simulation and Modelling

Building a statistical theory of turbulence from the ground up (i.e. starting from the Navier-Stokes equations) is a very difficult task, as we have just seen. We will therefore need to rely on some empirical understanding of turbulence. This can be achieved essentially by two means: laboratory experiments and numerical simulations. In this chapter, I explain the basic principles of direct numerical simulations, before touching briefly upon turbulence modeling techniques (§ 4.2), used in practical applications.

4.1 Direct Numerical Simulations

A reference for this section is Pope (2000, chap. 9).

Please note that the goal of this section is not to teach you how to run numerical simulations of turbulent flows in practice, but rather to address the fundamental question: "Can turbulence be solved by brute-force? Is it a computational problem or a physics problem?".

Arguably the most natural approach to numerical simulation of turbulent flows is to solve directly the Navier-Stokes equations. As we shall see, this requires to resolve the entire range of nonlinearly-coupled scales. For a long time, this requirement led to prohibitive numerical costs, and Direct Numerical Simulation (DNS) remained out-of-reach (in other words, DNS were restricted to very low Reynolds numbers). Technological progress (powerful computers, Fast Fourier Transform algorithm[1], and later, massive parallelization) brought DNS into the realm of possibilities. Here, I shall describe briefly the principle of *pseudospectral methods* (§ 3.2.1), which are the most efficient numerical methods for DNS of the Navier-Stokes equations. Notwithstanding, these methods still fall short of industry requirements, which still recourse to turbulence modelling (briefly touched upon in § 4.2). Besides, practical applications often impose domain geometries incompatible with pseudospectral methods: for the sake of brevity, we leave aside here all other types of discretizations (finite differences, finite elements, Lattice-Boltzmann methods,...)[2].

[1] Cooley and Tukey (1965). The basic idea of the algorithm was in fact known to Gauss.

[2] See e.g. Hinch (2020) and Durran (2010).

4.1.1 *Pseudospectral methods*

The principle For simplicity, let us assume that we are considering a cubic domain of linear length L with periodic boundary conditions in all directions[3] (i.e. a domain with the topology of a flat torus $\mathbb{R}^3/(L\mathbb{Z}^3)$), so that the set of wave vectors (pedantically the *Pontryagin dual* of the torus) is simply $2\pi/L\mathbb{Z}^3$. Then, all the integrals above become discrete sums.

[3] See Boyd (2001) for a more general presentation.

In practical computations, the equations must of course be discretized to be solved by a computer: let us introduce a truncation in spectral space and retain only N wave vectors in each direction.

A pure spectral method would compute explicitly the convolution product in (3.35). However, because Fast Fourier Transforms are relatively cheap, it is much more efficient to compute the non-linear term in real space, and then its Fourier transform. In other words, pseudospectral methods (Orszag and Patterson 1972; Rogallo 1981) actually solve the equation:

$$(\partial_t + \nu k^2)\hat{u}_i(\mathbf{k}) = -\frac{i}{2}\mathcal{P}_i^{\ jl}(\mathbf{k})\mathcal{F}[\mathcal{F}^{-1}[\hat{u}_j]\mathcal{F}^{-1}[\hat{u}_l]](\mathbf{k}). \tag{4.1}$$

Note that different implementations may actually compute differently the nonlinear term (depending on at which point they compute the derivative). The important point is that derivatives are computed in Fourier space and products in real space.

As an illustration, assuming there is no better way of evaluating the convolution product than the naive one, the number of operations required at each time step is $O(N^6)$. By contrast, the complexity of the Fast Fourier Transform algorithm is $O(N^3 \ln N)$.

Some more details The discretization introduced above is equivalent to considering a regular grid on the torus with N grid points in each direction. The grid points are described by vectors $\mathbf{x} = n_x L/N\mathbf{e}_x + n_y L/N\mathbf{e}_y + n_z L/N\mathbf{e}_z$ (you can think of it as a *Bravais lattice* if you wish), with integer coefficients $0 \leq n_x, n_y, n_z < N$. Equivalently, the wave vectors are $\mathbf{k} = k_x 2\pi/L\mathbf{e}_x + k_y 2\pi/L\mathbf{e}_y + k_z 2\pi/L\mathbf{e}_z$. Instead of the Fourier transform $\mathcal{F}$ we use the *Discrete Fourier Transform:*

$$\hat{u}_i(\mathbf{k}) = \sum_{\mathbf{x}} u_i(\mathbf{x}) e^{-i\mathbf{x}\cdot\mathbf{k}}, \tag{4.2}$$

i.e.

$$\hat{u}_i(k_x, k_y, k_z) = \sum_{n_x=0}^{N-1}\sum_{n_y=0}^{N-1}\sum_{n_z=0}^{N-1} u_i(n_x, n_y, n_z) e^{-\frac{2i\pi}{N}\left(n_x k_x + n_y k_y + n_z k_z\right)}. \tag{4.3}$$

It is clear that the Discrete Fourier Transform is N-periodic in each index. In other words, the set of wave vectors described above can be

translated by any vector with coordinates multiple of $2\pi/L$ in any direction. This means that the first half of the Fourier coefficients correspond to positive wave numbers and the second half to negative wave numbers. The largest wave number represented in each direction is $k_{\max} = N/2 \times 2\pi/L = N\pi/L$.

In principle, $\hat{u}_i(k_x, k_y, k_z)$ should be an array of N^3 complex numbers. This would occupy twice as much memory as in real space. Indeed, because of the Hermitian symmetry ($\hat{u}_i(N - k_x, N - k_y, N - k_z) = \hat{u}_i(k_x, k_y, k_z)^*$), one may choose arbitrarily a dimension (say the z dimension) and store only half the Fourier coefficients in this direction (i.e. $0 \leq k_z \leq N/2$). This is still more than would be strictly necessary.

The resolution is strongly linked to the choice of viscosity. The basic idea is that the smallest resolved scales must be smaller than the scales at which dissipation occurs. This can be achieved by using the Kolmogorov phenomenology (see § 6) and enforcing $k_{\max}\eta \geq 1$ (actually, for the small scales to be well-resolved, it should be slightly larger), i.e. $\nu \geq \epsilon^{1/3} k_{\max}^{-4/3}$. ϵ is unknown in principle, but in practice we can more or less control its value. Clearly, higher resolutions give access to smaller viscosities, i.e. higher Reynolds numbers. Indeed, the above inequality gives an estimate of the resolution required to reach a given Reynolds number: $N \sim Re^{3/4}$.

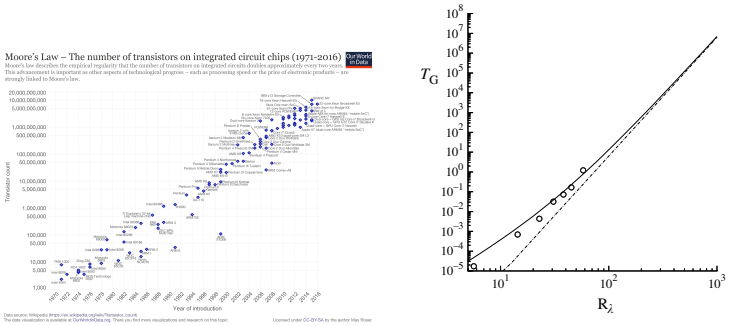

Figure 4.1: Moore's law (left) and time in days required to perform DNS on a gigaflop computer (typical commercial computer of the 2000s) as a function of the Reynolds number (Pope 2000, Fig. 9.3).

The time-step also depends on the resolution through the Courant-Friedrichs-Lewy (CFL) condition: in physical terms, the time-step should be smaller than the smallest eddy turnover time $\ell/U \sim 1/(Uk_{\max})$, with $U \sim 1$, and the viscous time $1/(\nu k_{\max}^2)$. In practice, Courant numbers much smaller than unity are used: $U_{\rm rms} dt/dx \approx 0.05$. Hence, one should halve the time-step when doubling the resolution. This means that the computational cost[4] for doubling the Reynolds number increases roughly by a factor 8.

To give ideas of state-of-the-art resolutions, record-breaking[5] DNS were for instance 4096^3, $R_\lambda = 1200$ (Kaneda et al. 2003) or 8192^3, $R_\lambda = 1300$ (Yeung, Zhai, and Sreenivasan 2015).

[4] For a total integration time T, the number of time steps increases linearly with resolution N — it can be expressed as NT_0/N_0 for a reference resolution N_0 — so, assuming the computational cost of one time step is dominated by the FFT, the total computational cost is $C = N(T_0/N_0)N^3 \ln N = O(N^4 \ln N) = O(Re^3 \ln Re)$.

[5] In 2019 a new record was set at $N = 12288$.

The time elapsed between the two simulations slightly underperforms a crude estimate based on a naive interpretation of Moore's law, according to which resolution should double every 6 years (Fig. 4.1). This is essentially due to the fact that the later run better resolved the small-scales. Note that simulations of this kind (say $N = 10000$), using double precision (64-bit floating point numbers, i.e. 8 bytes), require about 8TB of memory to store each component of the velocity field at each time.

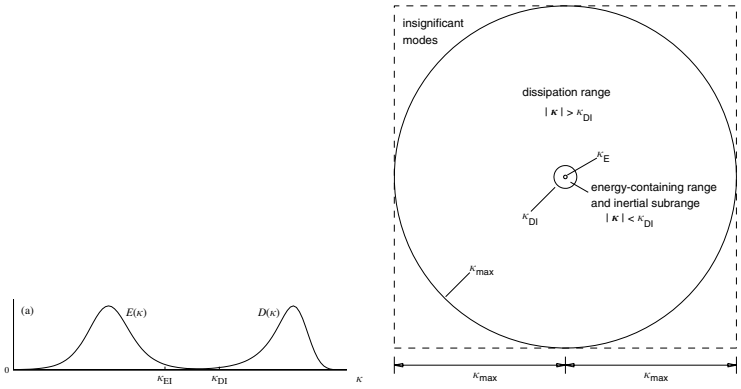

Figure 4.2: Left: sketch of the energy and dissipation spectra. Right: Solution domain in wavenumber space for a pseudo-spectral DNS of homogeneous isotropic turbulence (Pope 2000, Figs. 6.28 & 9.4).

It should be noted that much of the computational effort is actually dedicated to resolving the dissipation range (Fig. 4.2): typically this represents more than 99% of the modes.

Aliasing errors The multiplication required to compute the non-linear term of the Navier-Stokes equations introduces modes with wave number larger than $k_{\max}$ (Fig. 4.3).

Because of the discretizations, we cannot distinguish between wave numbers k and $k + 2\mathbb{Z}k_{\max}$. The Fourier mode k computed by the Discrete Fourier Transform is therefore the sum of all the Fourier coefficients with wave numbers differing from k by an integer multiple of $2k_{\max}$ (this is well explained in Pope (2000, Appendix F)). This phenomenon is known as *aliasing*.

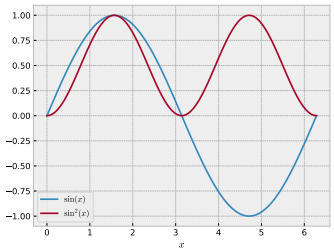

Figure 4.3: The deceptively simple principle of the *aliasing* phenomenon: $\sin(x)^2 = (1 - \cos(2x))/2$.

A simple strategy to remove aliasing errors is to use a larger domain. For instance, for actually resolving wave numbers up to $k_{\max}$, we may represent wave numbers up to $2k_{\max}$ (i.e. double the resolution) and enforce $\hat{u}_i(\mathbf{k}) = 0$ for $k_{\max} < k \leq 2k_{\max}$. This implies an eightfold increase of the computational cost. Because this additional computational burden is unaffordable, more efficient dealiasing techniques have been developed (e.g. Patterson and Orszag 1971).

Hyperviscosity A cheap way to reduce the size of the dissipative range (and therefore increase the inertial range) is to replace the

Laplacian Δ in the Navier-Stokes equations by some power of it: $-(-\Delta)^p$. In Fourier space, it amount to replacing the $\nu k^2 \hat{u}_i(\mathbf{k})$ term by $\nu_H k^{2p} \hat{u}_i(\mathbf{k})$. For $p = 1$, we have regular dissipation; otherwise, we call this rudimentary turbulence model *hyperviscosity* (Borue and Orszag 1995).

4.2 *Turbulence modelling*

The philosophy of DNS is to resolve explicitly all the relevant scales. An alternative is to model the unresolved scales. This requires to define properly the dynamical fields at different scales: this is what we do in § 4.2.1.

4.2.1 *Filtered velocity field*

Let us introduce a filtering function $G(\mathbf{x})$, typically with compact support or with a fast decay (Fig. 4.4).

We assume that G is normalized: $\int d\mathbf{x} G(\mathbf{x}) = 1$ and isotropic: $G(\mathbf{x}) = G(\|\mathbf{x}\|)$, with a slight abuse of notation.

Now let us define the dilatation $G_\ell(x) = G(x/\ell)/\ell^3$, and the filtered velocity field (a convolution with the kernel G_ℓ)

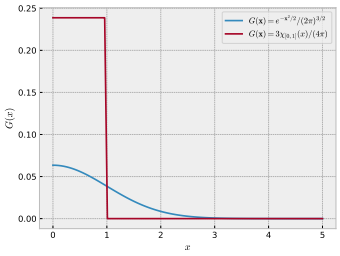

Figure 4.4: Example of a filtering function.

$$u_i^\ell(\mathbf{x}) = (G_\ell \star u_i)(\mathbf{x}), \tag{4.4}$$

$$= \int d\mathbf{y} G_\ell(\mathbf{x}-\mathbf{y}) u_i(\mathbf{y}) = \int d\mathbf{y} G_\ell(\mathbf{y}) u_i(\mathbf{x}+\mathbf{y}). \tag{4.5}$$

Note that as $\ell \to 0$,

$$u_i^\ell(\mathbf{x}) = \int d\mathbf{z} \ell^3 G_\ell(\ell\mathbf{z}) u_i(\mathbf{x}+\ell\mathbf{z}) = \int d\mathbf{z} G(\mathbf{z}) u_i(\mathbf{x}+\ell\mathbf{z}) \to u_i(\mathbf{x}) \int d\mathbf{z} G(\mathbf{z}) = u_i(\mathbf{x}). \tag{4.6}$$

In general, the filtering operator is not a projector. If we decompose the velocity fields into its filtered and residual parts: $u_i(\mathbf{x}) = u_i^\ell(\mathbf{x}) + u_i'(\mathbf{x})$, then in general $G_\ell \star u_i' \neq 0$.

Because the filtering operator is a convolution, its action in Fourier space is simply a product: $\hat{u}_i^\ell(\mathbf{k}) = \hat{G}_\ell(\mathbf{k}) \hat{u}_i(\mathbf{k})$, with $\hat{G}_\ell(\mathbf{k}) = \int G_\ell(\mathbf{x}) e^{-i\mathbf{k}\cdot\mathbf{x}} d\mathbf{x}$ the *transfer function*. It follows that the filtered energy spectrum is simply $E_\ell(k) = |\hat{G}_\ell(k)|^2 E(k)$.

4.2.2 *Filtered Navier-Stokes equations*

It is clear that the filtering operator commutes with the time derivative and (using integration by part) also with spatial derivatives.

$\partial_i u_j^\ell(\mathbf{x}) = (G_\ell \star \partial_i u_j)(\mathbf{x})$.

The filtered Navier-Stokes equations read

$$\partial_t u_i^\ell + \partial^j G_\ell \star (u_i u_j) = -\partial_i p^\ell + \nu \partial_j \partial^j u_i^\ell + f_i^\ell, \tag{4.7}$$

$$\partial^i u_i^\ell = 0, \tag{4.8}$$

In general $G_\ell \star (u_i u_j) = (u_i u_j)^\ell \neq u_i^\ell u_j^\ell$!

i.e.

$$\partial_t u_i^\ell + u_j^\ell \partial^j u_i^\ell = -\partial_i p^\ell + \nu \partial_j \partial^j u_i^\ell + f_i^\ell - \partial^j \tau_{ij}^\ell, \tag{4.9}$$

$$\partial^i u_i^\ell = 0, \tag{4.10}$$

with the *residual stress tensor* or *subgrid stress tensor*

$$\tau_{ij}^{\ell} = (u_i u_j)^{\ell} - u_i^{\ell} u_j^{\ell}. \tag{4.11}$$

These equations are not closed equations for the filtered velocity field.

4.2.3 Scale-by-scale energy budget

Let us use filtering to provide an alternative view of the scale-by-scale energy budget. We define $E_>(\ell) = \langle u_i^{\ell} u^{i\ell} \rangle / 2$ the kinetic energy at scales larger than ℓ.

Using the filtered Navier-Stokes equations (4.9) and incompressibility, we obtain

$$\partial_t E_>(\ell) = -\Pi(\ell) + \nu \langle u_i^{\ell} \Delta u^{i\ell} \rangle + \langle f_i^{\ell} u^{i\ell} \rangle, \tag{4.12}$$

with

$$\Pi(\ell) = \langle u^{i\ell} \partial^j \tau_{ij}^{\ell} \rangle = -\langle S^{ij\ell} \tau_{ij}^{\ell} \rangle. \tag{4.13}$$

$S_{ij}^{\ell} = \frac{\partial_i u_j^{\ell} + \partial_j u_i^{\ell}}{2}$.

Again, there are three contributions to the scale-by-scale energy budget: energy injection by the forcing, viscous dissipation, and inertial transfer. Π is the energy flux across scales. It corresponds to the work exerted by scales larger than ℓ onto scales smaller than ℓ. When $\Pi(\ell) > 0$, the energy is transferred, by the nonlinear term, on average from scales larger than ℓ to scales smaller than ℓ. This is called a *direct energy transfer*. When $\Pi(\ell) < 0$, the converse is true. This is called an *inverse energy transfer*.

4.2.4 Large-eddy simulations

The idea is to close the equations (4.9) by prescribing τ_{ij}^{ℓ} as a function of u_i^{ℓ}. This amounts to modelling the unresolved scales; the goal is essentially to regularize the large-scale field, i.e. dissipate energy. Because turbulence efficiently dissipate energy by transferring it to smaller (unresolved) scales where viscous dissipation can act efficiently, the turbulence model should mimick this effect by dissipating energy more efficiently than viscosity would do at the resolved scale.

It is therefore a natural idea that the divergence of the subgrid stress should act like an enhanced viscosity. This can be achieved by taking τ_{ij}^{ℓ} proportional to the filtered rate of strain:

$$\tau_{ij}^{\ell} = -2\nu_{\ell} S_{ij}^{\ell}. \tag{4.14}$$

The coefficient ν_{ℓ} is called *eddy viscosity*. A classical choice is the *Smagorinsky model*: $\nu_{\ell} = (C_S \ell)^2 \sqrt{2 S_{ij}^{\ell} S^{ij\ell}} > 0$. In this model, the rate of transfer of energy to the subgrid scales is $\Pi(\ell) = 2\nu_{\ell} \operatorname{Tr}(S^{\ell 2}) > 0$.

More elaborate models exist: see for instance Pope (2000, chap. 13).

4.3 *Reynolds-averaged equations*

Above we have separated the velocity field into two components using filtering in real space. Only a coarse-grained version of the velocity field, describing the large-scale eddies, is resolved in numerical simulations, while the effect of small-scale eddies are modeled. Alternatively, one may separate the flow into a statistical average $U_i = \langle u_i \rangle$ and fluctuations: $u'_i = u_i - U_i$. [6] This decomposition is known as *Reynolds decomposition*. The equation for the mean-flow is easily deduced from the Navier-Stokes equations:

$$\partial_t U_i + U_j \partial_j U_i = -\partial_i P + \nu \partial_j \partial^j U_i - \partial^j \langle u'_i u'_j \rangle. \tag{4.15}$$

[6] Assuming that ensemble averages may be estimated as time averages, one may also interpret the mean-flow itself as the time average velocity. In that case, the time derivative of the mean-flow vanishes.

This equation is known as the *Reynolds-averaged Navier-Stokes equation*. We observe that the mean-flow satisfies an equation very close to the Navier-Stokes equations themselves, except for the addition of a term in the right-hand side, (the opposite of) the divergence of the so-called *Reynolds stresses* $\langle u'_i u'_j \rangle$. This tensor encodes the effect of the turbulent fluctuations on the mean-flow. Its trace corresponds to the Turbulent Kinetic Energy (TKE), $k = \langle u'_i u^{i'} \rangle / 2$. We also introduce the *deviatoric part*, $a_{ij} = \langle u'_i u'_j \rangle - 2k\delta_{ij}/3$, which is the part actually transporting momentum: $\partial^j \langle u'_i u'_j \rangle = \partial^j a_{ij} - \frac{2}{3}\partial_i k$ and the second term can be absorbed into a modified mean pressure. When the flow is irrotational, the Reynolds stresses have no effect on the mean-flow. Indeed, since the vorticity vanishes, we have $\langle u'_i (\partial_j u^{i'} - \partial^i u'_j) \rangle = 0 = \partial_j k - \partial^i \langle u'_i u'_j \rangle$. Hence,

$$\partial^i \langle u'_i u'_j \rangle = \partial_j k, \tag{4.16}$$

and the whole Reynolds stress divergence can be absorbed into a modified mean pressure. This relation is known as the *Corrsin-Kistler equation*.

Unfortunately the equations for the mean-flow are not closed: to compute the mean-flow, one also needs to compute the Reynolds stresses. Many models have been developed. The simplest mdoels are based on the concept of *turbulent viscosity*: it is assumed that the deviatoric component of the Reynolds stresses is proportional to the mean strain rate[7]: $a_{ij} = -2\nu_T \langle S_{ij} \rangle = -2\nu_T (\partial_i U_j + \partial_j U_i)$. In that case, the Reynolds-averaged Navier-Stokes equations reduces to the standard Navier-Stokes equations with a modified effective viscosity $\nu_{eff} = \nu + \nu_T$. Typically the turbulent viscosity ν_T is much larger than the molecular viscosity ν.

[7] See Pope (2000, Chap. 10) for a discussion of this hypothesis.

The most crude models assume that the turbulent viscosity is constant in the homogeneous directions of the flow. If the mean-flow varies in the direction x for instance, the turbulent viscosity is given by $\nu_T = \frac{U(x)\delta(x)}{R_T}$ where $\delta(x)$ is a characteristic length scale in the direction of the mean-flow and R_T a constant chosen empirically for the flow of interest. The main problem of this approach is that its applicability is limited to well-known flows.

However, the turbulent viscosity needs not be a constant. Below we present briefly some of the classical models to estimate it.

4.3.1 *Mixing-length theory*

This model assumes that a space-dependent length scale $\ell_m(\mathbf{x})$ characteristic of momentum mixing by turbulence is known, and determines the turbulent viscosity as $\nu_T = \ell_m u* = \ell_m^2 |\nabla U|$.

4.3.2 *k-ϵ model*

The idea is to estimate the characteristic velocity for the turbulent viscosity using kinetic turbulent energy rather than the velocity gradient as in the mixing-length model: $\nu_T = c\ell_m\sqrt{k}$. While the mixing-length ℓ_m is still specified, the kinetic energy should be computed dynamically.

5
Empirical Characterization of Homogeneous Isotropic Turbulence

5.1 Anomalous dissipation

As the viscosity goes to zero (i.e. as the Reynolds number goes to infinity), the energy dissipation ϵ goes to a finite constant:

$$\lim_{\nu \to 0} \lim_{t \to \infty} \epsilon_\nu(t) = \epsilon > 0. \tag{5.1}$$

This limit can only depend on the macroscopic properties of the flow. Dimensional analysis yields the formula known as the *Taylor estimate* for the energy dissipation rate:

$$\epsilon = \frac{U^3}{L}. \tag{5.2}$$

As shall become clear very soon, the Taylor estimate may be seen as a measure of the magnitude of the nonlinear term in the energy budget $\mathbf{u} \cdot (\mathbf{u} \cdot \nabla)\mathbf{u}$.

Figure 5.1 shows measurements of the energy dissipation rate as

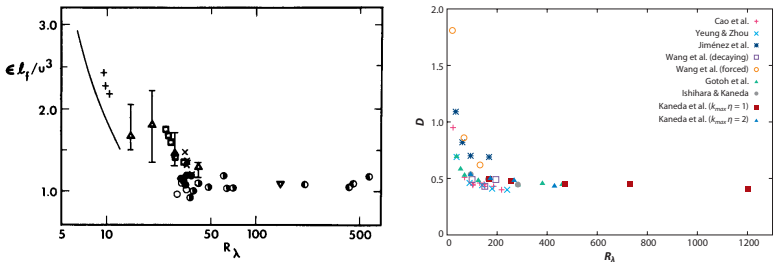

Figure 5.1: Energy dissipation rate as a function of the Reynolds number at the Taylor microscale R_λ in grid turbulence experiments (left, figure from Sreenivasan (1984)) and DNS (right, $D = \epsilon L/U^3$, figure from Ishihara, Gotoh, and Kaneda (2009)).

a function of the Reynolds number (at the Taylor microscale, see § 3.1.5) for various experiments and DNS runs.

We know from equation (3.24) that $\epsilon_\nu \propto \nu\langle(\partial_\parallel u_\parallel)^2\rangle$: a direct corollary of anomalous dissipation is that the velocity gradients become arbitrarily large in the limit of vanishing viscosity. In other words, we expect the velocity field to become everywhere non-differentiable in this limit. Similarly, using that in a stationary state $\epsilon_\nu = 2\nu\Omega$ (§ 2.5)

we see that the enstrophy should also diverge in this limit, i.e. rapid vortex stretching should take place.

As we have seen in the introduction (§ 1.2), this result has dramatic practical consequences: it is equivalent to the drag force acting on an object moving through a fluid increasing quadratically with the object velocity, instead of linearly for low velocities.

5.2 2/3 law in real space: second-order structure function

Let us define the *longitudinal velocity increment*:

$$\delta u_{\parallel}(\mathbf{x}, \mathbf{r}) = [\mathbf{u}(\mathbf{x}+\mathbf{r}) - \mathbf{u}(\mathbf{x})] \cdot \mathbf{r}/r, \tag{5.3}$$

and the *longitudinal structure functions*:

$$S_n(r) = \langle (\delta u_{\parallel}(\mathbf{x}, \mathbf{r}))^n \rangle. \tag{5.4}$$

The structure function is independent of $\mathbf{x}$ because of the homogeneity hypothesis and independent of the orientation of the separation vector $\mathbf{r}$ because of the isotropy hypothesis. The longitudinal velocity increment $\delta u_{\parallel}$ can be interpreted as a characteristic velocity at scale r.

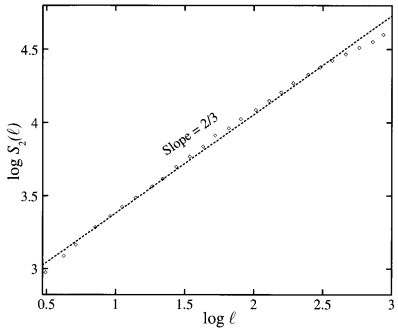

Figure 5.2: Second-order structure function obtained in the time domain (translated to the space domain using the Taylor hypothesis, see § A) in the Modane wind tunnel of ONERA. Figure reproduced from the book of Frisch (1995, Fig. 5.1), original data from Y. Gagne and E. Hopfinger.

Experimental results (hence, at large but finite Reynolds number), such as the one shown in Fig. 5.2, indicate that there exists a range of scales r such that the second-order longitudinal structure function behaves like a power law:

$$S_2(r) \sim r^{2/3}. \tag{5.5}$$

This relation holds in a range of scales called the *inertial range*: $\eta \ll r \ll L$ (where η is the *Kolmogorov scale*, see Eq. 6.1), i.e. for scales which feel neither the effect of molecular viscosity, neither the boundaries of the domain.

In the limit of vanishing viscosity, the Kolmogorov scale goes to zero, and the 2/3-law is consistent with the above remark (§ 5.1) that singularities develop in the velocity field: it essentially says that $\delta u_{\parallel} \sim r^{1/3}$, and $\partial_{\parallel} u_{\parallel} = \lim_{r \to 0} \delta u_{\parallel}/r$, which diverges.

5.3 2/3 law in Fourier space: the energy spectrum

The longitudinal structure function $S_2(r)$ is a second order statistical quantity for velocity; intuitively we expect it to be related to the energy spectrum. Hence, the 2/3-law should have a counterpart in spectral space.

5.3.1 A rough argument

Let us consider an eddy of size r, or equivalently scale $k = r^{-1}$, with typical kinetic energy $S_2(r)$, or equivalently $kE(k)$. Then the 2/3 law corresponds to an energy spectrum $E(k) \sim k^{-5/3}$. The $k^{-5/3}$ spectrum is ubiquitous in 3D turbulence. Examples from the ONERA S1 wind tunnel (in the time domain, which can be related to spatial scales using the *Taylor hypothesis*, see § A) and from a DNS are shown in Fig. 5.3. Read § 5.1 in the book by Frisch (1995) for more examples.

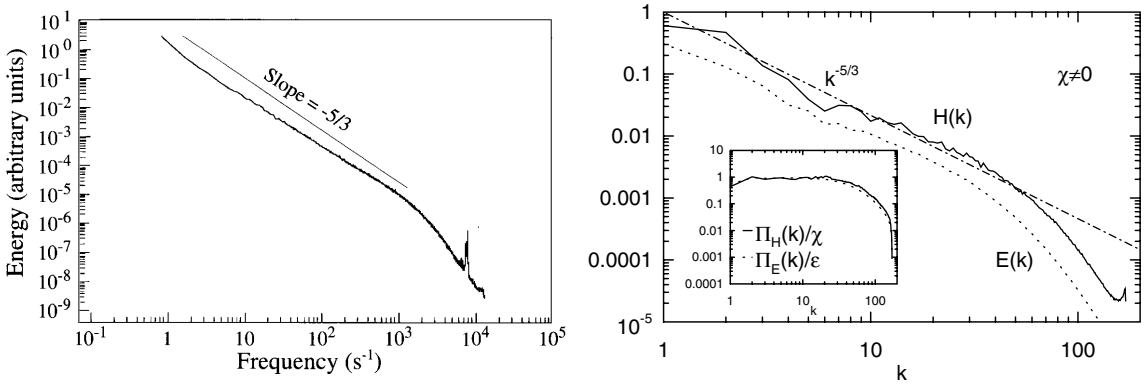

Figure 5.3: Energy spectrum in a wind tunnel (left, Frisch (1995)) and in a DNS of homogeneous isotropic turbulence in a box (right, Chen et al. (2003)).

5.3.2 A more precise relation

Let us first note that the second-order structure function $S_2(r)$ can be related to the longitudinal velocity autocorrelation function f introduced in Eq. (3.5):

$$S_2(r) = 2[f(0) - f(r)], \tag{5.6}$$

and therefore also to the velocity covariance tensor:

$$U_i^{\,i}(r) = 3f(r) + rf'(r) = 3U_{\text{rms}}^2 - \frac{3}{2}S_2(r) - \frac{r}{2}S_2'(r). \tag{5.7}$$

The energy spectrum is also related to the trace of the velocity covariance $U_{ij}(\mathbf{r})$, through the relation $E(k) = 2\pi k^2 \hat{U}_i^i(\mathbf{k})$. Let us simplify this relation by using the fact that the trace of the velocity covariance

tensor depends only on the norm of the vector:

$$\hat{U}_i^i = \frac{1}{(2\pi)^3}\int U_i^i(r)e^{-i\mathbf{kr}}d\mathbf{r}, \tag{5.8}$$

$$= \frac{1}{(2\pi)^2}\int_0^\pi \sin\theta d\theta \int_0^{+\infty} r^2 dr U_i^i(r)e^{-ikr\cos\theta}, \tag{5.9}$$

$$= \frac{2}{(2\pi)^2}\int_0^{+\infty} \frac{r}{k}\sin(kr)U_i^i(r)dr, \tag{5.10}$$

from which it follows that

$$E(k) = \frac{1}{\pi}\int_0^{+\infty} kr\sin(kr)U_i^i(r)dr, \tag{5.11}$$

and conversely,

$$\frac{U_i^i(r)}{2} = \int_0^{+\infty} E(k)\frac{\sin(kr)}{kr}dk. \tag{5.12}$$

As a consequence, for $r \ll L$,

$$\underbrace{\frac{3}{2}U_{\text{rms}}^2}_{=E} - \frac{1}{4r^2}\frac{d}{dr}[r^3 S_2(r)] = \underbrace{\int_0^{\frac{2\pi}{L}} E(k)\underbrace{\frac{\sin(kr)}{kr}}_{\approx 1}dk}_{\approx E} + \int_{\frac{2\pi}{L}}^{+\infty} E(k)\frac{\sin(kr)}{kr}dk. \tag{5.13}$$

Assuming that $S_2(r) = Ar^\alpha$ and $E(k) = Bk^\beta$, we obtain

$$-\frac{3+\alpha}{4}Ar^\alpha = Br^{-\beta-1}\int_{\frac{2\pi r}{L}}^{+\infty} u^{\beta-1}\sin u du, \tag{5.14}$$

which yields the relationship $\alpha = -\beta - 1$, provided that the integral depends weakly on r.

An argument relating the second order structure function and the energy spectrum, similar to the one presented here, can be found in the book by Lesieur (2008, § 6.4.5), although the book proceeds in a different order. Yet another formulation of the same relation can be found in Frisch (1995, § 4.5).

5.4 *Velocity PDF*

Batchelor (1953, § 8)

The PDF of the one-point velocity $u_i(\mathbf{x})$ is found experimentally to be close to Gaussian (see FIg. 5.4). This result has been known for a very long time (Simmons and Salter 1934); this is remarkable, given that no digital treatment of experimental data was available at the time.

On the other hand, the joint distribution of the velocity at multiple points $u_{i_1}(\mathbf{x}_1), \ldots, u_{i_n}(\mathbf{x}_n)$ is not a normal distribution. Fig. 5.5 shows for instance that the flatness $\langle \delta u_\parallel(\mathbf{r})^4\rangle / \langle \delta u_\parallel(\mathbf{r})^2\rangle^2$ is close to 3 only when the velocity at the two points becomes statistically independent, and that the skewness $\langle \delta u_\parallel(\mathbf{r})^3\rangle / \langle \delta u_\parallel(\mathbf{r})^2\rangle^{3/2}$ remains finite all the way to the integral scale.

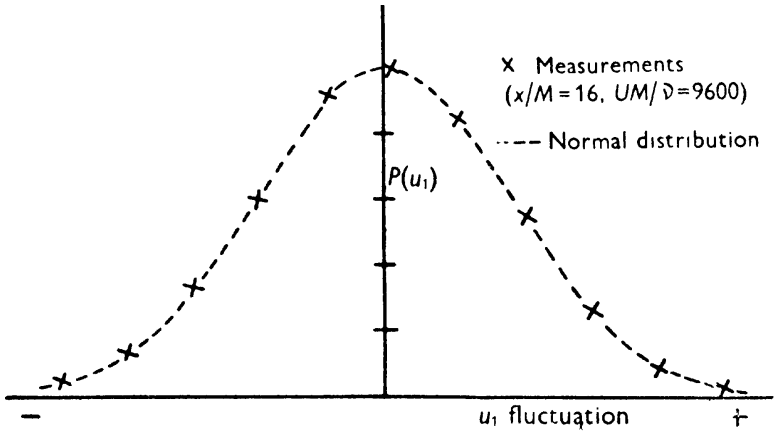

Figure 5.4: PDF of the velocity at one point in grid turbulence (Batchelor 1953).

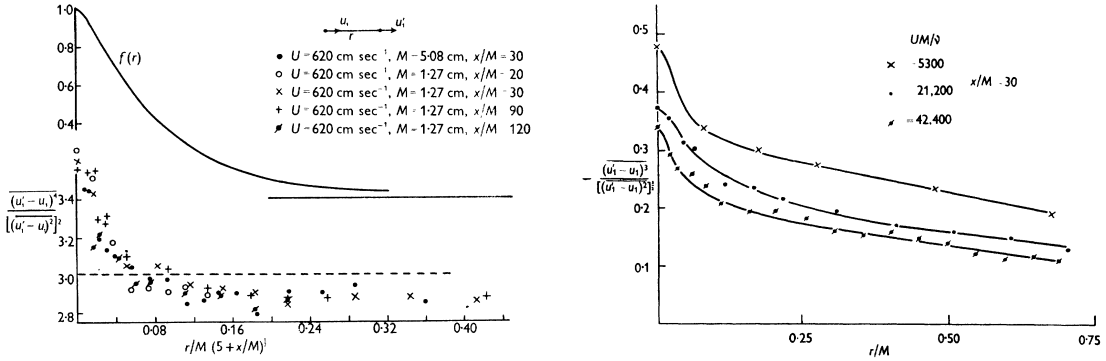

Figure 5.5: Flatness (left) and skewness (right, Stewart (1951)) of the velocity increment in grid turbulence (Batchelor 1953).

The statistical properties at small distances can also be studied by considering the longitudinal velocity gradient $\partial_\parallel u_\parallel$. Its PDF is not Gaussian, as Fig. 5.6 reveals. In particular, it has negative skewness (negative velocity gradients are more probable than positive velocity gradients), as shown in Fig. 5.7. We will further study the statistical properties of velocity increments (and in particular, the deviations from Gaussianity) in the chapter about intermittency (Chap. 7).

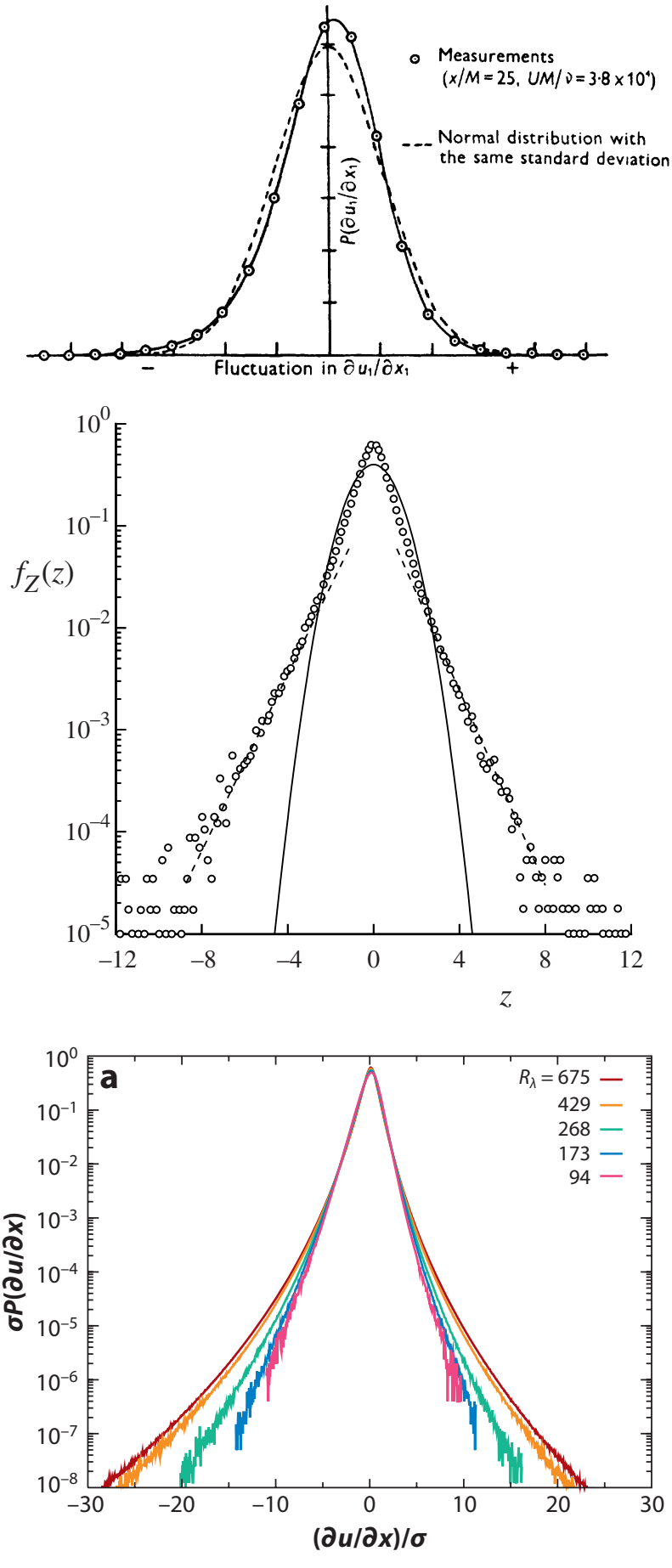

Figure 5.6: PDF of the longitudinal velocity gradient in grid turbulence (top, Batchelor (1953)),in the atmospheric boundary layer (middle, $z = (\partial u_1/\partial x_1)/\langle(\partial u_1/\partial x_1)^2\rangle^{1/2}$, **VanAtta1970**), and in DNS (bottom, Ishihara, Gotoh, and Kaneda (2009).

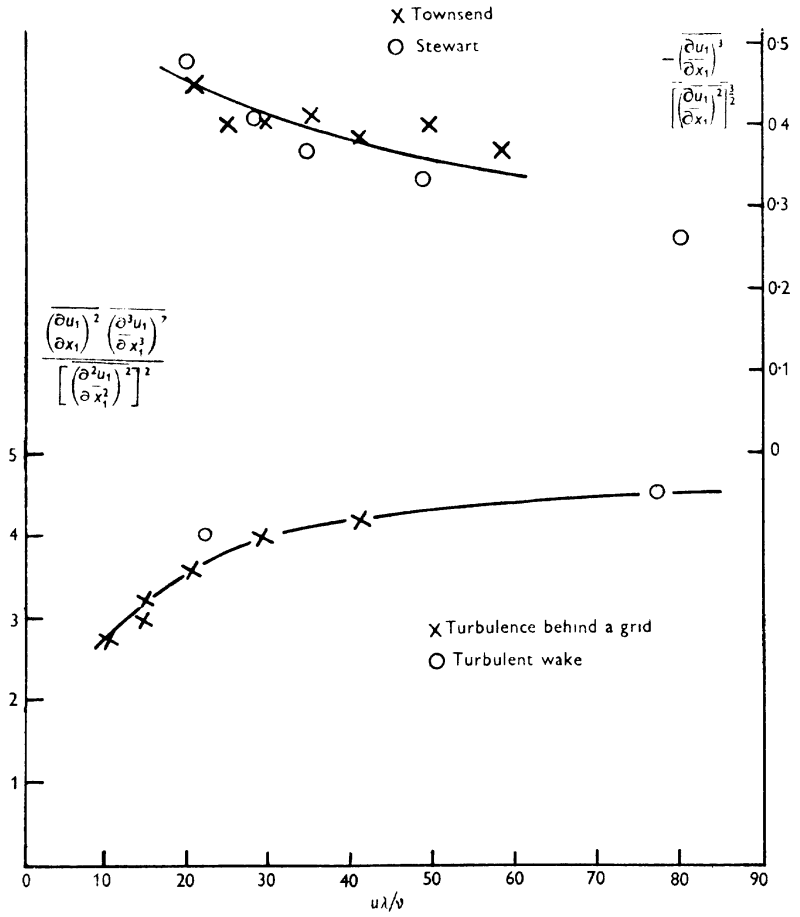

Figure 5.7: Skewness of the longitudinal velocity gradient in grid turbulence as a function of the Reynolds number (Batchelor 1953).

6
Kolmogorov theory of fully developed turbulence

THIS IS THE CORE CHAPTER of this course, which delves into the most important results of classical turbulence theory.

The main reference for this chapter is the book by Frisch (1995) (chapter 6).

6.1 *Phenomenology*

6.1.1 *Kolmogorov theory (1941)*

Kolmogorov scale There is only one way to build a length scale based on viscosity ν and energy dissipation rate ϵ: it is the *Kolmogorov scale*

$$\eta = \left(\frac{\nu^3}{\epsilon}\right)^{1/4}. \tag{6.1}$$

Phenomenology is an approach of a physical problem which does not rely on fundamental principles (such as momentum conservation) but rather on a qualitative understanding of the phenomenon, using for instance dimensional analysis, scaling hypotheses or other physical arguments.

Figure 6.1: Andrey Nikolaevich Kolmogorov (1903–1987).

As we will show later, the Kolmogorov scale can be interpreted as the scale at which viscous dissipation balances inertia:

$$\mathbf{u}\cdot(\mathbf{u}\cdot\nabla)\mathbf{u} \sim \nu\mathbf{u}\cdot\Delta\mathbf{u},$$

i.e. the scale at which the Reynolds number is of order one: $U\eta/\nu \sim 1$.

First Kolmogorov assumption of universality: At large but finite Reynolds numbers, all the small-scale statistical properties are uniquely and universally determined by the scale r, the average energy dissipation rate ϵ and the viscosity ν (or equivalently, r, ϵ and η).

Second Kolmogorov assumption of universality: In the limit of infinite Reynolds numbers, all the small-scale statistical properties are uniquely and universally determined by the scale r and the average energy dissipation rate ϵ.

Energy spectrum By a simple dimensional argument, it follows from the first universality assumption that there exists a universal function F such that the energy spectrum reads:

$$E(k) = F(k\eta)\epsilon^{2/3}k^{-5/3}. \tag{6.2}$$

In agreement with the second universality assumption, the function F has a finite limit for $\eta \to 0$, referred to as the Kolmogorov constant and denoted C_K. It should take a universal value (independent of the flow), and experiments report $C_K \approx 1.5$.

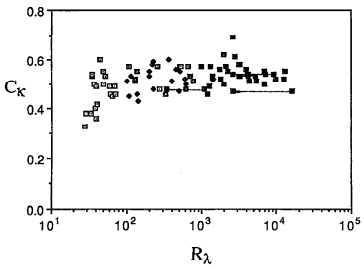

Figure 6.2: Measurements of the Kolmogorov constant as a function of the Reynolds number R_λ for many flows (Sreenivasan 1995). The constant measured is the one of the 1D energy spectrum, which is related to the constant of the isotropic spectrum by a factor $55/18 \approx 3$ (see § C.2).

Structure functions Similarly, under the first universality assumption, dimensional analysis gives the form of the structure function of order n:

$$S_n(r) = F_n\left(\frac{\eta}{r}\right)(\epsilon r)^{n/3}, \tag{6.3}$$

with F_n a universal function. This becomes, in the limit $\eta \to 0$

$$S_n(r) = C_n(\epsilon r)^{n/3}, \tag{6.4}$$

where $C_n = F_n(0)$ are universal constants. Experimental measurements give the value $C_2 \approx 2.0$.

6.1.2 *The inertial range*

The Kolmogorov theory predicts $S_2(r) \sim r^{2/3}$. As briefly alluded to earlier, this scaling cannot hold for all r.

In the limit $r \to 0$, it would lead to a non-differentiable velocity field at fixed viscosity, but we need the velocity field (at fixed ν) to be twice differentiable for the Navier-Stokes equations to make sense. In fact, for a smooth field[1], a Taylor expansion ($u_\parallel(\mathbf{x}+\mathbf{r}) = u_\parallel(\mathbf{x}) + r_i\partial^i u_\parallel(\mathbf{x}) + o(r)$) yields

$$\begin{aligned}
S_2(r) &= r^i r^j \langle \partial_i u_\parallel \partial_j u_\parallel \rangle, && (6.5)\\
&= -r^i r^j \frac{\partial}{\partial x^i}\frac{\partial}{\partial x^j} f(x)|_{\mathbf{x}=0}, && (6.6)\\
&= -r^i r^j \frac{\partial}{\partial x^i}\frac{x_j}{x} f'(x)|_{\mathbf{x}=0}, && (6.7)\\
&= -r^i r^j \left[\frac{x_i x_j}{x^2} f''(x) + \frac{\delta_{ij}}{x} f'(x) - \frac{x_i x_j}{x^3} f'(x)\right]_{\mathbf{x}=0}, && (6.8)\\
&= -r^2 f''(0), && (6.9)\\
&= r^2 \langle (\partial_\parallel u_\parallel)^2 \rangle, && (6.10)\\
&= \frac{\epsilon r^2}{15\nu} = U_{\text{rms}}^2 \left(\frac{r}{\lambda}\right)^2. && (6.11)
\end{aligned}$$

[1] Based on the Taylor expansion we expect $S_2(r) \sim r^2$ for a smooth field without doing the computation, but computing the tensor structure allows for properly matching the different ranges.

You might notice that the tricks used in this computation are very similar to those used in § 3.1.6.

Alternatively, one can find the same result by working with the more general rank-4 velocity gradient covariance tensor:

$$\begin{aligned}
S_2(r) &= \frac{r^i r^j r^k r^l}{r^2}\langle \partial_i u_j \partial_k u_l \rangle,\\
&= 2\frac{r^i r^j r^k r^l}{r^2}\langle (\partial_\parallel u_\parallel)^2 \rangle \left[\delta_{ij}\delta_{kl} - \frac{1}{4}\delta_{ik}\delta_{jl} - \frac{1}{4}\delta_{jk}\delta_{il}\right],\\
&= r^2\langle (\partial_\parallel u_\parallel)^2 \rangle,
\end{aligned}$$

but that just leads to unnecessarily more complicated computations.

Note that this computation also means that $F_n(\xi) \sim \frac{1}{15}\xi^{-4/3}$ for $\xi = \eta/r \to +\infty$, i.e. $r \to 0$ at fixed η. This is not incompatible with the definition of the constants C_n, which is the limit $\eta \to 0$ at fixed r.

The scale at which equations (6.4) and (6.11) match, denoted η, can be easily computed:

$$\eta = (15C_2)^{3/4}\left(\frac{\nu^3}{\epsilon}\right)^{1/4}. \tag{6.12}$$

We recover, up to a numerical factor, the Kolmogorov scale identified by dimensional analysis (Eq. 6.1).

In the limit $r \to +\infty$, $S_2(r)$ must go to a constant. Indeed, the longitudinal autocorrelation function $f(r) = \langle u_\parallel(\mathbf{x})u_\parallel(\mathbf{x}+\mathbf{r})\rangle$ decays to zero at infinity, and $S_2(r) = 2U_{\text{rms}}^2 - 2f(r) \longrightarrow 2U_{\text{rms}}^2$. Let us define a (large) scale L such that $S_2(L) = 2U_{\text{rms}}^2$. This scale should correspond, up to an order one numerical factor, to the integral scale (see § 3.1.4) in the freely decaying case or the pumping scale in the forced case. Then, matching with equation (6.4), we can relate that scale to the energy dissipation rate:

$$L = \left(\frac{2}{C_2}\right)^{3/2}\frac{U_{rms}^3}{\epsilon}, \text{ or equivalently, } \epsilon = \left(\frac{2}{C_2}\right)^{3/2}\frac{U_{rms}^3}{L}. \tag{6.13}$$

i.e. $L = \left(\frac{2}{C_2}\right)^{3/2} L_0$.

This is, up to a numerical factor, the Taylor estimate (5.2) for the energy dissipation rate.

The Kolmogorov scale can be compared to the Taylor microscale and the integral scale[2]:

$$\lambda/L_0 \sim Re^{-1/2} \sim R_\lambda^{-1}, \tag{6.14}$$

$$\lambda/\eta \sim Re^{1/4} \sim R_\lambda^{1/2}. \tag{6.15}$$

Note in particular that $R_\lambda \sim \sqrt{Re}$.

All those estimates, except $\lambda/\eta \sim R_\lambda^{1/2}$, rely on the Taylor estimate $\epsilon = U_{rms}^3/L_0$.

We can now estimate the size of the inertial range, for which the scaling law (6.4) holds:

$$\frac{\eta}{L} \sim Re^{-3/4}. \tag{6.16}$$

This explains how the Reynolds number measures the range of scales which are coupled by nonlinearity. In a way, it gives a rough estimate of the effective number of degrees of freedom of the system: in 3D, it goes like $Re^{9/4}$.

These arguments are summarized in Fig. 6.3: the 2/3-law is expected to hold in the inertial range $\eta < r < L$, where η is the Kolmogorov scale and L is approximately the integral scale or the pumping scale. Below η, the velocity field is regularized by viscosity.

[2] e.g. Tennekes and Lumley (1972, pp. 66–68)

$$\epsilon = \frac{U_{rms}^3}{L_0} = 15\nu\frac{U_{rms}^2}{\lambda^2}$$
$$\longrightarrow \frac{\lambda}{L_0} = 15\frac{\nu}{U_{rms}\lambda} \sim R_\lambda^{-1}$$
$$\longrightarrow \frac{\lambda^2}{L_0^2} = 15\frac{\nu}{U_{rms}L_0} \sim Re^{-1}$$
$$\epsilon = \nu^3\eta^{-4} = 15\nu U_{rms}^2\lambda^{-2}.$$

6.1.3 *Energy flux in the inertial range*

In spectral space The scale-by-scale energy budget in Fourier space (3.40) holds for a statistically stationary velocity field solution of the Navier-Stokes equations, i.e. by averaging E, Π and F over random Fourier

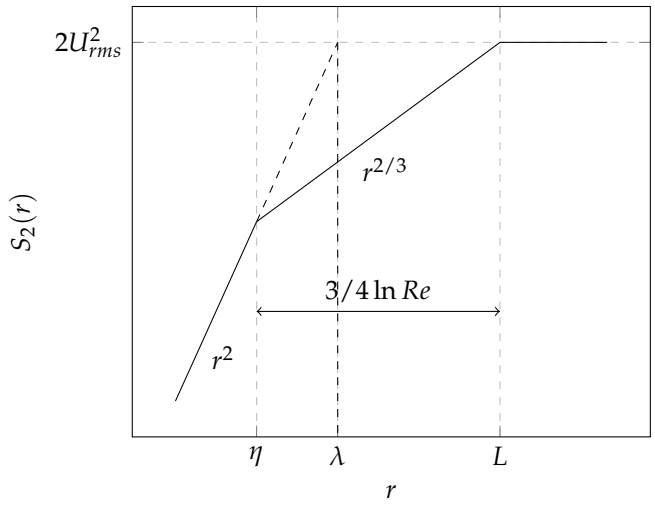

Figure 6.3: Skecth of the expected behavior of the second-order structure function, illustrating the inertial range and its boundaries.

modes distributed according to the invariant measure of the system. We obtain $2\nu k^2 E(k) = -\partial_k \Pi(k) + F(k)$. For fixed k, we can take the limit $\nu \to 0$ and the left-hand side vanishes. Now, we assume that the forcing acts at large scale, such that $\hat{f}(\mathbf{k}) = 0$ for $k > k_f$. Then, for $k > k_f$, the energy flux is constant: $\partial_k \Pi(k) = 0$. The equation for the cumulative energy spectrum in the limit $t \to \infty, \nu \to 0$ yields $\Pi(k) = \epsilon$ for $k > k_f$. In particular,

$$\lim_{k\to+\infty} \lim_{\nu\to 0} \lim_{t\to+\infty} \Pi(k) = \epsilon. \tag{6.17}$$

This simply means that in a stationary state, the average energy injected by the forcing (at the large scales) equals the energy flux through the inertial range equals the energy dissipation rate (in the dissipative range).

For finite $\nu > 0$, we expect $\Pi(k) \approx \epsilon$ should hold as long as dissipation is weak, i.e. $2\nu \int_0^k p^2 \underbrace{E(p)}_{C_K \epsilon^{2/3} p^{-5/3}} dp \ll \epsilon$. This is fulfilled for $k\eta \ll 1$: indeed, then $2\nu \int_0^k p^2 E(p) dp \leq 2C_K \nu \epsilon^{2/3} \int_0^k p^{1/3} dp = \frac{3}{2} C_K \epsilon (k\eta)^{4/3} \ll \epsilon$.

In real space The same reasoning applies based on the scale-by-scale energy budget for the filtered velocity field from § 4.2.3.

At finite ℓ, the viscous term goes to zero as $\nu \to 0$:

$$0 \leq -\nu \langle u_i^\ell \Delta u^{i\ell} \rangle = \nu \langle \partial_j u_i^\ell \partial^j u^{i\ell} \rangle, \tag{6.18}$$

$$= \nu \left\langle \int d\mathbf{y} \int d\mathbf{z} \partial_j G_\ell(\mathbf{x}-\mathbf{y}) \partial^j G_\ell(\mathbf{x}-\mathbf{z}) u_i(\mathbf{y}) u^i(\mathbf{z}) \right\rangle, \tag{6.19}$$

$$= \nu \int d\mathbf{y} \int d\mathbf{z} \partial_j G_\ell(\mathbf{x}-\mathbf{y}) \partial^j G_\ell(\mathbf{x}-\mathbf{z}) \langle u_i(\mathbf{y}) u^i(\mathbf{z}) \rangle, \tag{6.20}$$

$$\leq \underbrace{3\nu U_{\text{rms}}^2 \int d\mathbf{y} \int d\mathbf{z} \partial_j G_\ell(\mathbf{x}-\mathbf{y}) \partial^j G_\ell(\mathbf{x}-\mathbf{z})}_{\xrightarrow[\nu\to 0]{} 0}. \tag{6.21}$$

There is no dissipation anomaly in the filtered velocity field: as we push the dissipative range downscale, it ends up below the cutoff scale, and no explicit dissipation can occur.

We have used the Cauchy-Schwarz inequality: $\langle u_i(\mathbf{y}) u^i(\mathbf{z}) \rangle \leq \sqrt{\langle u_i(\mathbf{y}) u^i(\mathbf{y}) \rangle \langle u_i(\mathbf{z}) u^i(\mathbf{z}) \rangle} = 3U_{rms}^2$.

Therefore, in a statistically stationnary state,

$$\Pi(\ell) = \langle u_i^\ell f^{i\ell} \rangle, \tag{6.22}$$
$$= \langle u_i^\ell f^i \rangle, \tag{6.23}$$

Basically, $\mathbf{f}^\ell(\mathbf{x}) \approx \mathbf{f}(\mathbf{x})$ as soon as $\ell \ll \ell_f$ the correlation scale of the forcing.

Because the forcing is at large scales,

$$= \left\langle \int d\mathbf{y} G_\ell(\mathbf{y}) u_i(\mathbf{y}) f^i(0) \right\rangle, \tag{6.24}$$
$$= \int d\mathbf{y} G_\ell(\mathbf{y}) \langle u_i(\mathbf{y}) f^i(0) \rangle, \tag{6.25}$$
$$= \langle u_i(0) \int d\mathbf{y} G_\ell(\mathbf{y}) f^i(-\mathbf{y}) \rangle, \tag{6.26}$$
$$= \langle u_i(0) f^i(0) \rangle, \tag{6.27}$$
$$= \epsilon. \tag{6.28}$$

More precisely,

$$\lim_{\ell \to 0} \lim_{\nu \to 0} \lim_{t \to +\infty} \Pi(\ell) = \epsilon. \tag{6.29}$$

6.1.4 *The Richardson cascade picture*

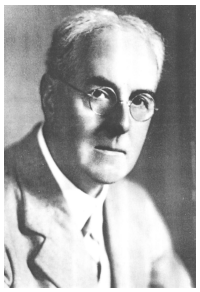

Figure 6.4: Lewis Fry Richardson (1881–1953). An interesting bibliography was written by Hunt (1998).

Let us now describe the physical picture of stationary homogeneous isotropic turbulence associated with the phenomenology described above. Let us assume that energy is continuously injected at large scales by some forcing mechanism, and that the system reaches a statistically stationary state. The large-scale structure of the flow depends on the details of the system: boundaries, stirring mechanism, etc. These scales contain most of the energy. Large-scale motion generates motion at smaller and smaller scales through nonlinear interactions. Energy is transferred in this process towards the small scales. No dissipation occurs through the inertial range, and the energy flux is constant. Below the Kolmogorov scale, viscous dissipation acts efficiently to ensure stationarity. This process is called the *energy cascade* [3]. This is why turbulent flows dissipate much more energy than laminar flows: turbulence transfers energy to scales where viscosity can dissipate it efficiently.

[3] sometimes *direct energy cascade* to distinguish it from the *inverse energy cascade* which occurs in 2D, see § **??**

Let us now consider an eddy of size ℓ, with typical velocity v_ℓ. We define the *eddy turnover time* $t_\ell = \ell / v_\ell$; it is the typical time during which the eddy should retain its structure, before being distorted due to the differential motion in its interior. t_ℓ is also the time scale for energy transfer from scales close to ℓ to scales smaller than ℓ: we may thus estimate the energy flux as $\Pi \sim v_\ell^3 / \ell$. Constancy of the energy flux in the inertial range yields the following scaling:

$$v_\ell \sim (\epsilon \ell)^{1/3}, \text{ and } t_\ell \sim \epsilon^{-1/3} \ell^{2/3}, \tag{6.30}$$

which also entails the scaling law for the structure functions — $S_n(\ell) \sim (\epsilon\ell)^{n/3}$ — and the energy spectrum. The energy flux constancy expressed at the integral scale yields the Taylor estimate (5.2) for the energy dissipation rate. Finally, estimating the typical time for diffusion at scale ℓ as $t_\nu = \ell^2/\nu$, we see that the eddy turnover time and the dissipation time coincide if and only if $\ell = \eta$ the Kolmogorov scale. This is another way to show that the Kolmogorov scale is the scale at which dissipative and inertial effects are comparable.

Note that the velocity scaling, applied to the Kolmogorov scale, shows that the Reynolds number at that scale is indeed one: $(\epsilon\eta)^{1/3}\eta/\nu \sim 1$.

The above phenomenology can be put in a more poetic manner:

> Big whorls have little whorls,
> Which feed on their velocity,
> And little whorls have lesser whorls,
> And so on to viscosity.
>
> L. F. Richardson (1922)

A graphic view can also be seen in Fig. 6.5. However, one should not expect to actually see an eddy breaking up through an hydrodynamic instability. No such thing exists, and the cascade process rather proceeds through energy transfers between incoherent velocity fluctations. Besides, individual interactions may transfer energy upscale or downscale; the positive average energy flux is only the result of a small imbalance between the two.

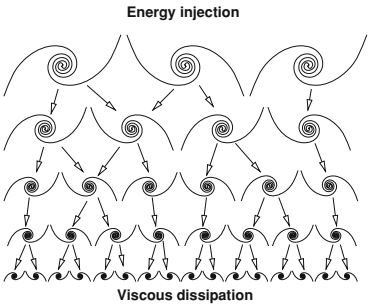

Figure 6.5: Schematic view of the Richardson energy cascade of homogeneous isotropic turbulence. Figure taken from Nazarenko 2010.

More results obtained using phenomenological arguments like the above can be found in Frisch (1995, Chap. 7), or in many other books about applications of turbulence (Tennekes and Lumley 1972; Vallis 2017)[4].

[4] A word of caution though: this kind of elegant and seemingly simple physical arguments can lead to all sorts of totally wrong predictions... Proceed with care!

Kolmogorov (1941)

6.2 *The 4/5-law*

6.2.1 *Karman-Howarth-Monin relation*

The Karman-Howarth-Monin relation describes the evolution of the second-order (two-point) correlation function.

Let us consider an incompressible velocity field $\mathbf{u}(\mathbf{x})$ solution of the Navier-Stokes equations subject to a random forcing $\mathbf{f}(\mathbf{x})$. We assume homogeneous statistics, and we note $\delta\mathbf{u} = \mathbf{u}(\mathbf{x}+\mathbf{r}) - \mathbf{u}(\mathbf{x})$.

Then, we have:

$$\partial_t \langle \mathbf{u}(\mathbf{x}) \cdot \mathbf{u}(\mathbf{x}+\mathbf{r}) \rangle = \frac{1}{2}\nabla_\mathbf{r} \cdot \langle (\delta\mathbf{u})^2 \delta\mathbf{u} \rangle + \langle \mathbf{u}(\mathbf{x}) \cdot [\mathbf{f}(\mathbf{x}+\mathbf{r}) + \mathbf{f}(\mathbf{x}-\mathbf{r})] \rangle + 2\nu\Delta_\mathbf{r} \langle \mathbf{u}(\mathbf{x}) \cdot \mathbf{u}(\mathbf{x}+\mathbf{r}) \rangle. \tag{6.31}$$

Proof. As a shorthand, we shall omit the position and denote with primes the variables at point $\mathbf{x}+\mathbf{r}$. From

the Navier-Stokes equations, we obtain easily

$$\begin{aligned}\partial_t\langle u^i u_i'\rangle = &-\langle u_i' u_j \partial^j u^i\rangle - \langle u_i u_j' \partial^j u'^i\rangle - \langle u_i' \partial^i p\rangle - \langle u_i \partial^i p'\rangle \\ &+ \nu\langle u_i' \partial_j \partial^j u^i\rangle + \nu\langle u_i \partial_j \partial^j u'^i\rangle + \langle u_i' f^i\rangle + \langle u_i f'^i\rangle.\end{aligned} \tag{6.32}$$

Using integration by parts and incompressibility, it can be seen that the pressure terms vanish: $\langle u_i' \partial^i p\rangle = \langle u_i \partial^i p'\rangle = 0$.

Using homogeneity, the viscous terms can be expressed as: $\nu\langle u_i' \partial_j \partial^j u^i\rangle + \nu\langle u_i \partial_j \partial^j u'^i\rangle = 2\nu\Delta_{\mathbf{r}}\langle u_i' u^i\rangle$, and the forcing terms read $\langle u_i' f^i\rangle + \langle u_i f'^i\rangle = \langle u_i(\mathbf{x})[f^i(\mathbf{x}+\mathbf{r}) + f^i(\mathbf{x}-\mathbf{r})]\rangle$.

It remains to treat the nonlinear term: using homogeneity and incompressibility,

$$\langle u_i' u_j \partial^j u^i\rangle + \langle u_i u_j' \partial^j u'^i\rangle = \frac{\partial}{\partial r_j}\langle u_i' u^i \delta u_j\rangle, \tag{6.33}$$

and using $u_i' u^i = (u_i u^i + u'_i u'^i - \delta u_i \delta u^i)/2$, we obtain

$$= \frac{1}{2}\frac{\partial}{\partial r_j}\langle u_i' u'^i \delta u_j\rangle + \frac{1}{2}\frac{\partial}{\partial r_j}\langle u_i u^i \delta u_j\rangle - \frac{1}{2}\frac{\partial}{\partial r_j}\langle \delta u_i \delta u^i \delta u_j\rangle. \tag{6.34}$$

The first two terms on the right hand side vanish because of homogeneity and incompressibility, which leaves us with the desired result. ■

This derivation is given in the book by Frisch (1995, § 6.2.1). An alternative derivation is given in the book by Monin and Yaglom (1971). The above relation was first derived with the additional assumption of statistical isotropy (Kármán and Howarth 1938), before being generalized by Monin (1959).

This relation illustrates the *closure problem*: the evolution of the second-order velocity correlation function depends on third-order statistics (the equation is not closed).

Finally, note that in the limit $\mathbf{r} = 0$, the Karman-Howarth-Monin relation reduces to the energy budget. The nonlinear term does not contribute in this limit, because as seen before, it conserves global energy. It only acts to redistribute energy between scales. We shall now see how the Karman-Howarth-Monin relation allows for deriving a quantitative result describing how the nonlinear term transfers energy across scales.

6.2.2 *Derivation of the 4/5-th law*

In this section we assume that the fields have isotropic statistics.

Energy budget in the inertial range Let us study the different terms of the Karman-Howarth-Monin relation under both limits $t \to +\infty$ (stationarity) and $\nu \to 0$ (fully developed turbulence):

- Because of stationarity, the left-hand side of equation 6.31 vanishes.
- For distances $r \ll \ell_f$ the correlation length of the forcing, $\langle u_i(\mathbf{x}) f^i(\mathbf{x}+\mathbf{r})\rangle = \langle u_i(\mathbf{x}) f^i(\mathbf{x}-\mathbf{r})\rangle \approx \langle u_i(\mathbf{x}) f^i(\mathbf{x})\rangle = \epsilon$.

- For fixed $\mathbf{r}$, $\Delta_{\mathbf{r}}\langle \mathbf{u}(\mathbf{x})\cdot\mathbf{u}(\mathbf{x}+\mathbf{r})\rangle$ remains finite as $\nu \to 0$ (similarly to the dissipative term at finite k or ℓ in the energy budgets derived in § 6.1.3), so the last term in the right-hand side of equation 6.31 vanishes in that limit.

Note that the two limits $\nu \to 0$ and $r \to 0$ do not commute:

$$\lim_{\nu\to 0}\lim_{r\to 0} \nu\Delta_{\mathbf{r}}\langle \mathbf{u}(\mathbf{x})\cdot\mathbf{u}(\mathbf{x}+\mathbf{r})\rangle = \epsilon > 0,$$

$$\lim_{r\to 0}\lim_{\nu\to 0} \nu\Delta_{\mathbf{r}}\langle \mathbf{u}(\mathbf{x})\cdot\mathbf{u}(\mathbf{x}+\mathbf{r})\rangle = 0.$$

We are left with

$$\lim_{r\to 0}\lim_{\nu\to 0}\lim_{t\to+\infty} \nabla_{\mathbf{r}}\cdot\langle(\delta\mathbf{u})^2\delta\mathbf{u}\rangle = -4\epsilon. \tag{6.35}$$

Relation (6.35) can readily be integrated into $\langle\delta\mathbf{u}^3\rangle = -\frac{4}{3}\epsilon\mathbf{r}$, which you might encounter, referred to as the 4/3-law (Dubrulle 2019). In the next paragraph, we reformulate it in terms of the longitudinal structure function $S_3(r) = \langle\delta u_\parallel^3\rangle$, which gives a 4/5 instead of a 4/3. The two are equivalent for isotropic turbulence; what follows is essentially manipulations of the tensor structure of the vector structure function to express the result in terms of the longitudinal velocity increments, which are easier to measure experimentally.

From the energy flux to the third-order structure function Using homogeneity and isotropy, the third-order velocity structure function $S_3(r)$ can be related to the tensor $S_{ij,k}(r) = \langle u_i(\mathbf{x})u_j(\mathbf{x})u_k(\mathbf{x}+\mathbf{r})\rangle$:

$$S_3(r) = \frac{r^i r^j r^k}{r^3}\langle\delta u_i\delta u_j\delta u_k\rangle, \tag{6.36}$$

$$= 2\frac{r^i r^j r^k}{r^3}[S_{ij,k}(r) + S_{ik,j}(r) + S_{kj,i}(r)]. \tag{6.37}$$

Now, the most general form for $S_{ij,k}$ is

$$S_{ij,k}(r) = A(r)\delta_{ij}\frac{r_k}{r} + B(r)\left(\delta_{ik}\frac{r_j}{r} + \delta_{jk}\frac{r_i}{r}\right) + C(r)\frac{r_i r_j r_k}{r^3}. \tag{6.38}$$

Injecting into the above equation, we obtain

$$\begin{aligned} S_3(r) = 2\frac{r^i r^j r^k}{r^3}\Big[&A(r)\delta_{ij}\frac{r_k}{r} + B(r)\left(\delta_{ik}\frac{r_j}{r} + \delta_{jk}\frac{r_i}{r}\right) + C(r)\frac{r_i r_j r_k}{r^3} \\ &A(r)\delta_{ik}\frac{r_j}{r} + B(r)\left(\delta_{ij}\frac{r_k}{r} + \delta_{jk}\frac{r_i}{r}\right) + C(r)\frac{r_i r_j r_k}{r^3} \\ &A(r)\delta_{kj}\frac{r_i}{r} + B(r)\left(\delta_{ik}\frac{r_j}{r} + \delta_{ij}\frac{r_k}{r}\right) + C(r)\frac{r_i r_j r_k}{r^3}\Big] \end{aligned} \tag{6.39}$$

$$= 2\frac{r^i r^j r^k}{r^3}\left[(A+2B)\delta_{ij}\frac{r_k}{r} + (A+2B)\delta_{ik}\frac{r_j}{r} + (A+2B)\delta_{jk}\frac{r_i}{r} + 3C\frac{r_i r_j r_k}{r^3}\right], \tag{6.40}$$

$$= 6(A+2B) + 6C. \tag{6.41}$$

Enforcing incompressibility: $\partial^k S_{ij,k} = 0$, we obtain relations between the functions A, B and C. Using the relations $\partial_k f(r) = r_k/r f'(r)$ and $\partial_k(r_i/r) = \delta_{ik}/r - r_i r_k/r^3$, we obtain:

$$\partial^k S_{ij,k}(r) = \left[A'(r) + 2\frac{A(r)+B(r)}{r}\right]\delta_{ij} + \left[2B'(r) + C'(r) - 2\frac{B(r)-C(r)}{r}\right]\frac{r_i r_j}{r^2}. \tag{6.42}$$

The two terms in brackets vanish: in principle these two relations allow to express B and C as functions of A. A particular combination of these two terms yields simpler computations: it corresponds to

taking the trace of the tensor: $\partial_k S_i^{\ jk} = 0$:

$$3\left[A'(r) + 2\frac{A(r)+B(r)}{r}\right] + \left[2B'(r) + C'(r) - 2\frac{B(r)-C(r)}{r}\right] = 0, \tag{6.43}$$

$$[3A'(r) + 2B'(r) + C'(r)] + \frac{2}{r}[3A(r) + 2B(r) + C(r)] = 0. \tag{6.44}$$

The only solution of the differential equation $y' + 2y/r = 0$ which is finite at $r = 0$ is the one which vanishes identiquely. This yields

$$\left\{\begin{array}{l} A' + \frac{2}{r}(A+B) = 0, \\ 3A + 2B + C = 0. \end{array}\right. \text{ i.e. } \left\{\begin{array}{l} B = -A - \frac{r}{2}A', \\ C = rA' - A, \end{array}\right. \tag{6.45}$$

from which $S_3(r) = -12A(r)$ follows.

Above, we have used the relation $\langle \delta u_i \delta u_j \delta u_k \rangle = 2(S_{ij,k} + S_{ik,j} + S_{kj,i})$ which yields in particular $\nabla_{\mathbf{r}} \cdot \langle (\delta \mathbf{u})^2 \delta \mathbf{u} \rangle = 4\partial^j S_{ij}^{\ \ i}$. On the other hand,

$$\partial^j S_{ij}^{\ \ i} = \partial^j (A + 4B + C)\frac{r_j}{r}, \tag{6.46}$$

$$= \frac{2}{r}(A + 4B + C) + A' + 4B' + C', \tag{6.47}$$

$$= -rA'' - 7A' - 8A/r. \tag{6.48}$$

Taking the limits $t \to +\infty$ and $\nu \to 0$, and $r \ll \ell_f$ in the Karman-Howarth-Monin relation, we consider the differential equation

$$rA'' + 7rA' + 8\frac{A}{r} = \epsilon. \tag{6.49}$$

Under the change of variable $y = A/r$, $x = \ln r$, the differential equation becomes

$$y'' + 6y' + 15y = \epsilon. \tag{6.50}$$

The general solution is of the form $y = \alpha e^{\rho_+ x} + \beta e^{\rho_- x} + \epsilon/15$, with $\rho_\pm = -3 \pm i\sqrt{6}$. The only solution with a finite limit when $x \to -\infty$ ($r \to 0$) is $y = \epsilon/15$, which yields

$$\lim_{r\to 0}\lim_{\nu\to 0}\lim_{t\to+\infty} \frac{S_3(r)}{r} = -\frac{4}{5}\epsilon. \tag{6.51}$$

This is the $4/5$-law.

Note that we are assuming that $S_3(r)/r$ does not diverge, which is not guaranteed *a priori* after taking the limit $\nu \to 0$, but is compatible with the phenomenology described above (according to which $\delta u_\parallel \sim r^{1/3}$) and supported by empirical evidence.

In the isotropic case, the Karman-Howarth relation can be written as:

$$\frac{\partial S_2}{\partial t} = -\frac{1}{3r^4}\frac{\partial}{\partial r}(r^4 S_3) - \frac{4}{3}\epsilon + \frac{2\nu}{r^4}\frac{\partial}{\partial r}\left(r^4 \frac{\partial S_2}{\partial r}\right), \tag{6.52}$$

which directly relates the structure functions S_2 and S_3 (Landau and Lifchitz 1971; Falkovich 2011). From here the $4/5$-law follows seemingly faster than in our derivation, but the above form of the Karman-Howarth relation actually involves most of the work we did above.

Finally, it should be noted that the $4/5$ law expresses the *irreversibility* of turbulence: under the time reversal transform, S_3 should change sign, but according to the $4/5$ law, $S_3 < 0$ as long as the energy dissipation rate $\epsilon > 0$ is finite.

6.3 Universality and self-similarity

6.3.1 Landau's objection to universality

Soon after Kolmogorov's 1941 theory was published, it was argued by Landau that the non-dimensional constants could not be universal[5].

The basic idea is to consider N experiments with different average energy dissipation rates ϵ_i. Assuming universality, we may write in each case $S_n^{(i)}(r) = C_n(\epsilon_i r)^{n/3}$. Now we further assume that the ensemble average still has the same scaling, with $S_n(r) = \sum_i S_n^{(i)}(r)/N$ and $\epsilon = \sum_i \epsilon_i / N$, which yields

$$\left(\frac{1}{N}\sum_{i=1}^{N}\epsilon_i\right)^{n/3} = \frac{1}{N}\sum_{i=1}^{N}\epsilon_i^{n/3}, \tag{6.53}$$

which only holds for all values of ϵ_i if $n = 3$.

Instead of relying on the Kolmogorov universality hypotheses, which directly postulates universality, one may think in terms of symmetries[6].

[5] see Frisch (1995, § 6.4)

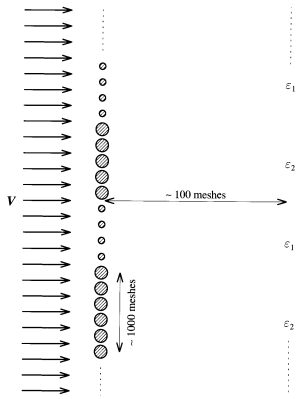

Figure 6.6: Exemple of grid turbulence setup illustrating Landau's objection (from Frisch (1995)).

[6] this is the presentation adopted in the book by Frisch (1995) from the beginning

6.3.2 Self-similarity in the Kolmogorov theory

Probability distribution function for longitudinal velocity increments under Kolmogorov's universality hypotheses Under the second universality hypothesis of Kolmogorov (see § 6.1), the PDF of the longitudinal velocity increment $\delta u_\parallel(r)$ of a statistically homogeneous and isotropic random field $\mathbf{u}$ can only depend on r, the average energy dissipation rate ϵ and the argument $\delta u_\parallel$ itself. Hence, dimensional analysis yields the following form:

$$p_r(\delta u_\parallel) = (\epsilon r)^{-1/3} p_0\left(\delta u_\parallel (\epsilon r)^{-1/3}\right), \tag{6.54}$$

where p_0 is a universal (non-dimensional) function. This means that the PDF retains its shape across scales. It can for instance be

The fact that p_r has the dimension of the inverse of a velocity can be seen easily by considering the normalization condition.

expressed using the PDF at large-scale:

$$p_r(\delta u_\parallel) = \left(\frac{r}{L}\right)^{-1/3} p_L\left(\delta u_\parallel \left(\frac{r}{L}\right)^{-1/3}\right). \tag{6.55}$$

This can also be expressed by considering the random variable $\delta u_\parallel(r)$: in law, $\delta u_\parallel(r) = (r/L)^{1/3}\delta u_\parallel(L)$.

Of course, computing the moments of the PDF (6.54), we recover the expected form for the structure functions: $S_n(r) = C_n(\epsilon r)^{n/3}$, with $C_n = \int_{\mathbb{R}} u^n p_0(u)du$. For larger and larger values of n, the coefficient C_n is more and more determined by the tails of the distribution p_0.

Self-similarity A random field $\phi(\mathbf{x})$ is said to be *self-similar* if there exists a real number h such that for all $\lambda \in \mathbb{R}$, the random fields $\phi(\lambda\mathbf{x})$ and $\lambda^h\phi(\mathbf{x})$ have the same probability law. Assuming the probability densities defined by $P[\phi(\mathbf{x}) \in [u, u+du]] = p_{\mathbf{x}}(u)du$ exist, self-similarity amounts to the condition[7]:

$$p_{\lambda\mathbf{x}}(u) = \lambda^{-h} p_{\mathbf{x}}(\lambda^{-h}u), \tag{6.56}$$

From (6.54), it is clear that, under the Kolmogorov universality assumptions, the velocity increments satisfy condition (6.56), and therefore, are self-similar.

[7] as can be seen from

$$P[\phi(\lambda\mathbf{x}) \in [u, u+du]] = p_{\lambda\mathbf{x}}(u)du,$$
$$P[\lambda^h\phi(\mathbf{x}) \in [u, u+du]] = P[\phi(\mathbf{x}) \in [\lambda^{-h}u, \lambda^{-h}(u+du)]]$$
$$= \lambda^{-h} p_{\mathbf{x}}(\lambda^{-h}u)du.$$

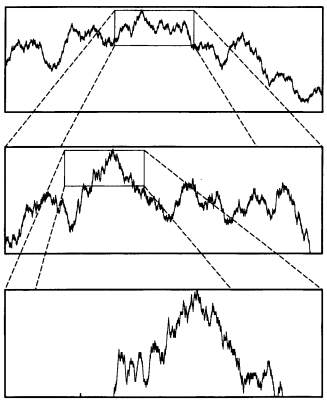

Figure 6.7: Self-similar random function: the statistical properties of the signal do not change when zooming in (Frisch 1995).

6.3.3 *Another look at Kolmogorov theory*

We have just shown that the Kolmogorov universality hypotheses imply self-similarity of the velocity increments. Let us now investigate the converse.

Let us make the following assumptions:

H1 — Symmetries In the limit of infinite Reynolds numbers, all the possible symmetries of the Navier-Stokes equations, usually broken by the mechanism producing the turbulent flow, are restored in a statistical sense at small-scales and away from the boundaries.

H2 — Self-similarity In the limit of infinite Reynolds numbers, the turbulent flow is self-similar at small scales, i.e. it possesses a unique scaling exponent h.

H3 — Dissipation anomaly In the limit of infinite Reynolds numbers, the turbulent flow has a finite non-vanishing mean rate of energy dissipation ϵ per unit mass.

Structure functions From the self-similarity hypothesis, we have $S_n(\lambda r) = \lambda^{hn} S_n(r)$, from which it follows that $S_n(r) \propto r^{hn}$. Using the 4/5-law, it follows that the scaling exponent is $h = 1/3$, and

$$S_n(r) = C_n(\epsilon r)^{n/3}, \tag{6.57}$$

with dimensionless constants C_n. The $4/5$-law also implies $C_3 = -4/5$, which is clearly universal, but we do not assume that the other constants are.

Furthermore, it can be directly checked that self-similarity implies the PDF (6.54) for longitudinal velocity gradients, using $p_{\lambda r}(u) = \lambda^{-h} p_r(\lambda^{-h} u)$.

7
Intermittency

7.1 The intermittency phenomenon

7.1.1 Non-Gaussianity of small-scale increments

K41 theory predicts that the PDF of longitudinal velocity increments retains its shape across scales (see Eq. (6.55)): if it is Gaussian at large scale, it remains Gaussian at all scales.

This is incompatible with observations (Fig. 7.1); while velocity increments have Gaussian statistics at large separations (like the velocity field itself), they develop fat tails as we move to smaller and smaller separations. This means that extreme (positive or negative) values of velocity increments are much more frequent in reality than predicted by Kolmogorov theory. Note that the PDF of velocity gradients is also non-Gaussian.

Self-similarity also makes Gaussian large-scale statistics incompatible with the 4/5-law: in Kolmogorov theory, skewness in the inertial range, required by the 4/5-law cannot be generated spontaneously.

It seems clear that the scale invariance symmetry is broken.

We shall briefly study in a problem set the *multifractal* model, which assumes that instead of just one (1/3), the velocity increment has a whole spectrum of scaling exponents (see Sec. 7.4).

7.1.2 Anomalous scaling

Let us introduce the scaling exponents of the structure functions:

$$S_n(r) \sim r^{\zeta(n)}. \tag{7.1}$$

Kolmogorov theory predicts $\zeta(n) = n/3$ (6.4).

In practice, we observe a deviation from Kolmogorov theory (see Fig. 7.3). This is called *anomalous scaling*, or *intermittency*. It means that, while low-order statistics (energy spectrum) are accurately described by Kolmogorov theory, higher-order statistics are not. For

Reference: Frisch (1995, Chapter 8)

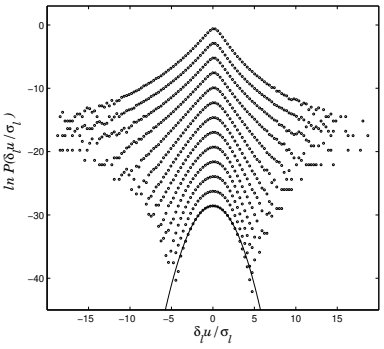

Figure 7.1: PDF of longitudinal velocity increments at various scales (figure by L. Chevillard).

For self-similar velocity increments, $S_3(r) = (r/L)\langle \delta u_{\parallel}(L)^3 \rangle$.

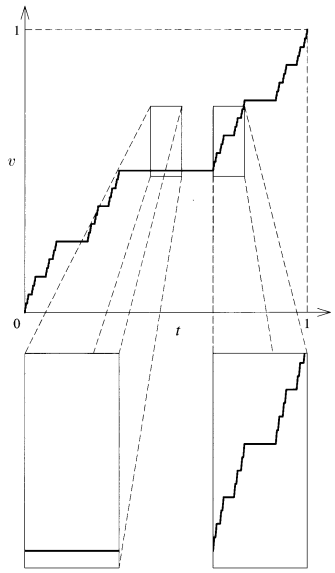

Figure 7.2: An example of an intermittent signal, the Devil's staircase, from Frisch (1995).

such observables, the energy cascade process cannot be characterized by the average energy dissipation rate ϵ alone; the fluctuations of the energy dissipation field matter. Phenomenological models considering ϵ as a random variable with known statistical properties provide a much better fit to the scaling exponents $\zeta(n)$ (Fig. 7.3).

It should be noted that anomalous scaling is not restricted to solutions of the Navier-Stokes equations. For instance, let us consider the problem of *passive scalar advection*:

$$\partial_t \theta + \mathbf{v} \cdot \nabla \theta = \kappa \Delta \theta, \tag{7.2}$$

where $\mathbf{v}$ is a random field. Instead of being described by the invariant measure for the Navier-Stokes equations, $\mathbf{v}$ can be taken as a Gaussian, white in time random field (this is the *Kraichnan model*). Under those circumstances, the anomalous exponents for the scalar $\langle \delta\theta^n \rangle \sim r^{\zeta(n)}$ have been computed analytically (Falkovich, Gawedzki, and Vergassola 2001). Another exemple is Burgers turbulence (e.g. Bec and Khanin 2007).

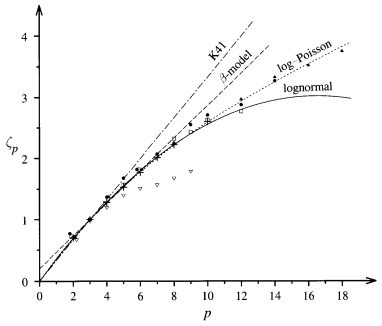

Figure 7.3: Scaling exponents $\zeta(n)$ as measured in experiments (points) and predicted by Kolmogorov theory or other models (Frisch 1995).

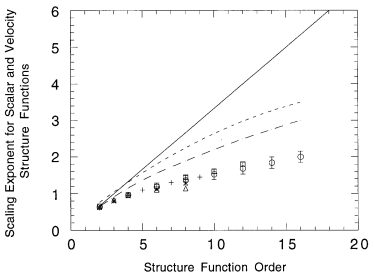

Figure 7.4: Scaling exponents for the passive scalar in lab experiments (points), for the velocity field (short dash), and Kolmogorov-Obhukov-Corrsin scaling (solid line).

7.2 *The log-normal model (KO62)*

7.2.1 *Fluctuations of the energy dissipation rate*

To account for the *intermittency* phenomenon, the K41 theory was revised with various models of the energy cascade. The first one was due to Kolmogorov (1962) and Obukhov (1962). We describe the main ideas below, at a qualitative level.

In Chapter 6, we obtained predictions for the statistical properties of the velocity field by assuming that they only depended on the average energy dissipation. In fact, energy dissipation is a random field (see Fig. 7.5), itself with complex statistical properties, deriving from the velocity field.

The *refined similarity hypothesis* replaces the average energy dissipation rate ε used in Chapter 6 by a local average of the energy dissipation field ε_ℓ:

$$\varepsilon_\ell(\mathbf{x}) = \frac{3}{4\pi\ell^3} \int_{\|\mathbf{x}-\mathbf{y}\| \leq \ell} \nu(\nabla \mathbf{u})^2 d\mathbf{y}. \tag{7.3}$$

This can be seen as a filtered version of the energy dissipation field.

All the statistical properties obtained above remain valid, only if they are understood as conditioned on the value of this local energy dissipation rate. Then, to obtain the unconditioned statistics, one should average over the probability distribution $p(\varepsilon_\ell)$ for the local energy dissipation rate ε_ℓ.

(Monin and Yaglom 1971, § 25.1 and 25.2)

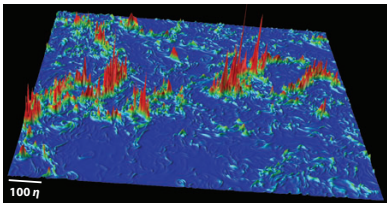

Figure 7.5: A snapshot of the dissipation field in a DNS (Ishihara, Gotoh, and Kaneda 2009).

7.2.2 *Structure functions*

Because it is linear in ε, the 4/5-law holds regardless of the probability distribution $p(\varepsilon_\ell)$. This means that the third-order structure function is only determined by the mean energy dissipation rate. On the other hand, other structure functions are affected by this approach; they depend on the full probability distribution of the energy dissipation rate. This holds for high-order structure functions but also for the energy spectrum, which should in principle exhibit *intermittency corrections*. As we shall see, these corrections are quite small for the energy spectrum.

7.2.3 *PDF of the energy dissipation rate*

(Monin and Yaglom 1971, pp. 611–612)

Kolmogorov (1962) and Obukhov (1962) suggested that the local energy dissipation rate follows a *log-normal* distribution (i.e. $\ln \varepsilon_\ell$ is a Gaussian random variable at all scales). They further assumed that, for large Reynolds numbers, the variance behaves as follows: $\sigma_\ell^2 \equiv \mathbb{E}(\ln \varepsilon_\ell - \mathbb{E}[\ln \varepsilon_\ell])^2 = \Lambda_0 - \mu \ln \ell$. The mean energy dissipation rate is given by $\mathbb{E}[\varepsilon_\ell] = e^{m_\ell + \sigma_\ell^2/2}$, with $m_\ell = \mathbb{E}[\ln \varepsilon_\ell]$. Because it should not depend on scale, we can impose $m_\ell = m - \sigma_\ell^2/2$, with $m = \ln \mathbb{E}[\varepsilon_\ell]$.

$$p(\varepsilon_\ell) = \frac{1}{\sqrt{2\pi\sigma_\ell^2 \varepsilon_\ell^2}} e^{-\frac{(\ln \varepsilon_\ell - m_\ell)^2}{2\sigma_\ell^2}}$$

7.2.4 *Intermittency corrections*

(Monin and Yaglom 1971, § 25.4)

A direct computation yields

$$S_n(\ell) = \mathbb{E}[C_n(\varepsilon_\ell \ell)^{n/3}] = C_n \ell^{n/3} e^{n m_\ell/3 + n^2 \sigma_\ell^2/18}, \tag{7.4}$$

$$= C_n e^{nm/3 + \Lambda_0 n(n-3)/18} \ell^{n/3 - \mu n(n-3)/18}, \tag{7.5}$$

$$= C_n (\mathbb{E}[\varepsilon_\ell]\ell)^{\frac{n}{3}} \left(\frac{\ell}{L}\right)^{-\mu n(n-3)/18}, \tag{7.6}$$

assuming $\Lambda_0 = \mu \ln L$ with L the integral scale. Hence, the scaling exponents are given by $\zeta_n = n/3 - \mu n(n-3)/18$. They are represented in Fig. 7.3; it is clear that they present a better fit to experimental data than the Kolmogorov 41 theory. However, the relative agreement holds only until approximately $n = 12$. In fact, the scaling exponents should ultimately become negative, which does not make much physical sense. Furthermore, the Kolmogorov-Obukhov theory breaks the Novikov inequality.

Because $\zeta_2 = 2/3 + \mu/9$, the energy spectrum should scale like $E(k) \propto k^{-5/3 - \mu/9}$.

In practice the measured value of the intermittency parameter is $\mu \approx 0.23$. Clearly, this corresponds to a very small correction for the energy spectrum.

7.3 *The β-model*

In § 7.2, we have assumed that the local energy dissipation rate has a log-normal distribution; we do not know where this distribution comes from. An alternative strategy is to modify the phenomenology of the energy cascade: the β-model is an example of such an approach, based on the velocity field. The idea is that the energy cascade is not "space filling": energy transfers to smaller scales occur in a localized manner in space. The location of "active" eddies form a subset of the domain, on which the velocity increments are still self-similar (in the inertial range). This set has a *fractal* structure, and it is characterized by its codimension D (i.e. it has dimension $3 - D$).

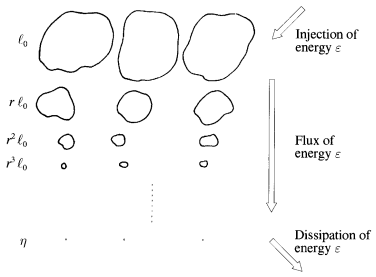

Figure 7.6: The cascade picture modified to account for intermittency according to the beta model (Frisch 1995).

The cascade phenomenology is then easily adapted from the Kolmogorov case (§ 6.1.4): the typical energy at scale ℓ is given by $p_\ell v_\ell^2$, where $p_\ell = (\ell/L_0)^{3-D}$ is the fraction of space filled with active eddies. The timescale for energy transfers to scale smaller than ℓ is still given by the eddy turnover time $t_\ell \sim \ell/v_\ell$, and requiring the energy flux to be constant in the inertial range, we obtain $\Pi_\ell \sim \epsilon \sim p_\ell v_\ell^3/\ell$, and therefore:

$$v_\ell \sim v_0 \left(\frac{\ell}{L_0}\right)^{1/3-(3-D)/3} \sim (\epsilon\ell)^{1/3} \left(\frac{\ell}{L_0}\right)^{-(3-D)/3}. \tag{7.7}$$

As mentioned above, the velocity increments are still self-similar, but the scaling exponent is now $h = 1/3 - (3-D)/3$. The structure functions can be obtained directly:

$$S_n(\ell) \sim p_\ell v_\ell^n \sim v_0^n \left(\frac{\ell}{L_0}\right)^{\zeta(n)}, \text{ with } \zeta(n) = \frac{n}{3} + (3-D)\left(1 - \frac{n}{3}\right). \tag{7.8}$$

The scaling exponents are still linear in n; we have only modified the slope of the line. Figure 7.3 shows that, with $D = 2.8$ it fits reasonably well the experimental data at low n, but not at all at large n.

We have still not explained why this model is called the β-model. This parameter comes from a discretization of the cascade: at each step eddies of size ℓ_n "break up" into eddies of size $\ell_{n+1} = \gamma\ell_n$, with $0 < \gamma < 1$. Then $p_{\ell_n} = \beta^n = \beta^{\frac{\ln(\ell_n/L_0)}{\ln\gamma}} = (\ell_n/L_0)^{3-D}$, hence $3 - D = \ln\beta/\ln\gamma$.

7.4 *The multifractal approach*

We have seen above that the self-similarity assumption means that the longitudinal velocity increment at scale ℓ is related to the increment at the integral scale through $\delta u_\parallel(\ell) = (\frac{\ell}{L})^h \delta u_\parallel(L)$, with the

choice $h = 1/3$ determined by the $4/5$-law. Experimentally, we observe $\delta u_\parallel(\ell)$ to be a Gaussian random variable at large-scale ($\ell = L$) but not at small scale (e.g. $\ell = \lambda$). We have discussed in 7.1 the manifestations of the breakdown of self-similarity.

An approach which has been suggested to account for intermittency is to represent the longitudinal velocity increment as the product of a Gaussian random variable corresponding to the velocity increment at the integral scale and a scale factor which is itself random. More precisely,

$$\delta u_\parallel(\ell) = \left(\frac{\ell}{L}\right)^h \times \delta u_\parallel(L), \tag{7.9}$$

with $\delta u_\parallel(L) \sim N(0, \sigma^2)$ and h a random exponent with PDF

$$p_\ell(h) = \frac{1}{\mathcal{Z}(\ell)} \left(\frac{\ell}{L}\right)^{1-\mathcal{D}(h)}, \tag{7.10}$$

and $\mathcal{D}(h)$ is a function independent of the scale ℓ.

It can be shown that the PDF for the velocity increment takes the form:

$$p_\ell(\delta u_\parallel) = \frac{1}{\sigma}\left(\frac{\ell}{L}\right)^{-h} \int p_0\left(\frac{\delta u_\parallel}{\sigma}\left(\frac{\ell}{L}\right)^{-h}\right) p_\ell(h) dh, \tag{7.11}$$

with $p_0(x) = e^{-x^2/2}/\sqrt{2\pi}$ the standard Gaussian distribution, which is interpreted as a sum of self-similar PDFs with different exponents h. The interpretation is that there exists a range of scaling exponents h, corresponding to coexisting self-similar energy transfers through scales occurring on regions in space with fractal dimension $\mathcal{D}(h)$.

The structure functions of even order can be shown to have power-law scalings: $S_{2n}(\ell) \sim \left(\frac{\ell}{L}\right)^{\zeta_{2n}}$, with $\zeta_n = \inf_h[nh + 1 - \mathcal{D}(h)]$ the Legendre-Fenchel transform of the multifractal spectrum $\mathcal{D}$ (assuming $\inf_h[1 - \mathcal{D}(h)] = 0$). As a consequence, ζ_n is always a concave function of n in this model.

The log-normal model (see § 7.2) is recovered with the choice $\mathcal{D}(h) = 1 - \frac{(h-c_1)^2}{2c_2}$, which yields $\zeta_n = c_1 n - \frac{c_2}{2} n^2$, which coincides with the KO62 prediction for the choice $c_1 = 1/3 + \mu/6$, $c_2 = \mu/9$.

Another well-known model which fits quite well the experimental data is the She-Leveque model[1], corresponding to the choice $\mathcal{D}(h) = -1 + 3\left[\frac{1+\ln(\ln(3/2))}{\ln(3/2)} - 1\right]\left(h - \frac{1}{9}\right) - \frac{3}{\ln(3/2)}\left(h - \frac{1}{9}\right)\ln\left(h - \frac{1}{9}\right)$. After a little bit of algebra, we get $\zeta_n = \frac{n}{9} + 2\left[1 - \left(\frac{2}{3}\right)^{\frac{n}{3}}\right]$. This model is compatible with the $4/5$-law, as it gives $\zeta_3 = 1$, and predicts a small correction to the $2/3$-law: $\zeta_2 \approx 0.7$.

[1] The model is presented in a less cryptic form in She and Leveque (1994).

8
The passive scalar problem

Let us consider the problem of passive scalar advection-diffusion:

$$\partial_t \theta + \mathbf{u} \cdot \nabla \theta = \kappa \Delta \theta. \tag{8.1}$$

We consider this as an abstract problem, with θ a dimensionless scalar field. In reality, it could represent the concentration of some chemical species for instance, or the temperature field. The velocity field $\mathbf{u}$ is prescribed (usually it is a random field) and we assume it is divergence free. It can be a solution of the Navier-Stokes equations, but it does not have to (see for instance the Kraichnan model in § **??**).

See for instance Lesieur (2008, § 6.10).

Adding a source term Q in the right-hand side of (8.1), passive scalar variance budget reads

$$\frac{d\Xi}{dt} = \langle Q\theta \rangle - \epsilon_\theta, \tag{8.2}$$

with $\Xi = \langle \theta^2 \rangle / 2$ the scalar variance and $\epsilon_\theta = -\kappa \langle \theta \Delta \theta \rangle = \kappa \langle (\nabla \theta)^2 \rangle$ the mean scalar variance dissipation rate.

Without forcing and dissipation ($Q = \kappa = 0$), all the norms of the scalar field are conserved (including the scalar variance Ξ), or more generally, $\int s(\theta(\mathbf{x}))d\mathbf{x}$ for any function s. The scalar field also remains bounded. These properties are the same as in 2D turbulence.

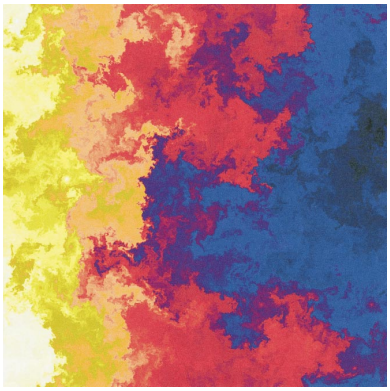

Figure 8.1: A snapshot of passive scalar turbulence (Falkovich, Gawedzki, and Vergassola 2001).

8.1 *Phenomenology*

We assume that the statistics of the velocity field are well described by Kolmogorov theory. We denote by ν the molecular viscosity of the fluid, and introduce the Prandtl number $Pr = \nu/\kappa$.

We further assume that the statistics of all the fields are stationary, homogeneous and isotropic, and denote by $\langle \cdot \rangle$ the average with respect to the invariant measure. The mean energy dissipation rate is $\epsilon = \langle \|\nabla \mathbf{u}\|^2 \rangle$.

The statistical properties of the scalar field are *a priori* governed by two non-dimensional numbers: the Reynolds number and the Prandtl number.

By analogy with the first Kolmogorov assumption of universality (see § 6.1), we may assume that the (small-scale) statistics of the scalar field are entirely determined by only five parameters: the scale r, the energy and scalar variance dissipation rates ϵ and ϵ_θ, the viscosity ν and the diffusivity κ.

If we assume that there exists and inertial range where neither dissipation nor diffusion are felt, dimensional analysis tells us that the scalar variance spectrum in that range should read

$$F_\theta(k) = C_\theta \epsilon_\theta^{-3\beta} \epsilon^{\beta} k^{2\beta-1}, \tag{8.3}$$

with β an undetermined exponant and C_θ a non-dimensional constant.

$$\begin{aligned}[F_\theta(k)] &= L,\\ [\epsilon_\theta] &= T^{-1},\\ [\epsilon] &= L^2.T^{-3},\\ [k] &= L^{-1}.\end{aligned}$$

By analogy with the Kolmogorov scale η, we introduce a scale η_θ where inertial effects and diffusion become comparable, i.e. the local Péclet number $\delta u \eta_\theta / \kappa$ is of order one. That scale depends on the scaling properties of the velocity increment δu, and two cases should be considered:

- If $\eta_\theta > \eta$, δu is in the inertial range and the Kolmogorov scaling $\delta u \sim (\epsilon r)^{1/3}$ should be used. We obtain $\eta_\theta/\eta \sim Pr^{-3/4}$. This corresponds to the $Pr < 1$ regime.

  In this regime, for $\eta < \eta_\theta < \ell < \ell_f$ in the *inertial-convective range*, the scalar variance dissipation rate can be estimated as the scalar variance at scale $k = \ell^{-1}$, $kF_\theta(k)$, divided by the eddy turnover time $\tau_k = 1/\sqrt{k^3 E(k)}$:

$$\epsilon_\theta \sim \frac{kF_\theta(k)}{\tau_k}, \quad F_\theta(k) \sim \epsilon_\theta \epsilon^{-1/3} k^{-5/3}. \tag{8.4}$$

  This is the *Kolmogorov-Obhukov-Corrsin* spectrum. It corresponds to the parameter $\beta = -1/3$ in the generic spectrum above.

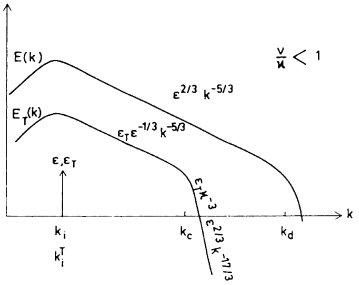

Figure 8.2: Schematic passive scalar spectrum in the $Pr < 1$ case (Lesieur 2008).

- If $\eta > \eta_\theta$, δu is in the dissipative range and we can estimate $\delta u \sim \nu/\eta$, which yields $\eta_\theta/\eta \sim Pr^{-1}$, with $Pr > 1$. We should still observe the Kolmogorov-Obhukov-Corrsin spectrum in the range of scales $\eta < \ell < \ell_f$. Now, in the range of scales $\eta_\theta < \ell < \eta$, called the *viscous-convective range*, the typical time scale becomes the viscous time $\tau_\nu \sim \eta^2/\nu$, from which we obtain:

$$\epsilon_\theta \sim \frac{kF_\theta(k)}{\tau_\nu}, \quad F_\theta(k) \sim \epsilon_\theta \sqrt{\frac{\nu}{\epsilon}} k^{-1}. \tag{8.5}$$

  This is known as the *Batchelor* spectrum. Note that it does not fit the general form by dimensional analysis above, which assumed that viscous effects were negligible.

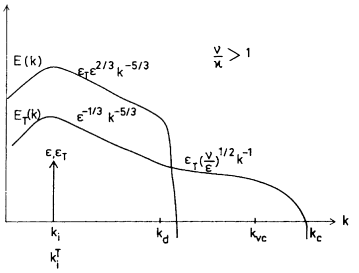

Figure 8.3: Schematic passive scalar spectrum in the $Pr > 1$ case (Lesieur 2008).

8.2 Karman-Howarth equation

Let us denote $\delta\theta = \theta(\mathbf{x}+\mathbf{r}) - \theta(\mathbf{x})$ the scalar increments, and $R = \langle\theta(\mathbf{x})\theta(\mathbf{x}+\mathbf{r})\rangle$ the scalar covariance. We assume homogeneous statistics, so that $\delta\theta$ and R only depend on $\mathbf{r}$.

The evolution of the scalar covariance is given by an equation analogous to the Karman-Howarth-Monin equation (6.31):

$$\partial_t R = \frac{1}{2}\nabla_{\mathbf{r}} \cdot \langle \delta\theta^2 \delta\mathbf{u}\rangle + \langle\theta(\mathbf{x})[Q(\mathbf{x}+\mathbf{r}) + Q(\mathbf{x}-\mathbf{r})]\rangle + 2\kappa\Delta_{\mathbf{r}} R. \quad (8.6)$$

It follows that, at scales smaller than the correlation scale of the source (or the scalar itself) and in a stationary state, we have the relation:

$$\langle \delta\theta^2 \delta\mathbf{u}\rangle = -\frac{4}{3}\epsilon_\theta \mathbf{r} + 2\kappa\nabla_{\mathbf{r}}\langle\delta\theta^2\rangle, \quad (8.7)$$

and in terms of longitudinal increments:

$$\langle \delta\theta^2 \delta u_\parallel\rangle = -\frac{4}{3}\epsilon_\theta r + 2\kappa\frac{d}{dr}\langle\delta\theta^2\rangle. \quad (8.8)$$

In particular, the relation $\langle \delta\theta^2 \delta u_\parallel\rangle = -4/3\epsilon_\theta r$ should hold in the inertial range corresponding to the direct cascade of scalar variance. This relation is analogous to the 4/5-law.

9
Closure methods

This chapter is mainly written after Lesieur (2008, Chap. 7).

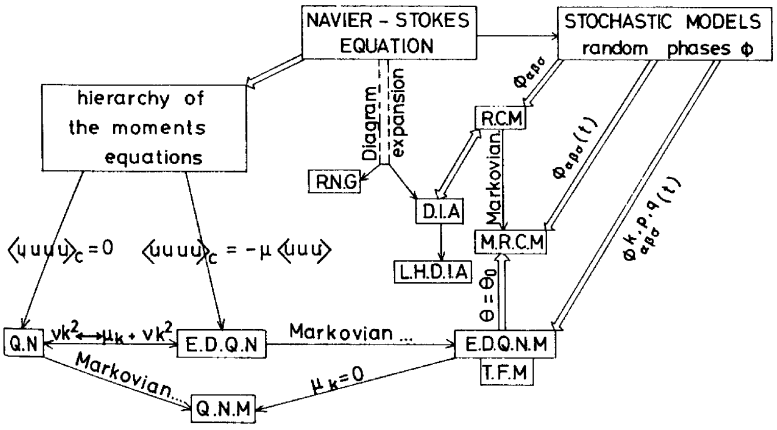

Figure 9.1: Schematic of the different closure theories (Lesieur 2008).

Let us write in a symbolic manner the first few equations in the hierarchy of moments:

$$(\partial_t + \nu(k^2 + k'^2))\langle \hat{u}_i(\mathbf{k})\hat{u}_j(\mathbf{k}')\rangle = \langle \hat{u}\hat{u}\hat{u}\rangle, \tag{9.1}$$

$$(\partial_t + \nu(k^2 + p^2 + q^2))\langle \hat{u}_i(\mathbf{k})\hat{u}_j(\mathbf{p})\hat{u}_l(\mathbf{q})\rangle = \langle \hat{u}\hat{u}\hat{u}\hat{u}\rangle. \tag{9.2}$$

Due to the non-linearity in the Navier-Stokes equations, moments of order n depend on moments of order $n+1$. This is the *closure problem* already alluded to earlier. In this chapter, we present some classical theories to close the hierarchy of moments and compute directly the statistics of homogeneous isotropic turbulence. All these theories are based on some arbitrary assumptions. While many closure theories have been suggested (see Fig. 9.1), we focus here on the *quasi-normal* family of closures.

9.1 *Quasi-normal closure*

Chou (1940), Millionshchikov (1941), Proudman and Reid (1954), Tatsumi (1957), and Tatsumi (1980)

It would be tempting to start by assuming that the Fourier coefficients of the velocity field have a joint Gaussian distribution (in this case, the statistics would be entirely determined by the velocity covariance tensor, which would satisfy a closed equation), however we have already seen before that non-Gaussianities are essential to the properties of homogeneous turbulence (for instance, according to Eq. (3.41), the energy flux across scales is due to a non-zero third order moment). Hence, the simplest (and earliest) closure approximation is to assume that the fourth-order cumulant vanishes, but third-order cumulants need not. In that case, fourth-order moments are given as combinations of second-order moments[1], which we shall write symbolically as $\langle \hat{u}\hat{u}\hat{u}\hat{u}\rangle = \sum\langle \hat{u}\hat{u}\rangle\langle \hat{u}\hat{u}\rangle$. Hence, Eq. (9.2) is replaced by

[1] For a centered Gaussian random variable, the fourth-order cumulant is $c_4 = m_4 - 3m_2$.

$$(\partial_t + \nu(k^2+p^2+q^2))\langle \hat{u}_i(\mathbf{k})\hat{u}_j(\mathbf{p})\hat{u}_l(\mathbf{q})\rangle = \sum\langle \hat{u}\hat{u}\rangle\langle \hat{u}\hat{u}\rangle, \tag{9.3}$$

and the hierarchy is closed. Integrating this equation allows to write explicitly third-order moments in terms of the velocity covariance. This expression can then be injected into Eq. (9.1) to obtain a closed equation for the velocity covariance in Fourier space $\hat{U}_{ij}(\mathbf{k})$, and then, after taking the trace, a closed equation for the energy spectrum:

$$(\partial_t + 2\nu k^2)E(k,t) = \int_0^t d\tau \int d\mathbf{p}d\mathbf{q}e^{-\nu(k^2+p^2+q^2)(t-\tau)}S(\mathbf{k},\mathbf{p},\mathbf{q},\tau), \tag{9.4}$$

with

$$S(\mathbf{k},\mathbf{p},\mathbf{q},\tau) = \frac{k^3}{pq}a(\mathbf{k},\mathbf{p},\mathbf{q})E(p,\tau)E(q,\tau) - \frac{k}{2pq}E(k,\tau)[p^2 b(\mathbf{k},\mathbf{p},\mathbf{q})E(q,\tau) + q^2 b(\mathbf{k},\mathbf{q},\mathbf{p})E(p,\tau)], \tag{9.5}$$

$$a(\mathbf{k},\mathbf{p},\mathbf{q}) = \frac{1-xyz-2y^2z^2}{2}, \quad b(\mathbf{k},\mathbf{p},\mathbf{q}) = \frac{p(xy+z^3)}{k}, \tag{9.6}$$

$$x = \frac{\mathbf{p}\cdot\mathbf{q}}{pq}, \quad y = \frac{\mathbf{k}\cdot\mathbf{q}}{kq}, \quad z = \frac{\mathbf{p}\cdot\mathbf{k}}{pk}. \tag{9.7}$$

Using $a(\mathbf{k},\mathbf{p},\mathbf{q}) = (b(\mathbf{k},\mathbf{p},\mathbf{q}) + b(\mathbf{k},\mathbf{q},\mathbf{p}))/2$, the equation can be further simplified into:

$$(\partial_t + 2\nu k^2)E(k,t) = \int_0^t d\tau \int d\mathbf{p}d\mathbf{q}e^{-\nu(k^2+p^2+q^2)(t-\tau)}\frac{k}{pq}b(\mathbf{k},\mathbf{p},\mathbf{q})[k^2E(p,\tau) - p^2E(k,\tau)]E(q,\tau). \tag{9.8}$$

This equation has been solved numerically: at large enough (but still very moderate) Reynolds numbers, the energy spectrum becomes negative (see Fig. 9.2). Similar results have been obtained for the spectrum of a passive scalar (O'Brien and Francis 1962). The reason

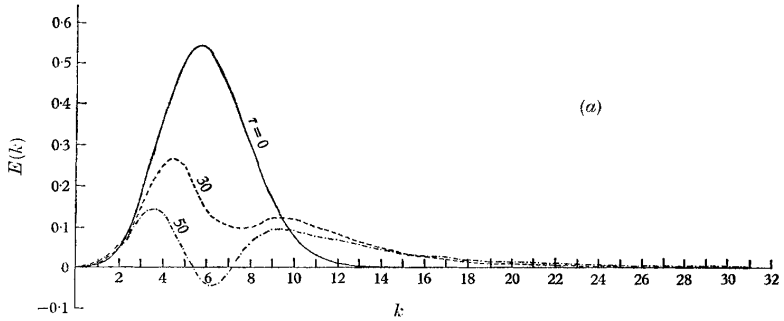

Figure 9.2: Numerical solution of Eq. (9.8): after some time the energy spectrum becomes negative (Ogura 1963).

for this behavior is that in the quasi-normal approximation, third order moments develop in an excessive manner. In reality, fourth-order cumulants (which are neglected here) should act to damp this growth. Better theories should account for this effect: we present below simple attemps to fix this problem.

9.2 *Eddy-damped quasi-normal markovian closure*

The first suggestion (Orszag 1970) to fix the *realizability* issue of the quasi-normal closure was to introduce explicitly a linear damping term for third-order moments in Eq. (9.3):

$$(\partial_t + \nu(k^2+p^2+q^2) + \mu_{kpq})\langle \hat{u}_i(\mathbf{k})\hat{u}_j(\mathbf{p})\hat{u}_l(\mathbf{q})\rangle = \sum \langle \hat{u}\hat{u}\rangle\langle \hat{u}\hat{u}\rangle, \quad (9.9)$$

For isotropic flows, it was suggested to construct the *eddy-damping rate* μ_{kpq} from the eddy-turnover time in a symmetric way: $\mu_{kpq} = \mu_k + \mu_p + \mu_q$ with $\mu_k = \sqrt{k^3 E(k)}$. If $E(k)$ is steeper than k^{-3}, μ_k becomes a decreasing function of k: the effect of damping is smaller towards smaller scales, which is counter-intuitive. As a consequence, the alternative choice $\mu_k = \sqrt{\int_0^k p^2 E(p)dp}$, which increases monotonically with k, has also been used (Pouquet et al. 1975, e.g.). The equation for the energy spectrum becomes:

$$(\partial_t + 2\nu k^2)E(k,t) = \int_0^t d\tau \int d\mathbf{p}d\mathbf{q} e^{-[\mu_{kpq}+\nu(k^2+p^2+q^2)](t-\tau)} \frac{k}{pq} b(\mathbf{k},\mathbf{p},\mathbf{q})[k^2E(p,\tau) - p^2E(k,\tau)]E(q,\tau), \quad (9.10)$$

referred to as the Eddy-Damped Quasi-Normal (EDQN) model.

In fact, the eddy-damping term is not sufficient to ensure *realizability* (positive energy spectrum). Orszag showed that this can be achieved by a process referred to as *Markovianization*. It consists in assuming that there is a time-scale separation between the characteristic time with which velocity covariance evolves (assumed to be on the order of the large eddy-turnover time, i.e. the characteristic time scale of energy containing scales) and the timescale

$[\mu_{kpq} + \nu(k^2 + p^2 + q^2)]^{-1}$ which controls the exponential damping of contributions to the third-order moment, assumed to be much smaller. The resulting equations are the Eddy-Damped Quasi-Normal Markovian (EDQNM) equations:

$$(\partial_t + 2\nu k^2)E(k,t) = \int d\mathbf{p}d\mathbf{q}\theta_{kpq}\frac{k}{pq}b(\mathbf{k},\mathbf{p},\mathbf{q})[k^2E(p,t) - p^2E(k,t)]E(q,t), \tag{9.11}$$

$$\theta_{kpq} = \int_0^t d\tau e^{-[\mu_{kpq}+\nu(k^2+p^2+q^2)](t-\tau)}. \tag{9.12}$$

In principle, μ_{kpq} depends on the energy spectrum so the integral defining θ_{kpq} should be computed dynamically at each timestep when solving numerically the EDQNM equations. It is customary to neglect this dependence, so that $\theta_{kpq} = (1 - e^{-[\mu_{kpq}+\nu(k^2+p^2+q^2)]t})/[\mu_{kpq} + \nu(k^2 + p^2 + q^2)]$.

The EDQNM approximation can be shown to be *realizable*: it always leads to positive energy spectra. A comparison with experimental data is shown in Fig. 9.3. The main advantage of this approach is that it has of course a much smaller numerical cost than solving the Navier-Stokes equations. Hence, very high "Reynolds numbers" can be achieved (see Fig. 9.4). This approach has been extended to anisotropic flows, where difficulties arise due to the existence of other relevant timescales characterizing the propagation of waves (Sagaut and Cambon 2008).

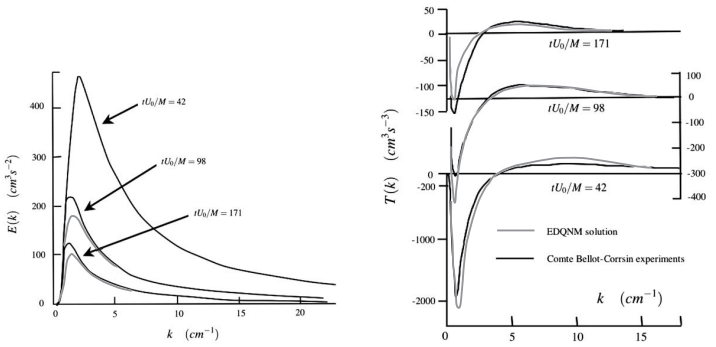

Figure 9.3: Comparison between experimental (black) and EDQNM data for the energy spectrum (left) and the energy transfer (right), from Sagaut and Cambon (2008, § 3.5).

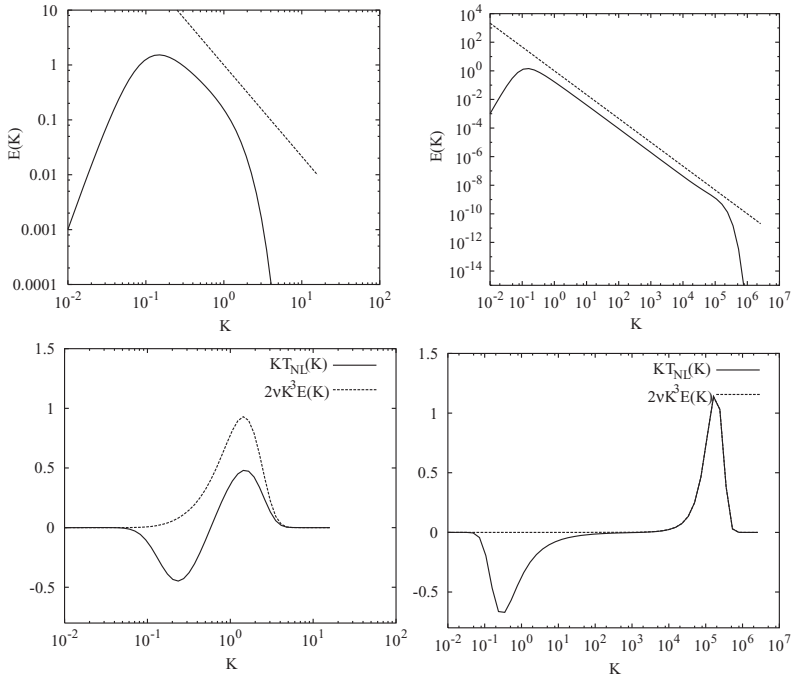

Figure 9.4: Energy spectrum (top) and transfer (bottom) for $R_\lambda = 30$ (left) and $R_\lambda = 10^5$ (right), from Sagaut and Cambon (2008, § 3.5).

Part II

Inhomogeneous or anisotropic flows

10
Free shear flows

10.1 Classical shear flows

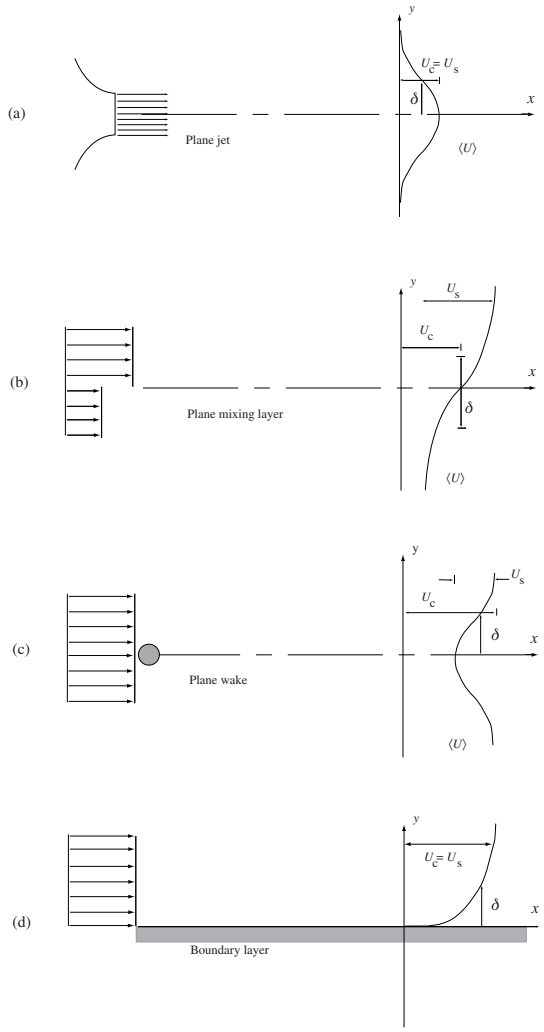

Figure 10.1: Classical shear flows (Pope 2000).

10.2 *The round jet*

We study a jet through a circular nozzle of diameter D. The fluid is injected into an ambient made of the same fluid, with density ρ and viscosity ν. The jet velocity U_J is constant across the nozzle. We denote x the axis orthogonal to the diameter of the nozzle and set $x_0 = 0$ the position of the nozzle.

We assume that the statistics of the flow are axisymmetric. It follows directly that the mean velocity field has only two non-vanishing components, the axial velocity U and the radial velocity V: $U(x,r)\mathbf{e}_x + V(x,r)\mathbf{e}_r$. We will denote the centerline velocity with a subset 0: $U_0(x) = U(x,0)$ and similarly for V. The half-width of the jet $r_{1/2}(x)$ is defined by $U(x, r_{1/2}(x)) = U_0(x)/2$.

10.2.1 *Experimental observations*

- self-similarity of the jet profile: $\xi = r/r_{1/2}(x)$, $U(x,r) = U_0(x)f(\xi)$ (Fig. 10.2).
- axial variations: spreading of the jet and centerline velocity (Fig. 10.3).
- lateral velocity: $V \ll U$, entrainment (Fig. 10.4).
- Reynolds stresses (Fig. 10.5).

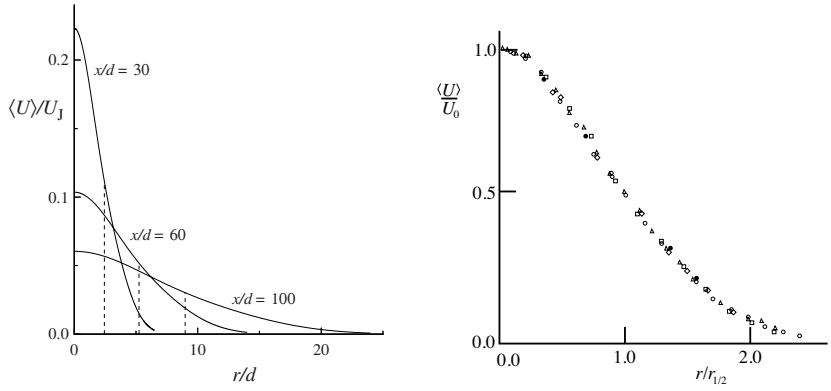

Figure 10.2: Left: velocity profile at several axial distances. Right: velocity profile rescaled by centerline velocity, as a function of radius normalized by half-width, exhibiting a self-similar character.

10.2.2 *Dimensional analysis*

From the problem parameters, we can construct two non-dimensional numbers: the Reynolds number $Re = U_J D/\nu$ and the axial distance x/D.

We assume that the large-scale properties of the jet do not depend on the Reynolds number. Then, the half-width of the jet should

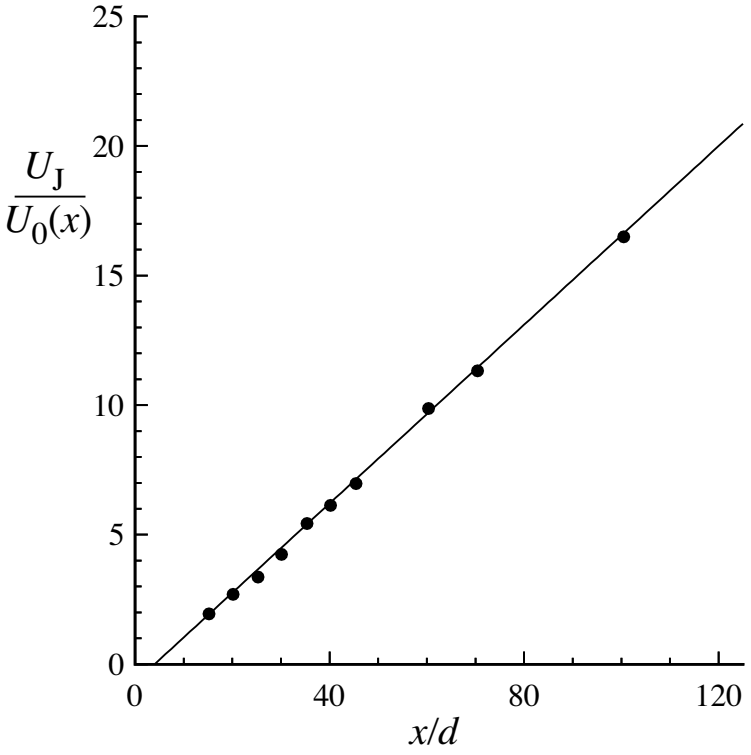

Figure 10.3: Inverse of the centerline velocity as a function of the axial distance.

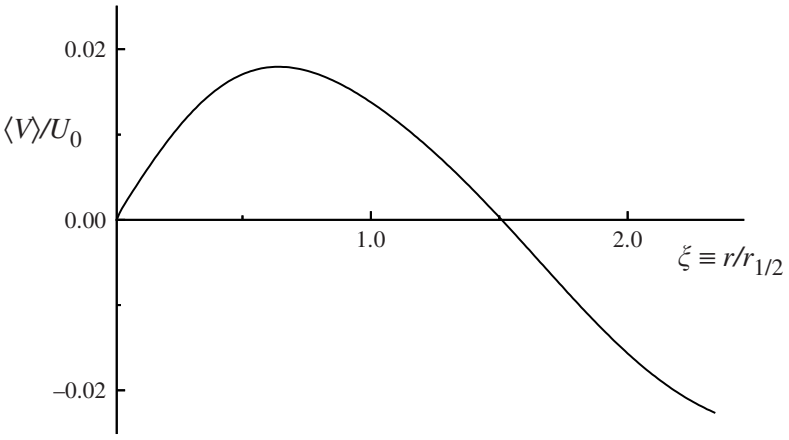

Figure 10.4: Self-similar profile of mean radial velocity.

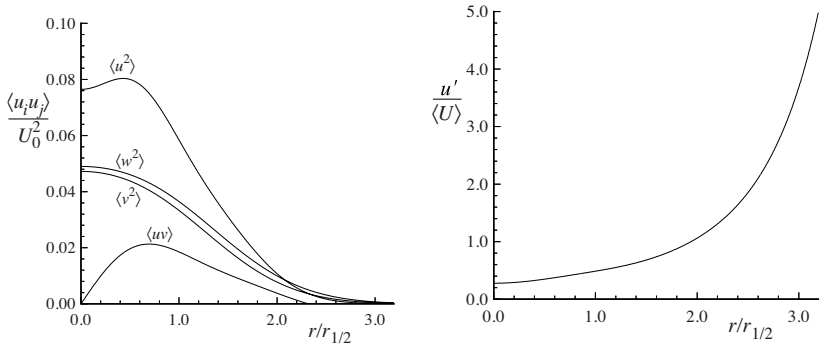

Figure 10.5: Left: Self-similar profile of the Reynolds stresses. Right: Self-similar profile of turbulence intensity.

satisfy $r_{1/2}(x) = R_0(x/d)x$ where R_0 is a universal function. Empirically, we observe that the function R_0 has a finite limit when $x/D \to +\infty$; we denote it $\tan\alpha$, $\alpha \approx 12.5$ is the angle of the jet. It does not depend on the properties of the fluid (viscosity, density) or the properties of the nozzle.

The flow rates of mass Q, momentum P and energy Π (across a plane orthogonal to the x axis) are proportional to $r_{1/2}^2 U_0$, $r_{1/2}^2 U_0^2$ and $r_{1/2}^2 U_0^3$, respectively. A momentum conservation argument yields that $r_{1/2}U_0$ is conserved, and from the paragraph above we deduce that $U_0 \propto 1/x$. It also follow that $Q \propto x$ (entrainment) and $\Pi \propto 1/x$. In section 10.2.3 we show these results in the context of the boundary layer approximation.

The flux of kinetic energy decreases with x due to kinetic energy dissipation, which is converted into heat. This flux is mostly due to the large scales of the flow, which do not depend on the Reynolds number: hence there remains a finite energy dissipation rate in the limit of infinite Reynolds number, another manifestation of the *dissipation anomaly*.

10.2.3 Momentum budget

Boundary-layer equations The mean axial and radial momentum equations read:

$$U\frac{\partial U}{\partial x} + V\frac{\partial U}{\partial r} = -\frac{1}{\rho}\frac{\partial P}{\partial x} + \nu\frac{\partial^2 U}{\partial x^2} + \frac{\nu}{r}\frac{\partial}{\partial r}\left(r\frac{\partial U}{\partial r}\right) - \frac{1}{r}\frac{\partial}{\partial r}r\overline{u'v'} - \frac{\partial}{\partial x}\overline{u'^2}, \tag{10.1}$$

$$U\frac{\partial V}{\partial x} + V\frac{\partial V}{\partial r} = -\frac{1}{\rho}\frac{\partial P}{\partial r} + \nu\frac{\partial^2 V}{\partial x^2} + \frac{\nu}{r}\frac{\partial}{\partial r}\left(r\frac{\partial V}{\partial r}\right) - \frac{1}{r}\frac{\partial}{\partial r}r\overline{v'^2} - \frac{\partial}{\partial x}\overline{u'v'}. \tag{10.2}$$

We first neglect all the terms involving V and the axial derivative of Reynolds stresses in the radial momentum equation:

$$\frac{1}{\rho}\frac{\partial P}{\partial r} = -\frac{1}{r}\frac{\partial}{\partial r} r\overline{v'^2}, \tag{10.3}$$

which after integration, yields

$$\frac{P}{\rho} = \frac{P_0}{\rho} - \overline{v'^2} + \int_r^{+\infty} \frac{1}{r'}\overline{v'^2} dr', \tag{10.4}$$

with P_0 the pressure in the free stream region ($r \to +\infty$).

In the equation for the mean axial momentum, we neglect the axial diffusion term to obtain:

$$U\frac{\partial U}{\partial x} + V\frac{\partial U}{\partial r} = -\frac{1}{\rho}\frac{\partial P_0}{\partial x} + \frac{\nu}{r}\frac{\partial}{\partial r}\left(r\frac{\partial U}{\partial r}\right) - \frac{1}{r}\frac{\partial}{\partial r} r\overline{u'v'} - \frac{\partial}{\partial x}(\overline{u'^2} - \overline{v'^2}) - \frac{\partial}{\partial x}\int_r^{+\infty} \frac{1}{r'}\overline{v'^2} dr'. \tag{10.5}$$

In the free stream the fluid is quiescent $\partial_x P_0 = 0$. We can again neglect the axial derivatives of the Reynolds stresses, even if this approximation is not so well controlled.

Finally, the boundary-layer equations for the round jet are:

$$U\frac{\partial U}{\partial x} + V\frac{\partial U}{\partial r} = \frac{\nu}{r}\frac{\partial}{\partial r}\left(r\frac{\partial U}{\partial r}\right) - \frac{1}{r}\frac{\partial}{\partial r} r\overline{u'v'}, \tag{10.6}$$

$$\frac{\partial U}{\partial x} + \frac{1}{r}\frac{\partial (rV)}{r} = 0. \tag{10.7}$$

Flow rate of mass, momentum and energy Simple budget arguments yield the (instantaneous) flow rates of mass Q, momentum P and energy Π across a plane orthogonal to the x axis:

$$Q(x) = 2\pi\rho \int_0^{+\infty} ru(x,r) dr, \tag{10.8}$$

$$P(x) = 2\pi\rho \int_0^{+\infty} ru^2(x,r) dr, \tag{10.9}$$

$$\Pi(x) = 2\pi\rho \int_0^{+\infty} r\frac{u^3(x,r)}{2} dr. \tag{10.10}$$

Writing the left-hand side of the boundary-layer equations in flux form (using the continuity equation), neglecting viscosity and multiplying by r yields

$$\frac{\partial (rU^2)}{\partial x} + \frac{\partial}{\partial r}(rUV + r\overline{u'v'}) = 0, \tag{10.11}$$

which upon integration becomes

$$\frac{d\overline{P}}{dx} = -2\pi\rho \left[rUV + r\overline{u'v'}\right]_0^{+\infty}, \tag{10.12}$$

$$= 0, \tag{10.13}$$

assuming that UV goes to zero sufficiently fast. In other words, the mean momentum flow rate $\overline{P}$ is conserved. Injecting the self-similar profile $U(x,r) = U_0(x)f(\xi)$, it can be expressed as

$$\overline{P}(x) = 2\pi\rho \int_0^{+\infty} rU^2(x,r)dr, \tag{10.14}$$

$$= 2\pi\rho r_{1/2}(x)^2 U_0(x)^2 \int_0^{+\infty} \xi f^2(\xi)d\xi, \tag{10.15}$$

and similarly,

$$\overline{Q}(x) = 2\pi\rho r_{1/2}(x)^2 U_0(x) \int_0^{+\infty} \xi f(\xi)d\xi, \tag{10.16}$$

$$\overline{\Pi}(x) = 2\pi\rho r_{1/2}(x)^2 U_0(x)^3 \int_0^{+\infty} r\xi f^2(\xi)d\xi. \tag{10.17}$$

It follows that the product $r_{1/2}(x)U_0(x)$ is conserved in the axial direction.

Self-similar solution of the boundary-layer equations Assuming $U(x,r) = U_0(x)f(\xi)$ with $\xi = r/r_{1/2}(x)$ and $\overline{u'v'} = U_0(x)^2 g(\xi)$, we obtain from the continuity equation

$$0 = f(\xi)U_o(x) - \frac{r}{r_{1/2}(x)^2}\frac{dr_{1/2}}{dx}U_0(x)f'(\xi) + \frac{1}{r}\frac{\partial}{\partial r}(rV), \tag{10.18}$$

$$rV = -r_{1/2}^2 U_0' \int_0^{\xi} \xi' f(\xi')d\xi' + r_{1/2}\frac{dr_{1/2}}{dx}U_0 \int_0^{\xi} \xi'^2 f'(\xi')d\xi', \tag{10.19}$$

$$= -r_{1/2}^2 U_0' \int_0^{\xi} \xi' f(\xi')d\xi' + r_{1/2}\frac{dr_{1/2}}{dx}U_0 \left[\xi^2 f(\xi) - 2\int_0^{\xi} \xi' f(\xi')d\xi'\right], \tag{10.20}$$

$$= -\frac{d}{dx}(r_{1/2}^2 U_0) \int_0^{\xi} \xi' f(\xi')d\xi' + r_{1/2}\frac{dr_{1/2}}{dx}U_0\xi^2 f(\xi). \tag{10.21}$$

Then, injecting this relation into the mean axial velocity equation (neglecting the viscous term), we obtain

$$[\xi f^2]\left\{\frac{r_{1/2}}{U_0}\frac{dU_0}{dx}\right\} - f' \int_0^{\xi} \xi' f(\xi')d\xi' \left\{\frac{r_{1/2}}{U_0}\frac{dU_0}{dx} + 2\frac{dr_{1/2}}{dx}\right\} = \frac{d}{d\xi}[\xi g(\xi)]. \tag{10.22}$$

It follows that

$$\frac{r_{1/2}}{U_0}\frac{dU_0}{dx} = C, \qquad \frac{dr_{1/2}}{dx} = S, \tag{10.23}$$

and therefore, $r_{1/2} = Sx$. We know from the previous section that the product $r_{1/2}U_0$ does not depend on x, so $C = S$ and $U \propto x^{-1}$.

Another consequence is that the flow rate of mass increases with axial distance x, which means that fluid is entrained from the quiescent region into the jet, and the flow rate of energy, on the other hand decreases as x^{-1}.

Turbulent viscosity hypothesis Solving the general equation for the self-similar profile in the above paragraph seems difficult... Instead, let us close the boundary-layer equations by making a uniform turbulent viscosity hypothesis: $\overline{u'v'} = -\nu_T \frac{\partial U}{\partial r}$ with ν_T constant. The boundary layer equation for axial momentum becomes:

$$U\frac{\partial U}{\partial x} + V\frac{\partial U}{\partial r} = \frac{\nu + \nu_T}{r}\frac{\partial}{\partial r}\left(r\frac{\partial U}{\partial r}\right). \tag{10.24}$$

This is the same equation as for a laminar boundary layer, replacing the viscosity ν by $\nu + \nu_T$. In general, the turbulent viscosity ν_T is much larger than the molecular viscosity ν. The solution of these equations was obtained by **Schlichting1933**: the self-similar profile is $f(\xi) = \frac{1}{(1+a\xi^2)^2}$ with $a = \sqrt{2} - 1$.

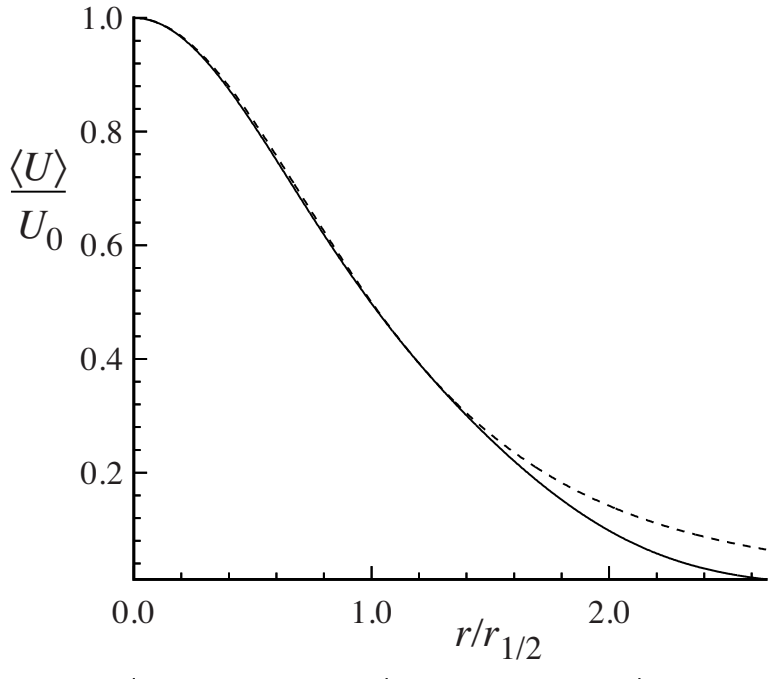

Figure 10.6: Mean velocity profile in the self-similar round jet: experimental data (solid line) and uniform turbulent viscosity solution (dashed line). From Pope (2000).

10.2.4 Energy budget

Reynolds decomposition: $u_i = U_i + u_i'$, $U_i = \bar{u}_i$. The Reynolds-averaged Navier-Stokes equations read

$$\partial_t \bar{u}_i + \bar{u}_j \partial^j \bar{u}_i = -\frac{1}{\rho}\partial_i \bar{p} + \nu \partial_j \partial^j \bar{u}_i - \partial^j \overline{u_i' u_j'}, \tag{10.25}$$

$$= -\frac{1}{\rho}\partial_i \bar{p} + 2\nu \partial^j \bar{S}_{ij} - \partial^j \overline{u_i' u_j'}, \tag{10.26}$$

which after multiplying by $\bar{u}^i$ yields the local mean energy budget:

$$\frac{\bar{D}}{\bar{D}t}\frac{\bar{\mathbf{u}}^2}{2} + \partial^j \left[\frac{\bar{p}}{\rho}\bar{u}_j - 2\nu \bar{u}^i \bar{S}_{ij} + \bar{u}^i \overline{u_i' u_j'}\right] = \underbrace{\partial^j \bar{u}^i \overline{u_i' u_j'}}_{-\mathcal{P}} - \underbrace{2\nu \bar{S}_{ij}\bar{S}^{ij}}_{\bar{\varepsilon}}. \tag{10.27}$$

Similarly, starting from the equation for fluctuations

$$\partial_t u_i' + \bar{u}_j \partial^j u_i' + u_j' \partial^j \bar{u}_i + u_j' \partial^j u_i' = -\frac{1}{\rho}\partial_i p' + 2\nu \partial^j S_{ij}', \tag{10.28}$$

we obtain after contracting with $u^{i\prime}$ and averaging:

$$\frac{\bar{D}}{\bar{D}t}k + \partial^j \left[\frac{\overline{p' u_j'}}{\rho} - 2\nu \overline{u^{i\prime} S_{ij}'} + \frac{1}{2}\overline{u_i' u^{i\prime} u_j'}\right] = \mathcal{P} - \underbrace{2\nu \overline{S_{ij}' S^{ij\prime}}}_{\varepsilon'}, \tag{10.29}$$

with $k = \frac{\overline{\mathbf{u}'^2}}{2}$ the turbulent kinetic energy. These equations both take the form of local conservation equations with additional source and sink terms. Upon integration over some volume, the divergence term becomes a flux across the surface enclosing the volume. This term describes the transport of mean or turbulent kinetic energy into or out of the volume.

The terms $\bar{\varepsilon}$ and ε' are the traces of a positive symmetric matrix, so they are always positive. They correspond to local dissipation of mean or turbulent kinetic energy, respectively.

Finally the term $\mathcal{P}$ can be interpreted as the kinetic energy exchanged locally between the mean-flow and the fluctuations. While we cannot know its sign *a priori*, it is in general positive and is referred to as the *production term*. It should be noted that turbulent kinetic energy is extracted from the mean-flow through the action of Reynolds stresses against the mean velocity gradient.

Note that

- Turbulent kinetic energy production is affected only by the main strain rate tensor: $\mathcal{P} = -\bar{S}^{ij}\overline{u_i' u_j'}$.

- Only the anisotropic part of the Reynolds stress tensor contributes to the production term: if $\overline{u_i' u_j'} = \frac{2}{3} k \delta_{ij} + a_{ij}$ then $\mathcal{P} = -\bar{S}^{ij} a_{ij}$.
- Using a turbulent viscosity model for Reynolds stresses: $a_{ij} = -2\nu_T \bar{S}_{ij}$, we obtain $\mathcal{P} = 2\nu_T \bar{S}^{ij} \bar{S}_{ij} \geq 0$. Here the production has the same form as the dissipation of mean kinetic energy $\bar{\varepsilon}$, replacing ν by ν_T.
- In the turbulent boundary layer approximation for the round jet (see § 10.2.3), the production term reads: $\mathcal{P} = -\overline{uv} \frac{\partial U}{\partial r}$, which becomes $\mathcal{P} = \nu_T \left(\frac{\partial U}{\partial r} \right)^2$ with a turbulent viscosity hypothesis.

We can revisit the anomalous dissipation issue from the evolution equation for turbulent kinetic energy (Eq. (10.29)). Indeed, assuming that the jet is self-similar, both k/U_0^2 and $\mathcal{P}/(U_0^3/r_{1/2})$ are self-similar and independent of the Reynolds number (asymptotically). In other words, both $\bar{D}k/\bar{D}t$ and $\mathcal{P}$ scale like $U_0^3/r_{1/2}$. We can therefore expect ε' to have the same scaling, so that $\varepsilon'/(U_0^3/r_{1/2})$ should be self-similar and independent of the Reynolds number. This is indeed observed in experimental measurements.

Note that for the round jet $\mathcal{P}/(U_0^3/r_{1/2}) = -\frac{\overline{u'v'}}{U_0^2} \frac{r_{1/2}}{U_0} \frac{\partial U}{\partial r}$

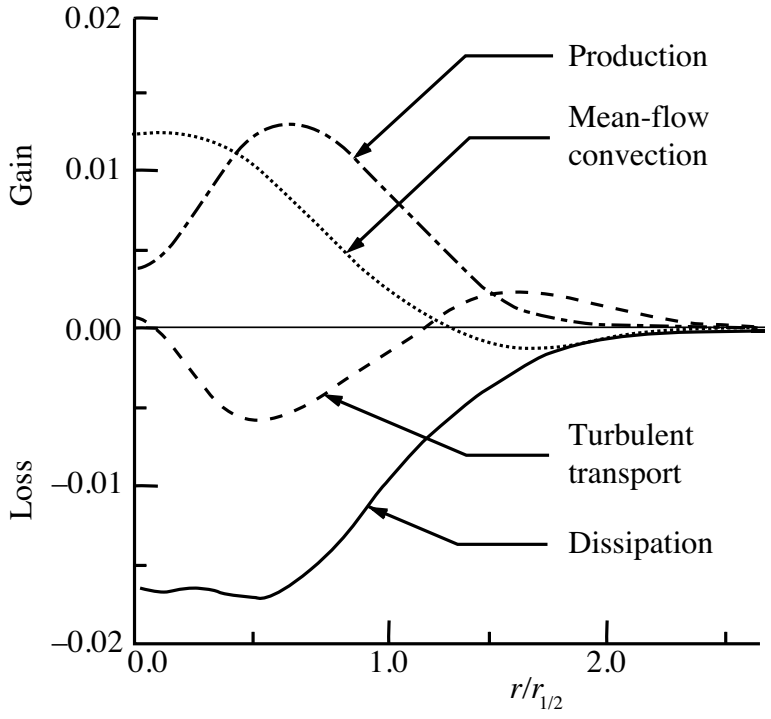

Figure 10.7: Various terms of the kinetic energy budget for the round jet (Pope 2000).

11
Density & Gravity

The notes for this chapter are still in a very early draft stage. They were written rapidly, and might still contain some mistakes or inaccurracies. Please treat them with caution and let me know if you find any problem.

Density was assumed to be constant in the previous chapters. Here, we show some consequences of density variations on the dynamics, in particular when the flow is subject to a gravity field.

11.1 Varying density and the equations of motion for a general fluid

The main reference for this section is Vallis 2017, Chap. 1

In chapter 2 we considered the Navier-Stokes equations for incompressible flows, assuming that the density is constant, and absorbed it into the pressure gradient. In that case, pressure is entirely determined from the incompressibility condition, so that no additional equation is required.

In general the momentum conservation equations read

$$\partial_t \mathbf{u} + \mathbf{u} \cdot \nabla \mathbf{u} = -\frac{1}{\rho} \nabla p + \nu \Delta \mathbf{u}, \tag{11.1}$$

which should be supplemented by the equations for the conservation of mass

$$\partial_t \rho + \nabla \cdot (\mathbf{u} \rho) = 0. \tag{11.2}$$

It remains to provide an equation relating pressure to density, and potentially other properties of the fluid, such as temperature or chemical composition of the fluid (e.g. humidity in the atmosphere, salinity in the ocean). This equation is referred to as an *equation of state*, which may be written $\rho = f(p, T, m_1, \dots, m_N)$ for a fluid which is a mixture of N species with mixing ratios m_i (note that in fact only $N - 1$ such variables are needed). Properties such as temperature and mixing ratios are transported by the flow and in turn satisfy advection equations, potentially with sources and sinks.

Below are some examples of an equation of state:

- A constant density fluid has the trivial equation of state $\rho =$ const. Then it follows from conservation of mass that the flow

is divergence-free and pressure is computed by solving the corresponding Poisson problem as in chapter 2.

- A *barotropic*[1] fluid has an equation of state of the form $\rho = f(p)$ (e.g. polytropic gas, $p = C\rho^\gamma$)
- If the fluid is an ideal gas, $p = \rho RT$ (e.g. dry air), or $p = \rho RT(1 + 0.61q)$ for moist air, with q the specific humidity (the ratio of the mass of water vapor contained in a parcel to the total mass). Note that the fluid is baroclinic then.
- For water, we do not have an exact equation of state. A possible approximation is to use a linear one: $\rho = \rho_0[1 - \beta_T(T - T_0) + \beta_p(p - p_0)]$ (fresh water), or $\rho = \rho_0[1 - \beta_T(T - T_0) + \beta_S(S - S_0) + \beta_p(p - p_0)]$ (for seawater), where S is the salinity. This approximation is not always good enough[2].

[1] A barotropic fluid is a fluid in which surface of constant pressure and surfaces of constant density coincide, or in other words: $\nabla p \times \nabla \rho = 0$. When this is not the case, the fluid is said to be *baroclinic*.

[2] See e.g. Vallis 2017, § 1.4 and § 1.7 for more details

For baroclinic flows, to close the equations, we need additional equations describing the composition of the flow:

$$\partial m_i + \mathbf{u} \cdot \nabla m_i = M, \tag{11.3}$$

where M represents sources and sinks, which depend on the particular case under study (see examples below), and a thermodynamic equation, which describes the evolution of the temperature field.

In fact, the most general form of the equations uses a slightly different equation of state and thermodynamic equation using the specific entropy η:

$$\eta = \eta(\rho, I, m_1, \dots, m_N), \tag{11.4}$$

$$\partial_t \eta + \mathbf{u} \cdot \nabla \eta = \frac{Q}{T}, \tag{11.5}$$

where I is the (specific) internal energy, Q corresponds to the heating rate of the flow, and the pressure and density can in turn be determined from the specific entropy:

$$\frac{1}{T} = \left(\frac{\partial \eta}{\partial I}\right)_{\rho, m_1, \dots, m_N}, \tag{11.6}$$

$$\frac{p}{T} = \left(\frac{\partial \eta}{\partial \alpha}\right)_{I, m_1, \dots, m_N}, \tag{11.7}$$

with $\alpha = 1/\rho$ the specific volume.

11.1.1 *Example: the ideal gas*

For an ideal gas, the equation of state is given by the equation[3]:

$$\eta = c_V \ln I + R_d \ln \alpha + \text{const}, \tag{11.8}$$

[3] The exact value of the constant can be computed in the case of a monoatomic gas; it is given by the Sackur-Tetrode formula.

the temperature and internal energy are proportional:

$$\frac{1}{T} = \left(\frac{\partial \eta}{\partial I}\right)_{\rho} = \frac{c_V}{I}, \tag{11.9}$$

$$\frac{p}{T} = \left(\frac{\partial \eta}{\partial \alpha}\right)_{I} = \frac{R_d}{\alpha}. \tag{11.10}$$

The latter equation yields the ideal gas law: $p = \rho R_d T$. In this case, the thermodynamic equation may be expressed in terms of the internal energy as:

$$\frac{DI}{Dt} + p\frac{D\alpha}{Dt} = Q, \tag{11.11}$$

or using the continuity equation

$$\frac{DI}{Dt} + p\alpha\nabla\cdot\mathbf{u} = Q, \tag{11.12}$$

or finally in terms of the temperature

$$c_V\frac{DT}{Dt} + p\alpha\nabla\cdot\mathbf{u} = Q. \tag{11.13}$$

11.2 *Fluid statics in a gravity field*

From now on we assume that the fluid is subject to a gravity field, which amounts to adding a body force $\mathbf{g} = -g\mathbf{e}_z$ to the right-hand side of Eq. (11.1).

11.2.1 *Hydrostatic balance*

The projection of the momentum equations on the vertical yields the following equation for vertical accelerations:

$$\frac{Dw}{Dt} = -\frac{1}{\rho}\frac{\partial p}{\partial z} - g. \tag{11.14}$$

For the fluid to be at rest, the pressure gradient and gravity forces must balance each other. This is *hydrostatic balance*:

$$\frac{\partial p}{\partial z} = -\rho g. \tag{11.15}$$

It means that pressure at any given level is determined by the weight of fluid above it. In particular, pressure is a monotonically decreasing function of height. This allows to use pressure as a vertical coordinate, instead of height; this practice is extremely frequent in atmospheric science.

Hydrostatic balance may be a useful approximation to the vertical momentum equation, even when the fluid is not at rest. For instance,

it is often approximately satisfied in large-scale geophysical flows, where vertical accelerations are much smaller than horizontal accelerations[4]. Nevertheless, this approximation does not always yield a sufficiently good approximation to the pressure field, whose horizontal gradient generate lateral motion.

[4] in the atmosphere, for instance, it only breaks down at horizontal scales on the order of the kilometer, and only the numerical models with the highest resolutions do not rely on it

11.2.2 *Application: vertical structure of the atmosphere and the dry adiabatic lapse rate*

We assume that the atmosphere can be considered as an ideal gas. We can rewrite the thermodynamic equation (11.11) using (specific) enthalpy $h = I + p\alpha$ instead of internal energy:

$$\frac{Dh}{Dt} - \alpha \frac{Dp}{Dt} = Q, \tag{11.16}$$

which, assuming hydrostatic balance, yields

$$\frac{D}{Dt}(h + gz) = Q. \tag{11.17}$$

We introduce a generalized enthalpy, often referred to as the *dry static energy*: $h + gz = c_P T + gz$. We have just shown that this quantity is conserved by adiabatic motion. The physical interpretation is that as a fluid parcel is moved adiabatically from the surface towards higher altitude, the potential energy gained is exactly balanced by the loss of internal energy due to the work of pressure forces (the gas cools down under adiabatic expansion). It follows that in the absence of a heating term, the temperature profile in an atmospheric column is given by the so-called *dry adiabatic lapse rate*:

$$\frac{dT}{dz} = -\frac{g}{c_p}. \tag{11.18}$$

For dry air, this gives a temperature gradient of about 10K/km. Observed average temperature profiles are typically less steep than the dry adiabatic lapse rate. We give a little more explanation in Sec. 11.2.3.

11.2.3 *Static stability*

In this section we would like to understand under which condition a column of ideal gas at rest in a gravity field is stable. Clearly, a necessary condition for stability is that the density should decrease with height: $\frac{\partial \rho}{\partial z} < 0$. Invoking hydrostatic balance, we can use pressure as a vertical coordinate, and the equivalent stability condition is that density increases with pressure. However, this condition is not sufficient: when a parcel of air is moved adiabatically over the vertical

column, it undergoes expansion or compression. The column is stable if the density of a parcel of air brought adiabatically to a reference level is an increasing function of pressure.

Because of the ideal gas law $p = \rho R_d T$, the density at a pressure level is entirely determined by the temperature at the same level. Let us choose our reference level with pressure $p_0 = \rho_0 R_d T_0$, where ρ_0 and T_0 are the density and temperature. For simplicity we choose the surface as our reference level, so that all the fluid parcels lie initially above that level. We take a parcel of air at pressure level p; initially it has a density ρ and a temperature T, satisfying $p = \rho R_d T$. We bring it adiabatically at the pressure level p_0 and we want to compute its temperature θ after it has been heated up by the work of pressure forces. Under adiabatic motion, dry static energy is conserved: $c_p dT + g dz = 0$, or using hydrostatic balance and the ideal gas law, $c_p dT - R_d T dp/p = 0$, which integrates to $\theta = T \left(\frac{p_0}{p}\right)^{R_d/c_p}$. θ is called the *potential temperature* of the parcel. The density of the parcel after adiabatic compression is $\rho' = p_0/(R_d\theta)$ and the stability condition is $\rho' < \rho_0$, i.e. $T_0 < \theta$. The static stability condition is that the potential temperature profile should increase with height, or equivalently decrease with pressure:

$$\frac{\partial \theta}{\partial z} > 0. \tag{11.19}$$

The marginal stability condition (potential temperature independent of height) corresponds to the dry adiabatic lapse rate for the temperature profile. Hence, the fact that the observed temperature profile is typically less steep can be interpreted as a consequence that the atmosphere is in general not statically stable. Note that the condition above is for dry air, and the atmosphere contains moisture. This affects the stability condition. In fact, the atmosphere is close to the marginal stability condition for moist air, which corresponds to a less steep vertical temperature gradient.

Moist convection is more complex, because water vapor can condense when a parcel of moist air is lifted upwards, thereby heating the parcel. See Vallis 2017, Chap. 18 for more details.

11.3 *The shallow-water equations*

Reference Vallis 2017, Chap. 3.

In section 11.1 we have explained how to take into account density variations in the equations of motion in a general way. Such density variations matter most when coupled to the effect of gravity. In section 11.2 we have introduced some effects of gravity in a static framework. We now turn to dynamical effects. We first do so in the simplest system, the shallow-water equations, where the density is assumed constant (which circumvents most of the difficulties of section 11.1) but the upper boundary is a free surface, so that deformations of the free surface lead to horizontal variations in the weight of the fluid column, and hence to restoring motions due to gravity.

Non-constant density will be considered in section 11.4.

11.3.1 *Equations of motion*

We consider a layer of fluid of constant density ρ_0 in a gravity field $\mathbf{g}$. We denote $\mathbf{v} = (\mathbf{u}, w)$ the three dimensional velocity field, $\mathbf{u}$ the horizontal velocity and w the vertical velocity. The depth of the fluid layer is denoted h, and we assume that the bottom is flat. On top of the fluid lies another fluid of negligible inertia ($\rho = 0$). We assume that hydrostatic balance holds, so that the vertical component of the momentum conservation equation is:

$$dp = -\rho_0 g dz, \tag{11.20}$$

which after integrating from the bottom to arbitrary height z yields

$$p(z) - p(z = h) = \rho_0 g(h - z), \tag{11.21}$$

because the overlying fluid has negligible inertia, $p(z = h) = 0$, and taking the horizontal gradient, we see that

$$\nabla_\perp p = \rho_0 g \nabla_\perp h. \tag{11.22}$$

In other words, the horizontal pressure gradient does not depend on the vertical coordinate. If the horizontal velocity field is initially independent of the vertical coordinate, it remains so at all times, and the advection term therefore becomes $\mathbf{v} \cdot \nabla \mathbf{u} = \mathbf{u} \cdot \nabla \mathbf{u}$. The horizontal momentum equation simplifies to

$$\partial_t \mathbf{u} + \mathbf{u} \cdot \nabla \mathbf{u} = -g \nabla h + \nu \Delta \mathbf{u}. \tag{11.23}$$

We have dropped the $\perp$ index for horizontal gradients, since there is no ambiguity anymore.

The continuity equation simplifies as well. Because density is constant, the three-dimensional continuity equation becomes simply $\nabla \cdot \mathbf{v} = 0 = \nabla_\perp \cdot \mathbf{u} + \partial_z w$, which we can integrate vertically from the bottom to the top of the fluid layer:

$$w(z = h) - w(z = 0) = -h \nabla \cdot \mathbf{u}, \tag{11.24}$$

and since $w = \frac{Dz}{Dt}$ and the bottom boundary condition imposes $w(z = 0) = 0$, we have

$$\frac{Dh}{Dt} = -h \nabla \cdot \mathbf{u}, \tag{11.25}$$

or equivalently,

$$\frac{\partial h}{\partial t} + \nabla \cdot (h \mathbf{u}) = 0. \tag{11.26}$$

Combined with the horizontal momentum equations, these are the *shallow-water equations*.

These equations are closed: due to the assumption of hydrostatic balance, the thermodynamic properties of the fluid do not matter for the dynamics (they are only passive). The only difference with the incompressible case studied before is that now the upper boundary is a free surface, with gravity as a restoring force. As we shall see now, this new ingredient is sufficient to generate new dynamical phenomena, such as waves.

11.3.2 Shallow-water waves

Non-rotating system Let us write H the average fluid layer depth and h' the deviations': $h = H + h'$. We consider the linearized equations:

$$\partial_t \mathbf{u} = -g\nabla h', \tag{11.27}$$

$$\partial_t h' + H\nabla \cdot \mathbf{u} = 0, \tag{11.28}$$

which, after taking the time derivative of the continuity equation, yields the wave equation

$$\frac{\partial^2 h'}{\partial t^2} = gH\Delta h'. \tag{11.29}$$

This equation admits wave solutions with phase speed $c = \sqrt{gH}$. The waves are not dispersive. They are called (surface) *gravity waves*.

Note that we could also have diagonalized the full linear system. This is most easily done by introducing the vorticity $\zeta = \partial_x v - \partial_y u$, the divergence $\delta = \partial_x u + \partial_y v$, the geopotential $\phi = gh$ and the Fourier transforms $\hat{\zeta}, \hat{\delta}, \hat{\phi}$. Then the linear system reads

$$\dot{X} + LX = 0, \text{ with } X = \begin{pmatrix} \hat{\zeta} \\ \hat{\delta} \\ \hat{\phi} \end{pmatrix} \text{ and } L = \begin{pmatrix} 0 & 0 & 0 \\ 0 & 0 & K^2 \\ 0 & -c^2 & 0 \end{pmatrix}. \tag{11.30}$$

It is clear that the spectrum of the system is $\{0, \pm iKc\}$. In addition to the two wave modes, there is a vorticity mode which does not propagate (its linear dynamics is trivial). We also see that the oscillations of the free surface are directly related to oscillations of the horizontal divergence.

Rotating system We can easily extend the analysis to a rotating shallow-water system. The linear momentum equation becomes:

$$\partial_t \mathbf{u} = -g\nabla h' - 2\Omega \times \mathbf{u}. \tag{11.31}$$

The same analysis as above leads to the dispersion relation:

$$\omega^2 = f^2 + c^2 K^2. \tag{11.32}$$

These waves are known as *Poincaré waves*.

11.4 The Boussinesq approximation

In section 11.2 we have only considered fluid at rest in a gravity field. Here, we return to dynamical effects. We first introduce an approximation to simplify the equations: we assume that density can be considered constant, except when it is combined with gravity. The rationale is that density fluctuations are small, but since the acceleration of gravity is large the product of the two may not be neglected.

11.4.1 The Boussinesq equations

Several flavors of the Boussinesq equations, or tightly related ones, such as the anelastic equations, exist. Here our goal is just to show a simple set of equations making use of the Boussinesq approximation to discuss internal gravity waves.

We decompose the density and pressure fields into a background state and fluctuations: $\rho = \rho_0 + \delta\rho$, $p = p_0 + \delta p$. We assume that hydrostatic balance applies in the background state: $dp_0 = -\rho_0 g dz$, and that the fluctuations are small: $\delta\rho \ll \rho_0$ and $\delta p \ll p_0$. ρ_0 is a constant and p_0 depends on z only.

The momentum equations now write:

$$(\rho_0 + \delta\rho)(\partial_t \mathbf{u} + \mathbf{u}\cdot\nabla\mathbf{u}) = -\nabla(p_0 + \delta p) + (\rho_0 + \delta\rho)\mathbf{g}, \tag{11.33}$$

$$= -\left(\frac{\partial p_0}{\partial z} + \rho_0 g\right)\mathbf{e}_z - \nabla\delta p + \delta\rho\mathbf{g}, \tag{11.34}$$

$$\partial_t \mathbf{u} + \mathbf{u}\cdot\nabla\mathbf{u} = -\frac{1}{\rho_0}\nabla\delta p + \frac{\delta\rho}{\rho_0}\mathbf{g}, \tag{11.35}$$

$$= -\nabla\phi + b\mathbf{e}_z, \tag{11.36}$$

with $\phi = \delta p/\rho_0$ a modified pressure and $b = -g\delta\rho/\rho_0$ the *buoyancy*.

The mass continuity equation writes:

$$\frac{D\delta\rho}{Dt} + (\rho_0 + \delta\rho)\nabla\cdot\mathbf{u} = 0, \tag{11.37}$$

which, assuming that the time scale in the derivative is the same as the advective time scale, can be approximated as

$$\nabla\cdot\mathbf{u} = 0, \tag{11.38}$$

i.e. incompressible flow.

Finally, the thermodynamic equation can be written as:

$$\frac{Db}{Dt} = B, \tag{11.39}$$

where B is some source term, proportional to the heating rate, that we do not write explicitly here[5].

In particular, in the adiabatic case, the set of closed equations

[5] It can be found, along with the derivation, starting from a form of the thermodynamic equation using pressure and density, in Vallis 2017, p. 72.

sometimes referred to as the *simple Boussinesq equations* is:

$$\partial_t \mathbf{u} + \mathbf{u} \cdot \nabla \mathbf{u} = -\nabla \phi + b \mathbf{e}_z, \tag{11.40}$$

$$\nabla \cdot \mathbf{u} = 0, \tag{11.41}$$

$$\partial_t b + \mathbf{u} \cdot \nabla b = 0. \tag{11.42}$$

Let us now write a simple variant of these equations: we assume that the background state is in fact a given density profile $\bar{\rho}$ which depends on z. The derivation above still applies for fluctuations $\delta\rho = \bar{\rho} + \rho'$, with $\rho' \ll \bar{\rho}$. Correspondingly, we decompose the buoyancy b into $\bar{b} = -g\bar{\rho}/\rho_0$ and $b' = -g\rho'/\rho_0$ so that $b = \bar{b} + b'$ with $b' \ll \bar{b}$ and the pressure δp into $\delta p = \bar{p} + p'$ with $p' \ll \bar{p}$, assuming hydrostatic balance: $d\bar{p} = -\bar{\rho} g dz$. ϕ also becomes $\phi = \bar{\phi} + \phi'$ in the obvious way. Clearly $\bar{b}\mathbf{e}_z - \nabla\bar{\phi} = 0$. The equations become:

$$\partial_t \mathbf{u} + \mathbf{u} \cdot \nabla \mathbf{u} = -\nabla \phi' + b' \mathbf{e}_z, \tag{11.43}$$

$$\nabla \cdot \mathbf{u} = 0, \tag{11.44}$$

$$\partial_t b' + \mathbf{u} \cdot \nabla b' = -N^2 u_z, \tag{11.45}$$

with $N^2 = \frac{d\bar{b}}{dz} = -\frac{g}{\rho_0}\frac{d\bar{\rho}}{dz}$ the (square of the) *buoyancy frequency*.

11.4.2 *Application: internal gravity waves*

Vallis 2017, § 2.10.4 and Chap. 7.

Let us start from the Boussinesq equations for flow over a mean density profile, Eqs. (11.43)– (11.45).

We linearize the equations and assume invariance in the y direction, to obtain:

$$\frac{\partial u}{\partial t} = -\frac{\partial \phi'}{\partial x}, \tag{11.46}$$

$$\frac{\partial w}{\partial t} = -\frac{\partial \phi'}{\partial z} + b', \tag{11.47}$$

$$\frac{\partial u}{\partial x} + \frac{\partial w}{\partial z} = 0, \tag{11.48}$$

$$\frac{\partial b'}{\partial t} = -N^2 w. \tag{11.49}$$

Fourier-transforming the equations, we obtain the dispersion relation for plane wave solutions:

$$\omega = \pm \frac{Nk}{\sqrt{k^2 + m^2}}, \tag{11.50}$$

$$= \pm N \cos\theta, \tag{11.51}$$

with $k = K\cos\theta$ the wave number in the zonal direction, $m = K\sin\theta$ the wave number in the vertical direction. Such waves are called *internal gravity waves*. The frequency of internal gravity waves is

bounded by the buoyancy frequency N. A notable feature of gravity waves is that the wave number does not appear in the dispersion relation: only the direction of the wave vector (i.e. the direction of propagation), and not its norm, determines the frequency.

We have assumed implicitly that $N^2 > 0$ (stable background density profile, according to § 11.2.3). Indeed, in that case perturbations to the background profile propagate but do not grow in amplitude. On the other hand, if $N^2 < 0$ the linear system above admits unstable modes with exponentially growing amplitude; the background stratification is unstable.

12
Geophysical Turbulence

The notes for this chapter are still in a very early draft stage. They were written rapidly, and might still contain some mistakes or inaccurracies. Please treat them with caution and let me know if you find any problem.

12.1 *Beta-plane turbulence*

Rhines (1975), Vallis (2017, § 12.1)

12.1.1 *Beta effect*

We start from the 3D momentum equations in a rotating frame of reference[1]:

$$\partial_t \mathbf{v} + \mathbf{v} \cdot \nabla \mathbf{v} = -\nabla p + \nu \Delta \mathbf{v} - 2\boldsymbol{\Omega} \times \mathbf{v}, \tag{12.1}$$

[1] We do not discuss carefully how to obtain these equations of motion (for instance the centrifugal force, etc); please refer to a geophysical fluid dynamics textbook for more details, for instance Vallis (2017, Chap. 2).

where the latter term is the Coriolis force. The Coriolis force contains two contributions: one involving horizontal velocities and one involving vertical velocities, which can be neglected compared to the first one. The projection of the Coriolis force on the plane normal to the sphere (i.e. its contribution to the horizontal momentum equations) decreases from the pole to the equator. This phenomenon is called *beta effect*, or *differential rotation*. As far as horizontal motions are concerned, it is as if the Earth was rotating faster as we move towards the poles. This effect has a major influence on the large-scale dynamics of the atmosphere and the ocean.

The horizontal momentum equations on the sphere therefore write[2]

[2] Here we bluntly assume that the motion is 2D.

$$\partial_t \mathbf{u} + \mathbf{u} \cdot \nabla \mathbf{u} = -\nabla p + \nu \Delta \mathbf{u} - f \mathbf{e}_r \times \mathbf{u}, \tag{12.2}$$

with $f = 2\Omega \sin\phi$ with ϕ the latitude.

The equations are sometimes projected onto a plane tangent to the sphere at a given latitude ϕ_0. A corresponding approximation is to expand the Coriolis parameter at first order: $f(\phi) = f(\phi_0) + \beta y + o(y)$, where $y = a\phi$ is the meridional Cartesian coordinate, a the radius of the planet, $\beta = \frac{2\Omega}{a}\cos\phi_0$ the planetary vorticity gradient. When only the first term (constant f) is retained, we talk about an *f-plane* approximation. When the second term is also kept, this is the *beta-plane approximation*.

12.1.2 *Barotropic vorticity equation*

We start from the horizontal momentum equations on a beta-plane:

$$\partial_t u + u\partial_x u + v\partial_y u = -\partial_x p + \nu\Delta u + (f_0 + \beta y)v, \tag{12.3}$$
$$\partial_t v + u\partial_x v + v\partial_y v = -\partial_y p + \nu\Delta v - (f_0 + \beta y)u. \tag{12.4}$$

We assume that the flow is two-dimensional (u and v do not depend on the vertical) and non-divergent and we introduce a *stream function*:

$$u = \frac{\partial\psi}{\partial y}, \quad v = -\frac{\partial\psi}{\partial x}, \tag{12.5}$$

and the *vorticity* $\zeta = -\Delta\psi = (\nabla \times \mathbf{u}) \cdot \mathbf{k}$. Taking the curl of the momentum equations, we obtain:

$$\partial_t \zeta + \mathbf{u} \cdot \nabla\zeta + \beta v = \nu\Delta\zeta, \tag{12.6}$$
$$\partial_t q + \mathbf{u} \cdot \nabla q = \nu\Delta q, \tag{12.7}$$

with $q = \zeta + \beta y$ the *potential vorticity*. To differentiate the two, ζ is sometimes called *relative vorticity*. βy is the planetary vorticity (associated to the rotation of the Earth).

This equation is often called *barotropic vorticity equation*.

The barotropic vorticity equation is very similar to the 2D Navier-Stokes equations, with potential vorticity playing the role of vorticity. In particular, it has analogous conservation laws: in the absence of forcing and dissipation, the energy and the Casimir invariants (including *potential enstrophy*) are conserved.

Nevertheless, the phenomenology is different from 2D turbulence. In particular, we observe the formation of zonal jets, like in planetary atmospheres (see Fig. 12.1). Note that when the term corresponding to the beta effect dominates in the barotropic vorticity equation, we expect $\beta v \approx 0$, which is a first hint that strong beta effect should constrain the velocity to be essentially zonal.

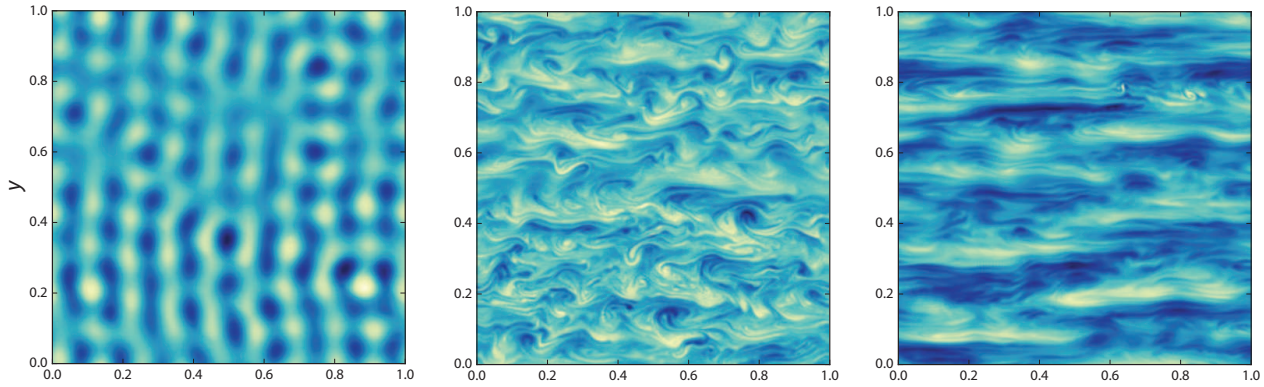

Figure 12.1: Vorticity field at different times (increasing from left to right) from numerical simulation of the barotropic vorticity equation (Vallis 2017, p. 450).

12.1.3 *Rhines scale*

Let us consider the magnitude of the different terms in the barotropic vorticity equation (neglecting molecular viscosity):

$$\begin{array}{cccc} \partial_t \zeta & +\mathbf{u}\cdot\nabla\zeta & +\beta v & = 0, \\ \frac{U}{LT} & \frac{U^2}{L^2} & \beta U & \end{array}$$

where U is a velocity scale and L a length scale. The inertial term and the beta effect are of the same order of magnitude when $L = L_R = \sqrt{U/\beta}$, which is called the *Rhines scale*[3]. Typically U is estimated as the root-mean square velocity. This reasoning assumes that the vorticity can be estimated as the root mean square velocity divided by the Rhines scale, which may actually be rather large. Hence other forms for this scale could be written. Nevertheless, we expect that at some large scale, the beta effect should dominate, while turbulence should dominate at smaller scales.

[3] Rhines (1975)

12.1.4 *Rossby waves*

We linearize the barotropic vorticity equation and look for plane wave solutions: $\psi = \psi_0 e^{i(kx+ly-\omega t)}$. These solutions are called Rossby waves. They obey the dispersion relation:

$$\omega = -\beta \frac{k}{k^2+l^2}. \tag{12.8}$$

The dispersion relation can be rewritten as

$$\left(k + \frac{\beta}{2\omega}\right)^2 + l^2 = \frac{\beta^2}{4\omega^2}, \tag{12.9}$$

which shows that the geometric locus of the wave vector is a circle, whose center and radius depend on the frequency. The group velocity $\mathbf{c}_g = \frac{\beta}{k^2+l^2}(\cos\alpha, \sin\alpha)$, where α is the angle between $\mathbf{e}_x$ and the wave vector $\mathbf{k}$, points from $\mathbf{k}$ towards the center of the circle.

12.1.5 *Deflection of the inverse cascade*

We would now like to understand the role of Rossby waves in energy transfers across scales, and in particular in the formation of anisotropic, zonal jets in beta plane turbulence. We start with a simple argument based on a comparison of timescales corresponding to different processes.

The eddy-turnover time, associated with the inverse cascade of 2D turbulence is $\tau_{NL} = 1/\sqrt{k^3 E(k)} \sim \varepsilon^{-1/3} K^{-2/3}$, with $K = \sqrt{k^2+l^2}$ the wave number. On the other hand, the timescale associated with Rossby wave propagation is the inverse of the frequency ω, which

depends explicitly on the zonal wave number k. We can therefore consider the product

$$\omega\tau_{NL} \sim \beta\varepsilon^{-1/3}kK^{-8/3}, \tag{12.10}$$
$$\sim \beta\varepsilon^{-1/3}K^{-5/3}\cos\theta, \tag{12.11}$$

with $k = K\cos\theta$. When this quantity is (much) smaller than unity, we expect the non-linear transfers to be much faster than wave propagation, and therefore we should observe an (isotropic) inverse cascade like in 2D. On the other hand, when it is (much) larger than unity, wave propagation dominates and the flow should be anisotropic.

The curves of equation $\omega\tau_{NL} = \text{const}$ correspond to "dumbell" shape curves. Hence, the inverse energy cascade is "deflected" by the Rossby waves towards the axis $k = 0$, which explains the formation of zonal structures (see Fig. 12.2).

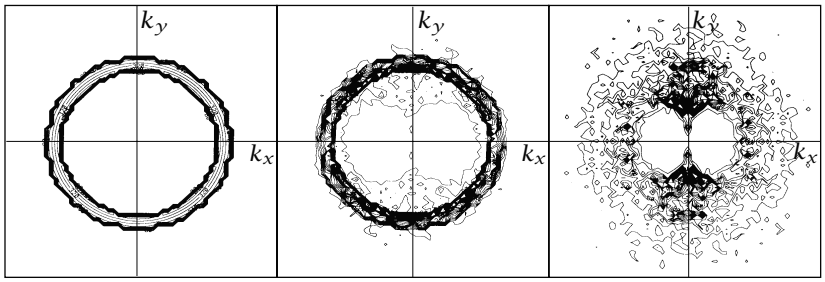

Figure 12.2: 2D energy spectrum from numerical simulations of the barotropic vorticity equation (Vallis and Maltrud 1993). Initially the spectrum is isotropic (left). As time proceeds, the energy condenses around the $k_x = 0$ axis (right).

12.1.6 *The* zonostrophic *energy spectrum of beta-plane turbulence*

If we neglect the anisotropic nature of the dispersion relation, the above reasoning yields a scale separating the inverse cascade regime and the wave regime: $L_\varepsilon = \left(\frac{\varepsilon}{\beta^3}\right)^{1/5}$. In fact, this scale is the same as the Rhines scale defined above, if we use the Taylor estimate for the energy dissipation rate $\varepsilon = U^3/L$, assuming that the correct scale in this formula is the Rhines scale L_R.

Now we would like to investigate the shape of the energy spectrum. Because of the inverse cascade, we have to add a dissipation mechanism at large scale to reach a steady state. We add Rayleigh friction to the barotropic vorticity equation:

$$\partial_t\zeta + \mathbf{u}\cdot\nabla\zeta + \beta v = \nu\Delta\zeta - \alpha\zeta. \tag{12.12}$$

Like in 2D turbulence, we can estimate easily the kinetic energy at steady-state, by assuming that it is entirely dissipated by the linear friction. It gives: $\varepsilon = 2\alpha E = 3\alpha U^2$. Injecting this estimate into the

Rhines scale yields a new scale $L_{\alpha\beta} = \left(\frac{\varepsilon}{3\alpha\beta^2}\right)^{1/4}$ which does not necessarily coincide with the separation scale between the nonlinear and the linear regimes derived above. This scale is in fact a combination of the scale L_ε and the classical friction scale $L_\alpha = \sqrt{\varepsilon/\alpha^3}$ at which the energy cascade is arrested in 2D: $L_{\alpha\beta} = L_\alpha^{1/6} L_\varepsilon^{5/6}$. One regime where we can have a physical interpretation of the competition between the different effects (nonlinearity, beta effect and friction) is the regime where friction is sufficiently small, so that the friction scale L_α (and the Rhines friction scale $L_{\alpha\beta}$) is large. Then it can be expected that the inverse energy cascade proceeds until the scale L_ε; once it is reached, the beta effect becomes dominant, the flow is anisotropic and jets should form until they reach a meridional scale $L_{\alpha\beta}$. In this regime it can be assumed that the energy spectrum does not depend on ε anymore, and dimensional analysis yields $E(k) = C_\beta \beta^2 k^{-5}$.

One drawback of this reasoning is that with such a steep spectrum, the eddy-turnover time decreases with increasing scale, and a definite friction scale cannot be defined anymore.

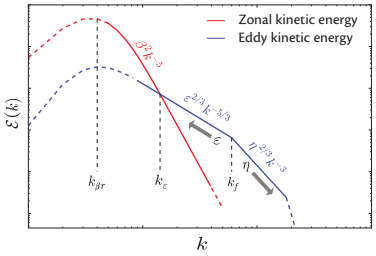

Figure 12.3: Schematic energy spectrum in the zonostrophic regime of beta-plane turbulence (Vallis 2017, Chap. 12).

12.1.7 *Momentum transport by Rossby waves*

In § 12.1.5, we have given an argument based on energy transfer in spectral space to explain the formation of zonal jets in beta-plane turbulence. In this section, we give a different argument, based on momentum transport properties of Rossby waves.

Let us carry out a Reynolds decomposition of the barotropic vorticity equation: we decompose the 2D velocity field into a mean-flow and fluctuations, and we assume that the mean flow is entirely in the zonal direction: $\mathbf{u} = U\mathbf{e}_x + \mathbf{u}'$, where the mean-flow is independent of x. The Reynolds-averaged Navier-Stokes equations for the mean-flow write

$$\partial_t U = -\partial_y \overline{u'v'} + \nu \Delta U. \tag{12.13}$$

The first term on the right hand side describes the acceleration due to all the non-zonally symmetric motions, like waves or turbulence. It takes the form of the divergence of a flux, $\overline{u'v'}$, which is a component of the Reynolds stress tensor, which is often called *eddy momentum flux* in the context of geophysical fluid dynamics. Because of the minus sign, the term $-\partial_y \overline{u'v'}$ is usually called *eddy momentum flux convergence*.

Now, it is easy to understand how Rossby waves transport momentum, and therefore accelerate the mean-flow through the eddy momentum flux convergence term. Indeed, for a plane Rossby wave we can compute directly the eddy momentum flux: $u = \partial_y \psi =$

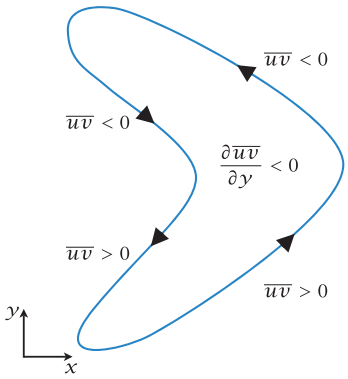

Figure 12.4: Momentum transport by Rossby waves (Vallis 2017, p. 544).

$-l\psi_0 \sin(kx + ly - \omega t)$, $v = k\psi_0 \sin(kx + ly - \omega t)$, and therefore:

$$\overline{u'v'} = -kl\frac{\psi_0^2}{2\pi}\int_0^{2\pi} \sin^2(kx + ly - \omega t)dx = -\frac{kl}{2}\psi_0^2. \tag{12.14}$$

On the other hand, the group velocity in the meridional direction is

$$c_g^y = \frac{\partial \omega}{\partial l} = \frac{2\beta kl}{(k^2 + l^2)^2}. \tag{12.15}$$

In particular, $c_g^y \overline{u'v'} < 0$: Rossby waves transport energy and momentum in opposite meridional directions. If Rossby waves propagate meridionally away from a source region, eddy momentum convergence in this region should be positive and the flow should accelerate towards the east. This is the fundamental mechanism through which Rossby waves can generate zonal jets. It plays an important part in the maintenance of the Jet Stream on Earth for instance[4].

[4] We have left aside for now the mechanism generating Rossby waves, which in that case is an instability of the jet called the *baroclinic instability*

Part III

Appendix

A
Taylor Hypothesis

Taylor (1938)

Until the (relatively recent) advent of velocimetry techniques based on lasers and high-speed cameras, most measurements were done with hot-wire devices, which only give access to the longitudinal (in the direction of the mean-flow) component of velocity at one point, as a function of time (see Fig. A.1). How do you extract information about the spatial structure of the velocity field from such a time series?

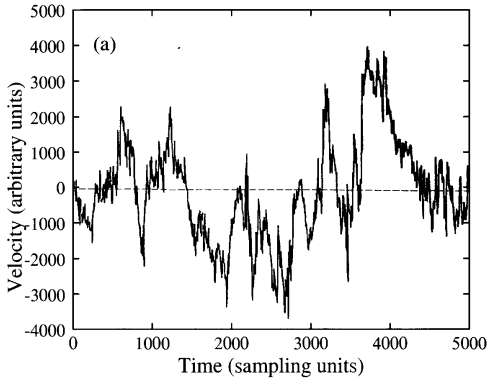

Figure A.1: Velocity signal recorded by a hot-wire in a wind tunnel, sampled at 5kHz (Frisch 1995).

Let us denote x the coordinate along the mean flow U, u the velocity in the reference frame of the laboratory and u' the velocity in the reference frame moving with the mean flow. We have

$$u(x,t) = U + u'(x - Ut, t). \tag{A.1}$$

As long as u' is typically much smaller than U, we can assume that the turbulence is essentially transported by the mean flow. This means that the spatial structure of the velocity field is *frozen* and travels as a block with speed U. When that happens, measuring $u(x_0, t)$ as a function of time at one point x_0 is equivalent to measuring $u(x, t_0)$ as a function of x at a given time. The validity of this approach is measured by the *turbulent intensity*: $I = \sqrt{\langle u'^2 \rangle}/U$, and we should have $I \ll 1$ for the Taylor hypothesis to be applicable [1].

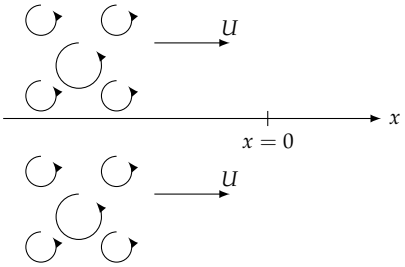

$$u'(x=0,t) = u'(x=-Ut, t=0)$$
$$u'(x,0) = u'(0, -\frac{x}{U})$$

[1] See Lumley (1965) and Pinton and Labbé (1994) about possible corrections to the Taylor hypothesis.

B
Some technical results

B.1 Isotropic functions: scalars, vectors and tensors

See Robertson (1940) or Batchelor (1953, § 3.3) for a more detailed presentation in the context of turbulence, or classical books on group theory for the background material.

Let us assume that $\mathbf{r}$ is a vector and $S(\mathbf{r})$, $\mathbf{V}(\mathbf{r})$ and $\mathbf{T}(\mathbf{r})$ are respectively a scalar, vector and rank-2 tensor function of $\mathbf{r}$. We assume that S, $\mathbf{V}$ and $\mathbf{T}$ are isotropic, i.e. the quantities $S(\mathbf{r})$, $\mathbf{a}\cdot\mathbf{V}(\mathbf{r})$ and $\mathbf{a}\cdot\mathbf{T}(\mathbf{r})\cdot\mathbf{b}$ for arbitrary vectors $\mathbf{a},\mathbf{b},\mathbf{r}$ are invariant under the action of $O(3)$. Then the most general form for these functions is:

$$S(\mathbf{r}) = S(r), \tag{B.1}$$

$$V_i(\mathbf{r}) = V(r) r_i, \tag{B.2}$$

$$T_{ij}(\mathbf{r}) = T_0(r)\delta_{ij} + T_1(r) r_i r_j. \tag{B.3}$$

I shall not write a fully rigorous proof here. In a nuthshell, this result follows from invariant theory, which states in particular that a function of vectors $\mathbf{x}^\alpha$, invariant under the action of rotations $SO(3)$ can be expressed in terms of scalar products $\mathbf{x}^\alpha\cdot\mathbf{x}^\beta$ and mixed products $\mathbf{x}^\alpha\cdot(\mathbf{x}^\beta\times\mathbf{x}^\gamma) = \det(\mathbf{x}^\alpha,\mathbf{x}^\beta,\mathbf{x}^\gamma)$. It follows that:

- $S(\mathbf{r})$, as a scalar invariant function of $\mathbf{r}$ only, can only be a function of $\mathbf{r}\cdot\mathbf{r}$.
- considering a vector $\mathbf{x}$, the scalar invariant $V_i(\mathbf{r})x^i$, which is also a linear function of $\mathbf{x}$, is proportional to $\mathbf{r}\cdot\mathbf{x}$.
- considering two vectors $\mathbf{x}$ and $\mathbf{y}$, the scalar invariant $T_{ij}(\mathbf{r})x^i y^j$, which is also a quadratic form, can be expressed in terms of the scalar products $\mathbf{x}\cdot\mathbf{y}$, $(\mathbf{r}\cdot\mathbf{x})(\mathbf{r}\cdot\mathbf{y})$ and the mixed products involving the three vectors, with coefficients depending on r^2 only. Because the mixed products are not invariant under reflections, their contribution vanishes if we impose $O(3)$ symetry, and we are left with the above result. If we only require symetry with respect to rotations ($SO(3)$), an additional term appears: $T_{ij}(\mathbf{r}) = T_0(r)\delta_{ij} + T_1(r)r_i r_j + T_2(r)\epsilon_{ijk}r^k$. Note that in general

$T_{ij}(\mathbf{r}) = T_{ji}(-\mathbf{r})$, so that reflection symmetry is equivalent to symmetry with respect to the two indices of the tensor.

C
The energy spectrum

In this section we discuss some additional aspects of the energy spectrum.

C.1 Model spectrum

Pope (2000, § 6.5.3)

In chapter 6 we will present a theory which accounts for the form of the energy spectrum in the inertial range, where it follows a power-law with a $-5/3$ slope; based on dimensional analysis, the spectrum is given by $E(k) = C\epsilon^{2/3}k^{-5/3}$ in that range. It can be useful to construct an analytical function which fits the observed spectrum, with the power law identified above in the inertial range but also in the energy-containing and dissipative scales. Such a model could take the form:

$$E(k) = C\epsilon^{2/3}k^{-5/3}f_L(kL)f_\eta(k\eta), \tag{C.1}$$

where $f_L(kL) \approx 1$ when $kL \gg 1$ and $f_\eta(k\eta) \approx 1$ when $k\eta \ll 1$. The specific forms which have been suggested are

$$f_L(kL) = \left(\frac{kL}{\sqrt{(kL)^2 + c_L}}\right)^{5/3+p_0}, \quad f_\eta(k\eta) = e^{-\beta[((k\eta)^4+c_\eta^4)^{1/4}-c_\eta]}, \tag{C.2}$$

where $p_0 = 2, c_L > 0, c_\eta > 0, \beta > 0$ are model constants. With such choices, the energy spectrum goes like k^2 at large scale. The alternative choice $p_0 = 4$, such that $E(k) \sim k^4$ at large scale, corresponds to the *van Karman spectrum*. The constant β is determined empirically; $\beta = 5.2$ is found to give good agreement with experimental data. The constants c_L and c_η are determined by requiring that $E(k)$ (resp. $2\nu k^2 E(k)$) integrates to E (resp. ϵ).

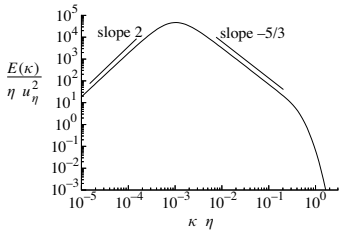

The model spectrum Eq. (C.1) for $R_\lambda = 500$.

C.2 *The one-dimensional spectrum*

Pope (2000, § 6.5)

Up to now we have only discussed the isotropic spectrum $E(k)$, corresponding to the kinetic energy integrated over a sphere of radius k in Fourier space. In isotropic flows, it is the most natural quantity to characterize the energy content over scales. Exploiting the constraints of homogeneity and isotropy, it can be computed easily even if we do not have access to the full velocity field, through the formula $E(k) = 2\pi k^2 \hat{U}_i^i(\mathbf{k}) = \frac{k^2}{(2\pi)^2} \int U_i^i(\mathbf{r}) e^{-i\mathbf{k}\cdot\mathbf{r}} d\mathbf{r}$, which only requires the knowledge of the longitudinal autocorrelation function $f(r)$.

Alternatively, we may measure one component of the velocity covariance tensor in an arbitrary direction (for simplicity let us choose a frame of reference such that this measurement direction is the first basis vector $\mathbf{e}_1$.), and compute (twice) its Fourier transform:

$$E_{ij}(k_1) = \frac{1}{\pi} \int_{-\infty}^{+\infty} U_{ij}(r\mathbf{e}_1) e^{-ik_1 r} dr, \tag{C.3}$$

and conversely,

$$U_{ij}(\mathbf{r}) = \frac{1}{2} \int_{-\infty}^{+\infty} E_{ij}(k_1) e^{ik_1 \mathbf{r}\cdot\mathbf{e}_1} dk_1. \tag{C.4}$$

From Eq. C.4 it follows that

$$E_{ij}(k_1) = 2 \int_{-\infty}^{+\infty} \int_{-\infty}^{+\infty} \hat{U}_{ij}(k_1, k_2, k_3) dk_2 dk_3. \tag{C.5}$$

Hence, the diagonal components of the one-dimensional spectrum correspond to integrating the kinetic energy density in Fourier space over a plane (here with fixed k_1). Note in particular that unlike the isotropic spectrum $E(k)$, the one-dimensional spectra $E_{ii}(k_1)$ contain contributions from wave vectors with wave numbers larger than k_1 (in fact, k_1 is the smallest wave number contributing to the spectrum). As usual, one can distinguish the longitudinal and transverse spectra $E_{11}(k_1)$ and $E_{22}(k_1) = E_{33}(k_1)$. Using homogeneity, they can be written $E_{ii}(k_1) = (2/\pi) \int_0^{+\infty} U_{ii}(r\mathbf{e}_1) \cos(k_1 r) dr$, and with our choice of frame of reference, $U_{11}(r\mathbf{e}_1) = f(r)$, $U_{22}(r\mathbf{e}_1) = U_{33}(r\mathbf{e}_1) = g(r)$, so that

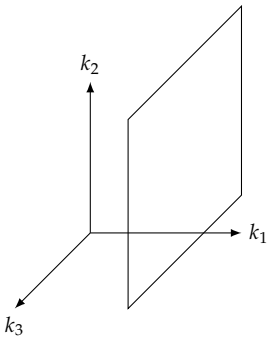

$$E_{11}(k_1) = \frac{2}{\pi} \int_0^{+\infty} f(r) \cos(k_1 r) dr, \quad E_{22}(k_1) = E_{33}(k_1) = \frac{2}{\pi} \int_0^{+\infty} g(r) \cos(k_1 r) dr, \tag{C.6}$$

and using the relation between the longitudinal and transverse autocorrelation function $g(r) = f(r) + rf'(r)/2$, we obtain the relation

$$E_{22}(k_1) = E_{11}(k_1) + \frac{1}{\pi} \int_0^{+\infty} rf'(r) \cos(k_1 r) dr, \tag{C.7}$$

integrating by parts,

$$= E_{11}(k_1) - \frac{1}{\pi}\int_0^{+\infty} f(r)[\cos(k_1 r) - r k_1 \sin(k_1 r)]dr, \quad \text{(C.8)}$$

$$= \frac{E_{11}(k_1)}{2} - \frac{k_1}{2}\frac{dE_{11}(k_1)}{dk_1} = -\frac{k_1^2}{2}\frac{d}{dk_1}\left(\frac{E_{11}(k_1)}{k_1}\right). \quad \text{(C.9)}$$

The longitudinal spectrum can also be related to the isotropic spectrum. Injecting $\hat{U}_{ii}(k_1, k_2, k_3) = E(k)(1 - k_i^2/k^2)/(4\pi k^2)$ into Eq. (C.5), we obtain

$$E_{11}(k_1) = \int_{-\infty}^{+\infty}\int_{-\infty}^{+\infty} \frac{E(k)}{2\pi k^2}\left(1 - \frac{k_1^2}{k^2}\right) dk_2 dk_3. \quad \text{(C.10)}$$

Changing to polar coordinates in the plane (k_2, k_3), with $k_r^2 = k_2^2 + k_3^2$, we get

$$= \int_0^{+\infty} \frac{E(k)}{k_1^2 + k_r^2}\left(1 - \frac{k_1^2}{k_1^2 + k_r^2}\right) k_r dk_r, \quad \text{(C.11)}$$

and under the new change of variable $k = \sqrt{k_r^2 + k_1^2}$,

$$= \int_{k_1}^{+\infty} \frac{E(k)}{k}\left(1 - \frac{k_1^2}{k^2}\right) dk. \quad \text{(C.12)}$$

Differentiating with respect to k_1, we get

$$\frac{dE_{11}(k_1)}{dk_1} = -2k_1 \int_{k_1}^{+\infty} E(k) k^{-3} dk < 0, \quad \text{(C.13)}$$

which shows that regardless of the shape of the isotropic spectrum, the longitudinal spectrum $E_{11}(k_1)$ is always a decreasing function of k_1. Differentiating again,

$$\frac{d^2 E_{11}(k_1)}{dk_1^2} = -2\int_{k_1}^{+\infty} E(k) k^{-3} dk + 2E(k_1) k_1^{-2}, \quad \text{(C.14)}$$

from which we obtain the isotropic spectrum in terms of the longitudinal spectrum:

$$E(k) = \frac{k^3}{2}\frac{d}{dk}\left(\frac{1}{k}\frac{dE_{11}(k)}{dk}\right). \quad \text{(C.15)}$$

From the above relations, we see that if the longitudinal spectrum has a power-law of the form $E_{11}(k_1) = C_1 k_1^{-p}$, then it is also the case for the transverse and isotropic spectra: $E_{22}(k_1) = C_2 k_1^{-p}$ and $E(k) = Ck^{-p}$ with $C_2 = (1+p)C_1/2$ and $C = p(2+p)C_1/2$. For $p = 5/3$, we have $C_2 = 4/3C_1$and $C = 55/18C_1$.

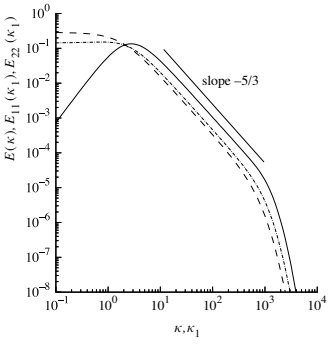

Comparison of the one-dimensional and isotropic spectra (Pope 2000).

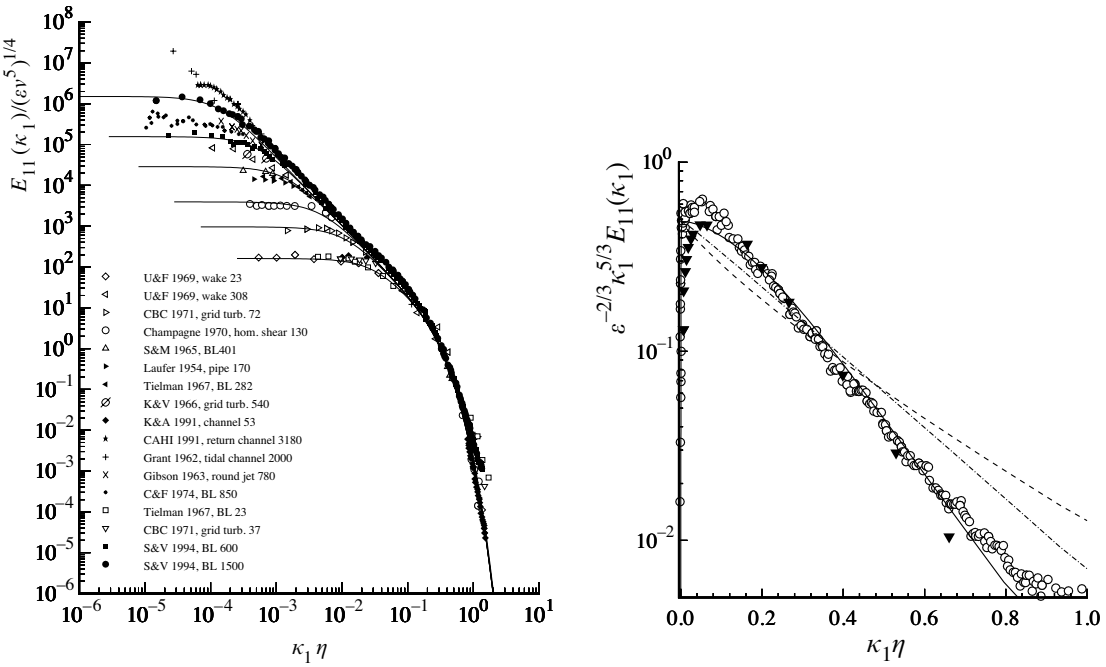

Figure C.1: Longitudinal velocity spectrum in various experiments (points) and using the model spectrum Eq. (C.1), in logarithmic coordinates (left) revealing the inertial range and energy containing range, and in linear-logarithmic coordinates (right), focusing on the dissipative range (Pope 2000, § 6.5.4).

C.3 *Refined study of the energy spectrum*

Fig. C.1 shows longitudinal spectra from a variety of measurements at different Reynolds numbers, rescaled based on Kolmogorov scalings (see Chap. 6). It shows that the spectrum seems to follow a universal curve at scales smaller than the energy containing scales. We also observe that the inertial range grows with increasing Reynolds number. These figures also illustrate the quality of the fit obtained from the model spectrum given by Eq. (C.1) (solid lines). By contrast, the alternative models $f_\eta(k\eta) = e^{-\beta_0 k\eta}$ (corresponding to $c_\eta = 0$) with $\beta_0 = 2.094$ (dashed line) and $f_\eta(k\eta) = e^{-\frac{3}{2}C(k\eta)^{4/3}}$ (dot-dashed line, Pao (1965)) do not describe as well the energy spectrum decay in the dissipative range.

Plotting the one-dimensional spectra in all directions in compensated form, as in Fig. C.2 allows to test isotropy. Although the measurements are made in a flow which is not isotropic (a turbulent boundary layer), the transverse spectra $E_{22}(k_1)$ and $E_{33}(k_1)$ are quite similar, in particular at small scales. The ratio $C_1'/C_1 \approx 1.4$ is close to $4/3$, which is the theoretical value for isotropic flows with a $-5/3$ power law spectrum.

Finally, this figure shows a departure from the Kolmogorov inertial range prediction towards the end of the inertial range (here, at $k\eta \approx 0.1$) where a bump appears in the compensated spectrum. This phenomenon[1] is referred to as the *bottleneck* of the energy cascade.

[1] also observed in high resolution direct numerical simulations, e.g. Kaneda et al. (2003) and Mininni, Alexakis, and Pouquet (2008).

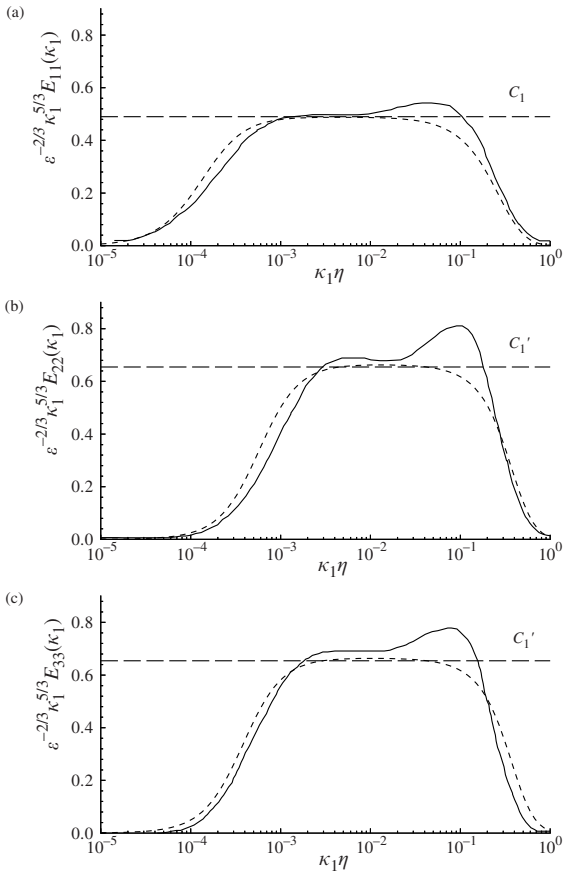

Figure C.2: Compensated one-dimensional spectra measured in a turbulent boundary layer at $R_\lambda = 1450$ (solid lines, Saddoughi and Veeravalli (1994)) and from the model spectrum Eq. (C.1) (dashed lines). Figure from Pope (2000, Fig. 6.17).

It means that the universal function F appearing in the Kolmogorov spectrum at finite Reynolds number (see § 6.1) is not a decreasing function of k, but rather increases throughout the inertial range, until a scale on the order of the Kolmogorov scale, and starts decreasing only within the dissipative range. This phenomenon is classically interpreted as a consequence of the fact that viscosity, which can still be seen from the lower end of the inertial range, inhibits triadic interactions involving modes close to the dissipative scales and thereby reduces slightly the energy transfer towards smaller scales, leading to an accumulation of energy at the door of the dissipative range (Falkovich 1994). An alternative interpretation is that the bottleneck is a signature of incomplete *thermalization* (Frisch et al. 2008). It has also been suggested to be related to helicity (Kurien, Taylor, and Matsumoto 2004).

In numerical simulations, the bottleneck effect increases with the use of hyperviscosity, which is one of the arguments against such numerical practice.

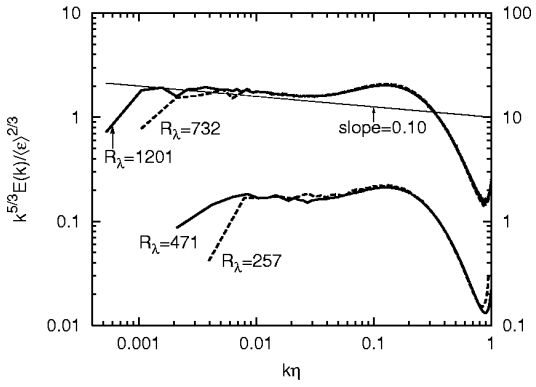

Figure C.3: Compensated isotropic energy spectrum $E(k)$ in high-resolution DNS of homogeneous isotropic turbulence (Kaneda et al. 2003).

C.4 *The energy spectrum in the energy-containing range*

Let us assume that the velocity-spectrum tensor $\hat{U}_{ij}(\mathbf{k})$ is at least twice differentiable at $\mathbf{k} = 0$, so that we can write the Taylor expansion[2]:

$$\hat{U}_{ij}(\mathbf{k}) = a_{ij} + a_{ijl}k^l + a_{ijlm}k^l k^m + o(k^2), \tag{C.16}$$

where the coefficients $a_{ij}, \cdots$ do not depend on $\mathbf{k}$. The incompressibility condition $k^i\hat{U}_{ij}(\mathbf{k})$ for all wave vectors $\mathbf{k}$ means that all the terms in the series must vanish: $a_{ij}k^i = a_{ijl}k^i k^l = a_{ijlm}k^i k^l k^m = 0$. In particular, $a_{ij} = 0$[3]. Besides, for any $\mathbf{k}$ the hermitian form $\hat{U}_{ij}(\mathbf{k})$ is positive (non-definite): for any vector $\mathbf{X}$, we have $X^i X^{j*}\hat{U}_{ij}(\mathbf{k}) \geq 0$. In particular, $a_{ijl}X^i X^{j*}k^l \geq 0$, but if $a_{ijl} \neq 0$ this quantity changes sign with $\mathbf{k}$, so necessarily $a_{ijl} = 0$. It follows that the first non-vanishing coefficient is a_{ijlm}: $\hat{U}_{ij}(\mathbf{k}) = a_{ijlm}k^l k^m + o(k^2)$, and therefore $E(k) = 2\pi k^2 a_{ijlm}k^l k^m + o(k^4)$ should scale like k^4 at small k (notwithstanding the tensor structure).

In numerical simulations, both the k^4 and an alternative k^2 scalings have been observed (Chasnov 1995), depending on the symmetries of the inital condition. The k^2 scaling has been explained theoretically by Saffman (1967). Note also that k^2 corresponds to a statistical equilibrium spectrum.

[2] Batchelor (1953, § 3.1)

[3] No such conclusion can be drawn for other coefficients: for instance $\epsilon_{ijl}k^i k^l = 0$ for all $\mathbf{k}$.

Bibliography

Batchelor, G. K. (1953). *The Theory of Homogeneous Turbulence*. Cambridge University Press.

Bec, J. and K. Khanin (2007). "Burgers turbulence". *Phys. Rep.* 447.1-2, pp. 1–66.

Bernard, D. (1999). "Three-point velocity correlation functions in two-dimensional forced turbulence". *Phys. Rev. E* 60.5, p. 6184.

Boffetta, G. and R. E. Ecke (2012). "Two-Dimensional Turbulence". *Ann. Rev. Fluid Mech.* 44, pp. 427–451.

Boffetta, G. and S. Musacchio (2010). "Evidence for the double cascade scenario in two-dimensional turbulence". *Phys. Rev. E* 82.1, p. 016307.

Borue, V. and S. A. Orszag (1995). "Forced Three-Dimensional Homogeneous Turbulence with Hyperviscosity". *EPL* 29.9, pp. 687–692.

Bouchet, F. and A. Venaille (2012). "Statistical mechanics of two-dimensional and geophysical flows". *Phys. Rep.* 515, pp. 227–295.

Boyd, J. P. (2001). *Chebyshev and Fourier spectral methods*. Courier Corporation.

Chasnov, J. R. (1995). "The decay of axisymmetric homogeneous turbulence". *Phys. Fluids* 7.3, pp. 600–605.

Chen, Q. et al. (2003). "Intermittency in the joint cascade of energy and helicity". *Phys. Rev. Lett.* 90, p. 214503.

Chou, P. (1940). "On an extension of Reynolds' method of finding apparent stress and the nature of turbulence". *Chin. J. Phys* 4.1.

Comte-Bellot, G. and S. Corrsin (1971). "Simple Eulerian time correlation of full-and narrow-band velocity signals in grid-generated, 'isotropic' turbulence". *J. Fluid Mech.* 48.2, pp. 273–337.

Cooley, J. W. and J. W. Tukey (1965). "An algorithm for the machine calculation of complex Fourier series". *Mathematics of computation* 19.90, pp. 297–301.

Dubrulle, B. (2019). "Beyond Kolmogorov cascades". *J. Fluid Mech.* 867, P1.

Durran, D. R. (2010). *Numerical methods for fluid dynamics: With applications to geophysics*. Vol. 32. Springer.

Eyink, G. and K. Sreenivasan (2006). "Onsager and the theory of hydrodynamic turbulence". *Rev. Mod. Phys.* 78, pp. 87–135.
Falkovich, G. (1994). "Bottleneck phenomenon in developed turbulence". *Phys. Fluids* 6.4, pp. 1411–1414.
– (2011). *Fluid Mechanics*. Cambridge University Press.
Falkovich, G., K. Gawedzki, and M. Vergassola (2001). "Particles and fields in fluid turbulence". *Rev. Mod. Phys.* 73.4, p. 913.
Feynman, R. P., R. B. Leighton, and M. L. Sands (1965). *The Feynman Lectures on Physics*. Addison-Wesley.
Frisch, U. (1995). *Turbulence, the legacy of A.N. Kolmogorov*. Cambridge University Press.
Frisch, U. et al. (2008). "Hyperviscosity, Galerkin truncation, and bottlenecks in turbulence". *Phys. Rev. Lett.* 101.14, p. 144501.
Hartmann, D. L. (2015). *Global physical climatology*. Vol. 103.
Herbert, C. (2014). "Restricted Partition Functions and Inverse Energy Cascades in parity symmetry breaking flows". *Phys. Rev. E* 89, p. 013010.
– (2015). "An Introduction to Large Deviations and Equilibrium Statistical Mechanics for Turbulent Flows". In: *Stochastic Equations for Complex Systems: Theoretical and Computational Topics*. Ed. by S. Heinz and H. Bessaih. Springer. Chap. 3, pp. 53–84.
Hinch, E. J. (2020). *Numerical Methods: Think before You Compute: A Prelude to Computational Fluid Dynamics*. Vol. 61. Cambridge University Press.
Hunt, J. C. R. (1998). "Lewis Fry Richardson and his contributions to mathematics, meteorology, and models of conflict". *Ann. Rev. Fluid Mech.* 30.1, pp. xiii–xxxvi.
Ishihara, T., T. Gotoh, and Y. Kaneda (2009). "Study of High–Reynolds Number Isotropic Turbulence by Direct Numerical Simulation". *Ann. Rev. Fluid Mech.* 41.1, pp. 165–180.
Kaneda, Y. et al. (2003). "Energy dissipation rate and energy spectrum in high resolution direct numerical simulations of turbulence in a periodic box". *Phys. Fluids* 15.2, pp. L21–L24.
Kármán, T. von and L. Howarth (1938). "On the statistical theory of isotropic turbulence". *Proc. R. Soc. London, Ser. A* 164, pp. 192–215.
Kellay, H. (2017). "Hydrodynamics experiments with soap films and soap bubbles: A short review of recent experiments". *Phys. Fluids* 29.11, p. 111113.
Kolmogorov, A. N. (1962). "A refinement of previous hypotheses concerning the local structure of turbulence in a viscous incompressible fluid at high Reynolds number". *J. Fluid Mech.* 13, pp. 82–85.

Kolmogorov, A. N. (1941). "Dissipation of energy in locally isotropic turbulence". *Dokl. Akad. Nauk. SSSR* 32, pp. 16–18. Reprinted in *Proc. R. Soc. Lond. A* **434**, 15–17 (1991).

Kraichnan, R. H. (1973). "Helical turbulence and absolute equilibrium". *J. Fluid Mech.* 59, pp. 745–752.

Kurien, S., M. A. Taylor, and T. Matsumoto (2004). "Cascade time scales for energy and helicity in homogeneous isotropic turbulence". *Phys. Rev. E* 69.6, p. 066313.

Landau, L. and E. Lifchitz (1971). *Physique Théorique, Tome VI: Mécanique des fluides*. Mir, Moscou.

Lee, T. D. (1952). "On some statistical properties of hydrodynamical and magneto-hydrodynamical fields". *Q. Appl. Math.* 10, pp. 69–74.

Lesieur, M. (2008). *Turbulence in Fluids*. 4th edition. Springer-Verlag, New York.

Lumley, J. L. (1965). "Interpretation of time spectra measured in high-intensity shear flows". *Phys. Fluids* 8.6, pp. 1056–1062.

Millionshchikov, M. (1941). "On the theory of homogeneous isotropic turbulence". In: *Dokl. Akad. Nauk SSSR*. Vol. 32. 9, pp. 611–614.

Mininni, P. D., A Alexakis, and A Pouquet (2008). "Nonlocal interactions in hydrodynamic turbulence at high Reynolds numbers: The slow emergence of scaling laws". *Phys. Rev. E* 77.3, p. 036306.

Moffatt, H. K. and A Tsinober (1992). "Helicity in laminar and turbulent flow". *Ann. Rev. Fluid Mech.* 24, pp. 281–312.

Monin, A. S. (1959). "The Theory of Locally Isotropic Turbulence". *Soviet Physics Doklady* 4, p. 271.

Monin, A. S. and A. M. Yaglom (1971). *Statistical Fluid Mechanics*. Vol. 2. MIT Press, Cambridge, MA.

Nazarenko, S. V. (2010). *Wave Turbulence*. Vol. 825. Lecture Notes in Physics. Springer.

O'Brien, E. E. and G. C. Francis (1962). "A consequence of the zero fourth cumulant approximation". *J. Fluid Mech.* 13.3, pp. 369–382.

Obukhov, A. M. (1962). "Some specific features of atmospheric turbulence". *J. Fluid Mech.* 13, pp. 77–81.

Ogura, Y. (1963). "A consequence of the zero-fourth-cumulant approximation in the decay of isotropic turbulence". *J. Fluid Mech.* 16.1, pp. 33–40.

Onsager, L. (1949). "Statistical hydrodynamics". *Il Nuovo Cimento* 6, pp. 279–287.

Orszag, S. A. (1970). "Analytical theories of turbulence". *J. Fluid Mech.* 41, pp. 363–386.

Orszag, S. A. and G. S. Patterson (1972). "Numerical simulation of turbulence". In: *Statistical models and Turbulence*. Springer, pp. 127–147.

Pao, Y.-H. (1965). "Structure of turbulent velocity and scalar fields at large wavenumbers". *Phys. Fluids* 8.6, pp. 1063–1075.
Patterson, G. S. and S. A. Orszag (1971). "Spectral calculations of isotropic turbulence: Efficient removal of aliasing interactions". *Phys. Fluids* 14.11, pp. 2538–2541.
Pinton, J.-F. and R. Labbé (1994). "Correction to the Taylor hypothesis in swirling flows". *Journal de Physique II* 4.9, pp. 1461–1468.
Pomeau, Y. (1995). "Statistical Approach (to 2D Turbulence)". In: *Turbulence: A Tentative Dictionary*. Ed. by P Tabeling and O Cardoso. Plenum Publishing Corporation.
Pope, S. B. (2000). *Turbulent Flows*. Cambridge University Press.
Pouquet, A. et al. (1975). "Evolution of high Reynolds number two-dimensional turbulence". *J. Fluid Mech.* 72, pp. 305–319.
Proudman, I and W. H. Reid (1954). "On the decay of a normally distributed and homogenous turbulent velocity field". *Philosophical Transactions of the Royal Society of London. Series A, Mathematical and Physical Sciences* 247.926, pp. 163–189.
Rhines, P. B. (1975). "Waves and turbulence on a beta-plane". *J. Fluid Mech.* 69, pp. 417–443.
Robertson, H. P. (1940). "The invariant theory of isotropic turbulence". In: *Mathematical Proceedings of the Cambridge Philosophical Society*. Vol. 36. 2. Cambridge University Press, pp. 209–223.
Rogallo, R. S. (1981). "Numerical experiments in homogeneous turbulence".
Ruelle, D. (2004). "Conversations on nonequilibrium physics with an extraterrestrial". *Physics Today* 57.5, pp. 48–53.
Saddoughi, S. G. and S. V. Veeravalli (1994). "Local isotropy in turbulent boundary layers at high Reynolds number". *J. Fluid Mech.* 268, pp. 333–372.
Saffman, P. (1967). "The large-scale structure of homogeneous turbulence". *J. Fluid Mech.* 27.3, pp. 581–593.
Sagaut, P. and C. Cambon (2008). *Homogeneous Turbulence Dynamics*. Cambridge University Press.
Salmon, R. (1980). "Baroclinic instability and geostrophic turbulence". *Geophys. Astrophys. Fluid Dyn.* 15, pp. 167–211.
She, Z. S. and E. Leveque (1994). "Universal scaling laws in fully developed turbulence". *Phys. Rev. Lett.* 72, pp. 336–339.
Siggia, E. D. (1981). "Numerical study of small-scale intermittency in three-dimensional turbulence". *J. Fluid Mech.* 107, pp. 375–406.
Simmons, L. F. G. and C Salter (1934). "Experimental investigation and analysis of the velocity variations in turbulent flow". *Proc. R. Soc. Lond. A* 145.854, pp. 212–234.
Sreenivasan, K. R. (1984). "On the scaling of the turbulence energy dissipation rate". *Phys. Fluids* 27.5, p. 1048.

– (1995). "On the universality of the Kolmogorov constant". *Phys. Fluids* 7.11, pp. 2778–2784.
Stewart, R. W. (1951). "Triple velocity correlations in isotropic turbulence". *Mathematical Proceedings of the Cambridge Philosophical Society* 47.1, 146–157.
Tatsumi, T (1957). "The theory of decay process of incompressible isotropic turbulence". *Proceedings of the Royal Society of London. Series A. Mathematical and Physical Sciences* 239.1216, pp. 16–45.
– (1980). "Theory of homogeneous turbulence". In: *Advances in Applied Mechanics*. Vol. 20. Elsevier, pp. 39–133.
Taylor, G. I. (1935). "Statistical theory of turbulence". *Proc. R. Soc. Lond. A* 151.873, pp. 421–444.
– (1938). "The spectrum of turbulence". *Proc. R. Soc. Lond. A* 164.919, pp. 476–490.
Tennekes, H. and J. L. Lumley (1972). *A First Course in Turbulence*. MIT Press.
Tritton, D. J. (2012). *Physical fluid dynamics*. Springer Science & Business Media.
Vallis, G. K. (2017). *Atmospheric and Oceanic Fluid Dynamics: Fundamentals and Large-scale Circulation*. Cambridge University Press.
Vallis, G. K. and M. E. Maltrud (1993). "Generation of mean flows and jets on a beta-plane and over topography". *J. Phys. Oceanogr.* 23, pp. 1346–1362.
Vincent, A. and M. Meneguzzi (1991). "The spatial structure and statistical properties of homogeneous turbulence". *J. Fluid Mech.* 225, pp. 1–20.
Warn, T (1986). "Statistical mechanical equilibria of the shallow water equations". *Tellus A* 38.1, pp. 1–11.
Yeung, P. K., X. M. Zhai, and K. R. Sreenivasan (2015). "Extreme events in computational turbulence". *Proc. Natl. Acad. Sci. U.S.A.* 112.41, pp. 12633–12638.
Zeitlin, V. (2018). *Geophysical fluid dynamics: understanding (almost) everything with rotating shallow water models*. Oxford University Press.
Zeman, O (1994). "A note on the spectra and decay of rotating homogeneous turbulence". *Phys. Fluids* 6, pp. 3221–3223.